UNIVERSITY OF CALIFORNIA,
IRVINE

Development and Function of Hematopoietic Cells

DISSERTATION

Submitted in partial satisfaction of the requirements
for the degree of

DOCTOR OF PHILOSOPHY

in Biological Sciences

by

Ankita Kiran Shukla

Dissertation Committee:
Assistant Professor Matthew A. Inlay, Chair
Associate Professor Mathew M. Blurton-Jones
Associate Professor Melissa B. Lodoen

2019

DEDICATION

To

My parents, Kiran and Rekha, for their unwavering support and blessings,

My younger sister, Urvi, for fulfilling the roles of best friend and older sister,

And my mentor and friend, Dr. Matt Inlay.

TABLE OF CONTENTS

LIST OF FIGURES

LIST OF TABLES

ACKNOWLEDGMENTS

I would like to begin by thanking the UC Irvine community for being extremely supportive throughout my undergraduate and graduate career. This includes not only the resources that UC Irvine offers as well as the warm and approachable faculty and staff, who, I have always felt, had my best interest in mind.

The biggest influence on my growth as a scientist was my mentor, Dr. Matthew Inlay. Matt gave me the freedom to pursue my curiosities and empowered me to believe in myself. I thank him for being the friendliest face in the audience for every talk I ever gave during graduate school. I appreciate him for allowing me to pursue an industry internship. I thank him for challenging me, supporting me, cheering me on, and being the example of a good leader. I always appreciated all his "Dad jokes" and thank him for laughing at all my puns in return.

My extraordinary experience in the Inlay lab was also a result of the supportive, friendly and kind lab mates. I want to thank Yasamine Ghorbanian for becoming the best friend, who I will cherish for a lifetime. Alborz Karimzadeh's wisdom about all things CD11a, second only to Matt, as well as his manly presence were invaluable in the lab. Tannaz Faal's morning discussions were ever so entertaining. I loved how seamlessly Erika Varady fit into our Inlay lab solidarity. I would like to thank Dr. Connie Inlay for her training and mentorship. I also would like to thank Vanessa Scarfone for all her FACS magic and insight about life in general.

My committee members, Drs. Mathew Blurton-Jones and Melissa Lodoen, whose feedback, experience and suggestions were crucial to the success of both my projects! I would also like to thank Dr. Eric Pearlman and Rebecca Taylor at the Institute for Immunology, for funding my research, as well as organizing events, like the Immunology Fair, that gave me opportunities to meet leaders in Immunology.

Apart from all the scientists I have mentioned thus far, my growth as a scientist would not have been possible without the support of my parents, Rekha and Kiran. They provide me with continuous love, positivity and blessings which complete my life. Their sacrifice of moving to the United States is what keeps me motivated at all times. I am grateful for the freedom to pursue what I enjoy in life. I will continue to make you proud. I love you.

Finally, I would like express my deepest love and appreciation for my sister, Urvi. I could not have asked for a better friend, roommate, partner in crime and dance. I love you more than anything in the world, second only to how much you love me.

CURRICULUM VITAE

Ankita Shukla

EDUCATION

University of California, Irvine

Doctor of Philosophy (Ph.D.) in Biological Sciences (June 2019)
Applied Project Management Certificate (December 2018)
Bachelor of Science (B.S.) in Developmental and Cell Biology (June 2012)
Bachelor of Arts (B.A.) in Anthropology (June 2012)

RESEARCH TRAINING

University of California, Irvine **September 2013- Present**
PhD Graduate Research
Advisor: Dr. Matthew Inlay

1. Alzheimer's Disease (AD)

I discovered a novel marker to distinguish microglia from infiltrating immune cells in mouse models of AD. I also identified amyloid plaque-associated myeloid cells are microglia, not infiltrating monocytes. My data is significant for therapeutic approaches targeting microglial phagocytic potential in AD. Through this project, I have gained a deep appreciation for the role of the immune system in brain diseases, which has now become my primary research interest.

2. Developmental Hematopoiesis

I use a novel lineage tracing model to assess whether adult Hematopoietic Stem Cells (HSCs) originate from the embryonic yolk sac or other hematopoietic tissues. My project will be the first to show contributions of the yolk sac to the adult HSC pool. Besides flow cytometry, immunohistochemistry and microscopy, I also became proficient in rigorous HSC transplantation techniques, retro-orbital injections in neonatal as well as adult mice, embryo harvests, intravenous and intraperitoneal injections through this project.

Allergan, PLC **Summer 2017**
Intern- Department of Immunology
Supervisor: Dr. Qing (Joe) Zhou

My internship project focused on the conversion of polyclonal to recombinant monoclonal antibody for use in total drug assay. I learned and mastered protein-protein and protein-small molecule binding kinetics to determine concentrations of drug present in samples. I also performed single and multiplex ELISA assays for functional validation studies. My project helped simplify peri-clinical validation assays and reduced expenses. My internship culminated in a company-wide adoption of my assay, interdepartmental recognition and invitation to return for the internship in successive summers. I have also built strong relationships with industry scientists, department directors, vice presidents and marketing heads etc.

Pomona College, Claremont. **2012- 2013**
Research Associate
Supervisor: Dr. Daniel Martinez

My research project focused on studying the migration of interstitial stem cells (I-cells) in chimeric, grafted species of hydra. I was also responsible for purchasing, training and managing undergraduate students and their projects, animal handling and other lab management tasks.

University of California, Irvine. Department of Molecular Biology & Biochemistry
Undergraduate Researcher
Supervisor: Dr. Christopher Hughes
I studied the role of *VEGF* signaling in arteriovenous malformations. I secured a competitive Undergraduate Research Opportunities Program Fellowship and funding for the project.

PUBLICATIONS

1. **Shukla AK**, McIntyre LL, Marsh SE, et al. (2018) CD11a expression distinguishes infiltrating myeloid cells from plaque-associated microglia in Alzheimer's disease. *Glia.* 1–13. https://doi.org/10.1002/glia.23575

2. Wigal SB, Raja P, **Shukla AK** (2013). An update on Lisdexamfetamine Dimesylate for the treatment of attention deficit hyperactivity disorder. *Expert Opinion on Pharmacotherapy* 14.1: 137-145. https://doi.org/10.1517/14656566.2013.754013

REPORTS IN PROGRESS

Shukla AK, Fabello JA, Inlay MA. Tracing hematopoietic stem cells derived from extra-embryonic mesoderm using the inducible HoxB6-CreER system. *To be submitted in 2019*

SELECTED FELLOWSHIPS AND AWARDS

- Experimental Hematology Award and Travel Stipend- ISEH (September 2018)
- Excellence in Cytometry Award -Southern California Flow Cytometry Association (April 2018)
- AAI Young Investigator Award -La Jolla Immunology Conference (October 2017)
- NIH T32 Immunology Research Fellowship (2016-2017)
- People's Choice Award -Associated Graduate Student Symposium (April 2016)
- Associated Graduate Students Travel Award (June 2016)

ORAL AND POSTER PRESENTATIONS BY PROJECT

CD11a expression distinguishes infiltrating myeloid cells from plaque-associated microglia in Alzheimer's Disease

Oral Presentations:
- Immunology Fair, Irvine CA. (December 2016, December 2018)
- SoCal Flow Summit, Irvine, CA. (April 2018)

Poster Presentations:
- La Jolla Immunology Conference (October 2018, October 2017)
- International Society of Stem Cell Research Annual Meeting, Boston, MA. (June 2017)

- Keystone Symposia- Neuroinflammation, Keystone, CO. (June 2017)

Hematopoietic stem cells derived from extra-embryonic mesoderm

Oral Presentations:

- International Society of Experimental Hematology Annual Meeting, Los Angeles, CA (September 2018)- *Lightening talk*
- Stem Cell Awareness Day Scientific Symposium, Irvine, CA. (November 2016)
- Southern California Flow Cytometry Summit, Irvine, CA. (April 2016)
- AGS Graduate Research Symposium, Irvine, CA. (April 2016)

Poster Presentations:

- International Society of Stem Cell Research Annual Meeting, San Francisco, CA. (June 2016)
- Cedars-Sinai Medical Center Graduate Symposium, Los Angeles, CA. (September 2015)

TEACHING AND MENTORING EXPERIENCE

UCI Undergraduate Research Mentor for Justin Fabello, Tiffany Tsai, and Nowshin Tabassum

CIRM Bridges to Stem Cell Research (CSU Fullerton) thesis Mentor for Leanne Hildebrand, who was accepted to multiple PhD programs.

Teaching Assistant

- Advanced Immunology Lab (2 quarters)
- Experimental Microbiology Lab (2 quarters)
- Biochemistry (2 quarters)
- Molecular Biology (1 quarter)

SCIENCE COMMUNICATION / OUTREACH EXPERIENCE

- "Ask-A-Scientist" Night, Irvine Unified School District, Ongoing – Consulting Scientist
- The Baccalaureates, College Application Essay Consultants – Founder/Consultant
- GPS-Biomed Elevator Pitch Competition, October 2016- Finalist
- Brews & Brains, December 2016- Invited Scientific Speaker

LEADERSHIP EXPERIENCE

- Associated Graduate Students (AGS) -Co-Chair, Professional Development Committee
- Graduate Research in Progress Seminars- Student Organizer
- The Baccalaureates, College Application Essay Consultants- Founder/Consultant

ABSTRACT OF THE DISSERTATION

Development and Function of Hematopoietic Cells

By

Ankita Shukla

Doctor of Philosophy in Biological Sciences

University of California, Irvine, 2019

Professor Matthew Inlay, Chair

This work focuses on the development and function of hematopoietic cells. First, this work identifies a novel marker CD11a, which distinguishes various tissue resident macrophage populations from bone-marrow derived cells that may colonize a tissue during inflammation. In the context of Alzheimer's disease, it is determined that myeloid cells that cluster around amyloid plaques are actually brain resident microglia, not infiltrating peripheral macrophages. Using CD11a, a novel quantification technique is also described, which demonstrated microglia proliferation and increased T cells infiltration in the AD mice. Additionally, we outline how CD11a expression patterns in various tissue resident macrophage (trMac) populations may help determine the developmental relationships between these cells. We corroborate other studies that microglia in the brain and Langerhans cells in the skin come from erythro-myeloid progenitors that arise in the embryonic yolk sac (YS). Additionally, we also provide evidence that some hematopoietic stem cells also arise from the mesoderm in extra-embryonic tissue, such as the YS, placenta as well as the vitelline vessels. Using the HoxB6-CreER lineage tracing system, we demonstrate that YS hematopoiesis is critical not just for trMacs, but also for HSC development.

INTRODUCTION

Opening Statement

The work presented here has two main focuses: determining the role of specific hematopoietic cells in the context of Alzheimer's Disease (AD), and defining the origins of hematopoietic stem cells (HSCs). First, this work will focus on microglia, the tissue resident macrophages (trMacs) of the brain, and their role in AD. Specifically, this work will provide a novel way to distinguish trMacs from peripheral immune cells that may contribute to disease pathology using CD11a as a marker. This work also explores the origins of trMacs, which arise early during embryonic development, seed tissues all over the embryo body and, in some cases, are replenished through self-renewal independent of HSCs throughout adult life. Secondly, the developmental origins of HSCs will be explored. Because HSCs can give rise to all cells of the blood and immune system, they have the potential for curing blood disorders and cancers. Defining the milieu in which they originate can help mimic this process *in vitro* to generate induced pluripotent stem cell (iPSC)-derived HSCs.

Overview of Alzheimer's Disease

Alzheimer's Disease (AD) is the sixth leading cause of death in the United States. It currently affects 5.8 million Americans, which is supposed to rise to 14 million by the year 2050. AD and other dementias cost the nation close to $300 Billion each year (Alzheimer's Association, 2019). This devastating disease is characterized by progressive memory loss, cognitive function, and eventually loss of basic daily functions. These symptoms arise from two main hallmarks of AD pathology: the deposition of extracellular beta-amyloid (Aß) peptides as well as intraneuronal tangles of hyperphosphorylated tau protein (Alzheimer, 1907; Hardy & Selkoe, 2002; Stelzmann,

Norman Schnitzlein, & Reed Murtagh, 1995). While, Aß is effectively cleared in heathy brains, the peptides are mis-cleaved and form neurotoxic aggregate in the AD brain (Hardy & Selkoe, 2002; Lemere et al., 2003) In addition, AD is also associated with significant synaptic loss, which leads to a lot of cell death in the brain (**Figure A**), and causes the cognitive decline (Carter & Lippa, 2005; DeKosky & Scheff, 1990; Masliah et al., 2001).

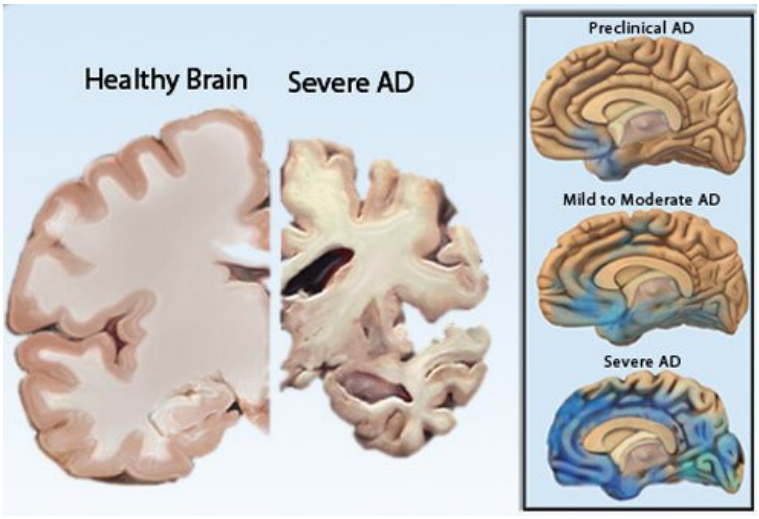

Figure A: Cell death in Alzheimer's Disease. Widespread cells death occurs and the brain shrinks dramatically in AD compared to a healthy brain. As disease progresses, cell death affects all regions of the brain, though the cortex is most severely affected in AD. *Image adapted from Alzheimer's Association.*

Currently, there are only five FDA-approved drugs which treat cognitive symptoms and mostly for mild to moderate stage AD (Alzheimer's Association 2019; Russ & Morling, 2012; Schneider, 2012). However, these drugs only mitigate symptoms and do not treat the disease-causing pathology or delay the progression of the disease (Ahmed et al., 2016; Canter et al., 2016; Schneider, 2012). Many drugs currently in development aim to do just this. Future drug targets include the parent amyloid precursor protein (APP), and the two enzymes responsible for mis-cleaving it in AD, beta- and gamma- secretases (Selkoe & Podlisny, 2002). Other drugs aim to target tau protein, which helps maintain the structure of neurons by associating with microtubules

(Citron, 2010; De Calignon et al., 2012; Kosik et al., 1986). However, clinical trials face challenges in understanding the disease, in addition to accurate and timely diagnosis and recruiting stage-appropriate participants.

Role of hematopoietic cells in AD

In recent years, tremendous efforts have been made to understand the role of the immune system in AD. The immune system consists of hematopoietic cells of myeloid and lymphoid lineages. The focus on neuroinflammation was prompted in part by the genome-wide association studies (GWAS) that implicated disease-related polymorphisms in genes related to the myeloid cells (Bradshaw et al., 2013; Griciuc et al., 2013; Guerreiro et al., 2012; Heneka et al., 2015; Siddiqui et al., 2017; Wang et al., 2016). The primary myeloid cell in the brain are the tissue-resident macrophages (trMacs), called microglia. Therefore, microglial ontogeny and function in health and disease have been studied extensively. Microglia, like other trMacs are derived from early precursors that originate in the yolk sac, which will be discussed later in this chapter as well as in Chapter 2. In the adult brain, microglia are maintained through local proliferation (Ajami et al., 2007; Elmore et al., 2014; Ginhoux et al., 2013; Mildner et al., 2007). In a healthy brain, microglia perform the role of immune surveillance and phagocytosis. In addition, they have recently shown to be critical for synaptic pruning, which is critical for neurogenesis (Hong et al., 2016; Nimmerjahn et al., 2005; Sierra et al., 2010; Stephan et al., 2012). In neuroinflammation, microglia become activated and alter their ramified morphology as well as surface marker expression and function. Activated microglia become more ameboid in shape, like other macrophages (Grete et al., 2015; Nimmerjahn et al., 2005). Additionally, activated microglia also

secrete many cytokines that may recruit peripheral macrophages from the blood (D'Mello et al., 2009; von Bernhardi et al., 2015).

Blood-Brain- Is it a Barrier or a Wall?

The brain was initially considered an "immune privileged" organ (Abbott et al., 2010; Schwartz & Kipnis, 2011); however the "leakiness" of the blood brain barrier (BBB) in AD has been more carefully studied in recent years. The BBB consists of endothelial cells which are supported by pericytes and astrocytes. The support cells are critical for functional barrier properties of the BBB (Daneman, 2012; Zenaro et al., 2017; Zhao et al., 2015). The barrier properties include tightly regulated transport of limited nutrients and metabolic waste in and out of the brain (Winkler et al., 2015; Winkler et al., 2011). While this exact property hinders therapeutics from entering the brain, barrier dysfunction may also be partially responsible for defect in Aß clearance in AD (Lemere et al., 2003; Winkler et al., 2015; Zhao et al., 2015). Another crucial function of the BBB is to prohibit pathogens as well as peripheral blood cells from entering the congested brain parenchyma. During neuroinflammation, barrier properties may be altered allowing peripheral immune cell infiltration into the brain parenchyma (Galea et al., 2007; Greter et al., 2005; Ransohoff, Kivisäkk, & Kidd, 2003; Shechter et al., 2013). If peripheral immune cells from the blood were to enter the limited and already crowded space of the CNS, does this infiltration exacerbate or ameliorate AD pathology?

In human AD and mouse models, myeloid cells have been observed to cluster around Aß plaques (Haga et al., 1989; Jay et al., 2015). However, whether these plaque-associated myeloid (PAM) cells are brain-resident microglia or peripheral monocytes-derived macrophages would depend on the permeability of the BBB in AD. This remains highly contested. GWAS implicated

two main AD risk genes, APOE and CD2AP, which are both important for the integrity of BBB (Lambert et al., 2013; Zhao et al., 2015; Zlokovic, 2013). However, other studies contest the leakiness of the BBB in human and mouse models of AD (Bien-Ly et al., 2015). However, infiltration of peripheral cells also relies on cytokines secreted by CNS cells that help recruit them into the parenchyma (D'Mello et al., 2009; Wang et al., 2016). These chemo-attractants are upregulated in AD brains (Cazareth et al., 2014; Goldeck et al., 2013; Moynagh, 2005; Tripathy et al., 2007). Thus, deciphering whether PAMs are microglia or peripheral macrophages relies on marker expression and morphology. To accurately define the role of immune cells in the AD, it is critical to unequivocally identify them. This will be the focus of Chapter 1.

CD11a

This work focuses on CD11a as a stable marker to distinguish infiltrating hematopoietic cells from the brain-resident microglia in the various neuroinflammatory contexts. CD11a (integrin αL; *Itgal*) and CD18 (integrin ß2) heterodimerize to form the Leukocyte Function Associated Complex 1 (LFA1). However, CD18 can form heterodimers with CD11b (to form Mac1or LFA2) as well as CD11c (to form LFA3). Thus, LFA1 is defined by the α subunit CD11a. LFA1 is an adhesion molecule which is expressed on the surface of all leukocytes (Hynes, 1987; Kishimoto et al., 1989). LFA1 interacts with ligands with extracellular matrix proteins and cell adhesion molecules, such as ICAM1 (Hynes, 2002). LFA1 is crucial for immunological synapse formation, migration of leukocytes as well as activation of lymphocytes (Larson & Springer, 1990; Shaw et al., 2004). Integrins, including LFA1, unfold upon activation. This conformation change from the folded position is required for migrating leukocytes in the blood stream to begin the process of rolling adhesion (Abram & Lowell, 2009; Lum et al., 2002). This adhesion to its ligand ICAM1,

allows neutrophils to extravasate into tissues (Abram & Lowell, 2009; Lum et al., 2002; Salas et al., 2006). Thus, CD11a is important for leukocyte extravasation into tissues during inflammation.

Certain chemokines and cytokines can also induce expression of and activation of the LFA1 integrin. Signaling cascades induced by the binding of selectins to their ligands have also been found to initiate the cell-intrinsic changes in LFA1 conformation to an active form. This "inside-out" signaling is thought to increase binding of LFA1 and ICAM1 (Abram & Lowell, 2009). LFA1-ICAM1 interaction is also important for the formation of immunological synapses between antigen-presenting cells and lymphocytes (Grakoui et al., 1999; Green et al., 2006; López-Rouríguez et al., 1995; Luo, Carman, & Springer, 2007; Semmrich et al., 2005). Indeed, multiple studies have demonstrated inadequate immune responses in CD11a knockout mice (Ghosh et al., 2014; Schmits et al., 1996). Thus, LFA1, and therefore CD11a, has also implications in antigen presentation. Given its widespread expression on almost all effector cells, as well as relevant immunological functions, in Chapter 1, we will explore whether CD11a can be used as a marker for peripheral cells and distinguish them from brain resident microglia.

Embryonic Origins of Adult Hematopoietic Cells

Questions related to the unique identity and function of tissue resident macrophages (trMacs) compared to their bone marrow-derived cousins is not limited to the CNS. Thus, CD11a expression on other trMacs, besides microglia, will be explored in Chapter 2. All macrophages share surveillance capabilities, which they use to respond to tissue-specific functions (A-Gonzalez et al., 2017; Godwin et al., 2013; Hoeffel & Ginhoux, 2018; Lavin et al., 2015; McGrath et al., 2015; Squarzoni et al., 2014; Thion et al., 2015). Additionally, as long-lived cells trMacs are more elastic responders to tissue-specific cues through epigenetic modifications (Álvarez-Errico et al.,

2015; Amit et al., 2016; Lavin et al., 2014). Thus, like microglia, all trMacs are promising targets for autoimmune diseases, neurodegenerative disorders as well as cancers. For a fuller understanding of trMac function, studies have relied on first understanding the mechanisms involved in their development. Important breakthrough in the field happened when studies reported that microglia, trMacs of the brain, and Langerhans Cells, trMacs of the skin, were resistant to high doses of irradiation, unlike all bone marrow derived cells (Ajami et al., 2007; Merad et al., 2002). This indicated that trMacs, at least in part, were derived from embryonic hematopoietic precursors.

The process of trMac development is as dynamic as the plurality of the functions that their embryonic precursors serve. Hematopoietic cells in the developing embryo have two main functions: to oxygenate developing tissues through differentiated red blood cells, and to establish the hematopoietic stem cell compartment. Thus, embryo hematopoiesis can be divided into two "waves": the primitive wave and the definitive wave (**Figure B)**. In mice, the primitive wave begins in the extra-embryonic mesoderm (EEM) of the yolk sac (YS) at embryonic day (e) 7.5. These cells consist mainly of nucleated erythrocytes, as well as early bipotent progenitors capable of producing erythroid cells and YS macrophages, known as erythro-myeloid progenitors (EMPs). These cells remain in the YS by forming blood islands with sparse endothelial cells away from the developing embryo (Ferkowicz & Yoder, 2005; Lux et al., 2008; Moore & Metcalf, 1970; J Palis, 2001; J Palis et al., 1999; James Palis, 2014). Until the establishment of blood circulation around e8.5-9.0, blood cells are only found in the YS. These cells begin to migrate throughout the embryo at the onset of circulation, including in the brain (Alliot et al., 1999; Alliot et al., 2006). Several fate mapping studies have shown microglia are derived from these early YS EMPs (Ginhoux et al., 2010b; Kierdorf et al., 2013b). Using fate mapping systems, strong evidence also

suggested the presence of hemogenic endothelial cells (HECs) that gave rise to these EMPs at e7.5 but not after E9.5 in the YS (Goldmann et al., 2016; Gomez Perdiguero et al., 2015a).

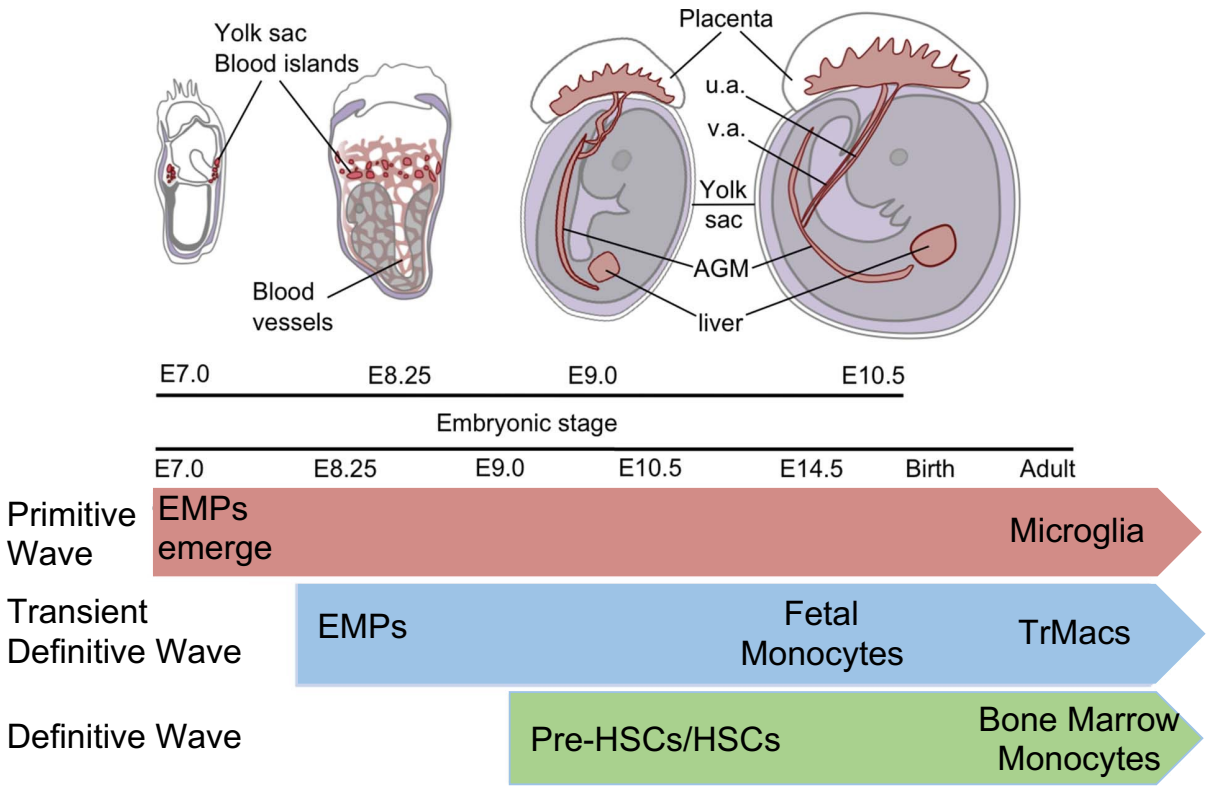

Figure B: Waves of hematopoietic cell development. The first blood cells appear in the yolk sac at e7.0 and consist mostly of nucleated "primitive" red blood cells along with early EMPs that give rise to YS macrophages, which seed the brain and give rise to microglia. The definitive wave begins at the onset of circulation around e8.5-9.0. Mature EMPS are found throughout the embryo at this time which can give rise to erythroid and myeloid cells and form the basis of tissue resident macrophages. Fetal monocytes that emerge at e12.5 replace some of these YS derived EMPs and give rise to adult tissue resident macrophages. HSCs and their precursors cells first emerge independently and well after EMPs have seeded different tissues. PreHSCs seed the fetal liver around e11.0 and give rise to mature, long-term and transplantable HSCs, which eventually seed the bone marrow after the mouse is born. *Image adapted from Hoeffel & Ginhoux, 2018.*

While primitive YS macrophages continue to colonize the whole embryo till e13.5, in adult mice, only microglia retained labeling in Runx1-CreEr model, suggesting that replacement of early macrophages in other tissues (Ginhoux et al., 2010; Hoeffel et al., 2012, Hoeffel et al., 2015).

Mature EMPS that rely on c-Myb activity emerge around e8.5-9.0 simultaneously with the establishment of circulation. These EMPs are capable of producing definitive, enucleated RBCs, megakaryocyte and myeloid progenitors, which produce macrophages through a monocyte precursor (McGrath et al., 2015; James Palis, 2016; Tober et al., 2007). However, the developmental relationship between the early and mature EMPs is unclear. In any case, these EMPs develop prior to and continue to flourish independent of HSC development (**Figure B).** Definitive hematopoiesis is initiated within the developing blood vessels of the YS at e8.5 placenta as well as within the embryo proper at e10.5 (Bertrand et al., 2010; Boisset et al., 2010; Hoeffel & Ginhoux, 2018; Kissa & Herbomel, 2010; Mikkola, Gekas et al., 2005).This is also when mature EMPs, defined as Ckit+, CD41+, and $FC_{\gamma}R$+, arise that give rise to most myeloid and mature erythroid cells (McGrath et al., 2015; Naito et al., 1990). While these EMPs are transient, they see various tissues and give rise to most trMac population in the adult (Gomez Perdiguero et al., 2015a). Namely, EMPs give rise to microglia in the brain, Langerhans cells in the epidermis, Kupffer cells in the liver, as well as lung Alveolar macrophages etc.

In recent years, another population of fetal myeloid cells was discovered that is thought to replace most YS EMPs, and in turn give rise to trMacs, except in the brain. At e12.5, fetal monocytes begin to develop in the fetal liver (Hoeffel et al., 2012, 2015; Hoeffel & Ginhoux, 2018b). These FL monocytes colonize every tissue by e13.5. Indeed, lineage tracing studies found evidence that myeloid precursors are replace by the FL monocytes after e14.5 in skin, as well lunch trMac populations (Ginhoux & Merad, 2010; Guilliams et al., 2013; Guillaume Hoeffel & Ginhoux, 2018a; Guillaume Hoeffel et al., 2012; Sheng, Ruedl, & Karjalainen, 2015). Another lineage tracing study show that all tissue resident macrophage populations are labeled after e14.5 in a fetal liver monocytes-specific system, and concluded that most trMacs are derived from these

monocytes that replace prior YS macrophages that may have seeded the tissues (Guillaume Hoeffel et al., 2015). The exact developmental relationship between this between the early and late myeloid progenitors still need to be explored.

Where do HSCs come from?

Concurrent with EMP development, the HSC compartment also begins to form at various sites in the developing embryos. *Bona fide* HSCs have three hallmark characteristics: longetivity, multipotency and engraftability. These stem cells last throughout the lifetime, are able to give rise to blood cells of all lineages and are able home to the bone marrow niche upon transplantation (see **Figure C**). Multipotent hematopoietic progenitors have been observed to emerge from HEC in murine embryos starting at e9.5 (Batsivari et al., 2017; Gekas et al., 2005; Inlay et al., 2014; Rhodes et al., 2008; Swiers et al., 2010). These are thought to be the putative precursors to HSCs, or Pre-HSCs. These pre-HSCs are capable of producing all mature blood lineages, but can only engraft in newborn recipients, or need to be matured first *ex vivo* (Taoudi et al., 2008; M. C. Yoder, Hiatt, & Mukherjee, 2002; M. Yoder & Hiatt, 1997a; Yoder et al., 1997b). Though Pre-HSCs number peak at e11.5, they are still considered a rare population (Inlay et al., 2014; F. Zhou et al., 2016). Studies have shown that the first transplantable, a.k.a "repopulating units" or HSCs, appear in the YS, placenta, the dorsal aorta of the Aorta-Gonad-Mesonephros (AGM) region as well as vitelline and umbilical vessels at e10.5 (Bertrand et al., 2004; de Bruijn & Speck, 2000; Gekas et al., 2005; Kumaravelu et al., 2002; Müller et al., 1994). After e11.5, all of hematopoiesis takes place in the FL until the bone marrow niche is established (Müller et al., 1994). Thus far, numerous studies established development of HSCs takes place in multiple waves as well as signals required for it. There is, however, a lot of debate about the birth place of HSCs.

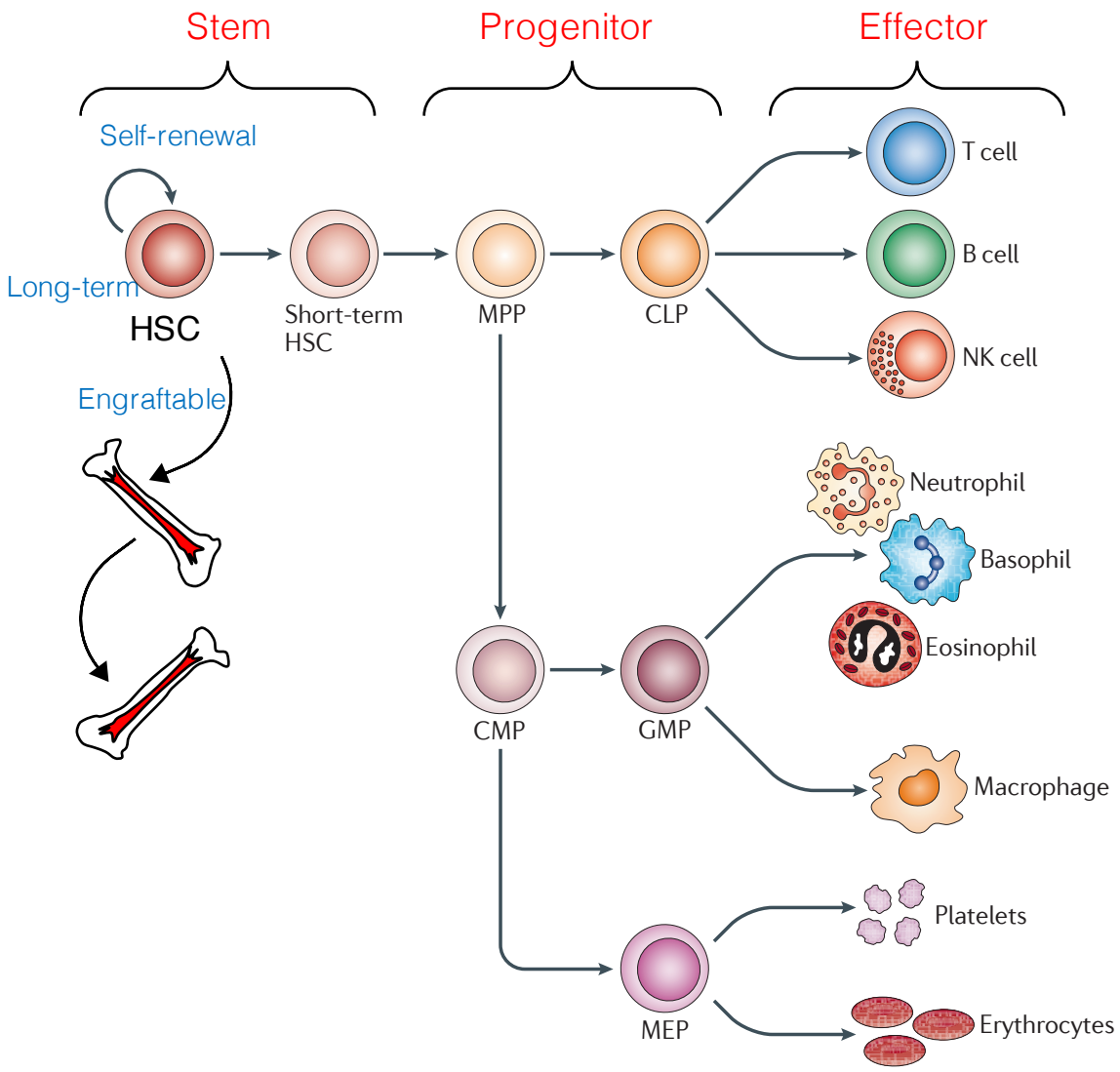

Figure C: The hematopoietic tree. Long-term HSCs give rise to all the cells of our immune system. HSCs are able to long-lived due to their ability self-renew. They are capable of homing to their niche in the bone marrow. HSCs themselves are quiescent, but other downstream multipotent progenitors (MPPs), which are not as self-renewing, are able to give rise to lineage-committed myeloid (CMP) and lymphoid (CLP) progenitors. These two make up the two main branches of mature hematopoietic cells. The myeloid lineage can be further broken down into granulocyte/macrophages progenitors (GMPs) and megakaryocyte/erythrocyte progenitors (MEPs). Mature hematopoietic cells are the effectors cells of the immune system and cannot self-renew, engraft, or give rise to any other cell types. *Image adapted from King & Goodell, 2011.*

As a result of all the contention, two models of hematopoiesis have emerged. A fundamental question that still plagues the field is whether HSCs, and all hematopoietic cells, come from the early precursors that appear in the YS blood islands (Moore & Metcalf, 1970), or if they arise in independent events from non-hematopoietic precursors, such as the hemogenic endothelial cells (Antas et al., 2013; Nishikawa et al., 1998). These models are referred to as the "Single Origin Model" and the "Multiple Origin Model," respectively. A large body of evidence from Elaine Dzierzak's research group and others supports the notion of endothelial-to-hematopoietic transition (Ciau-Uitz et al., 2014; Cumano et al., 1996; Cumano et al., 2001; Ditadi et al., 2015; Koh et al., 2015; Medvinsky & Dzierzak, 1996; Nguyen et al., 2014). Time lapse imaging studies also showed evidence of hematopoietic cells, which expressed markers for progenitors such as Ckit and Sca1, budding off the dorsal aorta and entering circulation (Boisset 2010). Thus, it is now well accepted that hematopoietic cells come from an endothelial precursor, but the whether these specialized endothelial cells exist beyond the walls of the dorsal aorta remains highly controversial. Thus, Chapter 3 will explore the contribution of the mesoderm that exists outside the embryo proper, namely in the YS, placenta and vitelline vessels, to the pool of adult, multipotent and engraftable HSCs.

Closing Statement

The studies presented here, establish CD11a as a novel marker for peripheral hematopoietic cells also provide an efficient and reliable way to distinguish trMacs brain from peripheral monocyte-derived macrophages. CD11a was used to determine that the plaque-associated myeloid cells in the AD brains are microglia and not peripheral myeloid cells. Moreover, the studies also show that it is actually lymphoid cells, specifically T lymphocytes, that are significantly increased in these AD murine brains. Moreover, our studies explored and confirmed the expression of CD11a

on other trMacs, like Langerhans Cells in the skin and postulated that the difference in CD11a expression compared to peripheral myeloid cells is linked to their HSC-independent ontogeny. Additionally, our studies on HSC development provide novel evidence that at least some HSCs are derived from the EEM, favoring the multiple origin model of HSCs. Though they do not diminish the contribution of the DA in giving rise to pre-HSCs, our work suggests that the YS and PL deserve further study to determine the molecular mechanisms that help pre-HSCs arise there. The YS, especially, would be much easier to study via imaging of cultured embryos. Additionally, our lineage tracing studies confirm previous findings that the pathway for trMacs development is independent from that of pre-HSCs and HSCs. Interestingly, trMacs are also not HoxB6 derived. Together, this work has identified the contributions of extra-embryonic tissues during HSC development and delineated the function of brain-resident versus peripheral hematopoietic cells in the context of Alzheimer's Disease.

CHAPTER 1: CD11A EXPRESSION DISTINGUISHES INFILTRATING MYELOID CELLS FROM PLAQUE-ASSOCIATED MICROGLIA IN ALZHEIMER'S DISEASE.

INTRODUCTION

Microglia are the resident immune cells of the central nervous system (CNS). They play critical roles in synapse formation (Parkhurst et al., 2013), maintaining the neuronal network by synaptic pruning (Paolicelli et al., 2011; Schafer et al., 2012; Stephan et al., 2012; Stevens et al., 2007)as well as immune surveillance (Nimmerjahn et al., 2005). Microglia also clear apoptotic cells, myelin or synaptic debris through phagocytosis (Sierra et al., 2010). As the resident immune cells of the CNS, understanding microglial involvement in neuroinflammatory contexts, such as Alzheimer's Disease (AD), is critical for understanding pathology and for targeting these cells for therapy. During many neuroinflammatory conditions, microglia become activated and the brain parenchyma can be infiltrated by peripheral immune cells. Indeed, single-cell studies have recently confirmed the presence of distinct bone marrow-derived immune cell types within compartments of the CNS in mouse models of AD (Mrdjen et al., 2018). The presence of these intruding cells further mystifies the exact role of infiltrating versus brain-resident immune cells in inflammation and neurodegeneration observed in AD.

The biggest hallmark of AD neuropathology is the deposition of insoluble beta amyloid (Aß) plaques throughout the brain. Aß plaques are frequently surrounded by myeloid immune cells, defined primarily by their expression of classical myeloid markers, including Iba1, CD11b, and CD45. However, these markers are not unique to microglia and any infiltrating peripheral monocytes and their macrophage progeny also express these markers (F. C. Bennett et al., 2018), complicating the ability to determine the origin(s) of plaque-associated cells. The significance of these plaques-associated myeloid (PAM) cells in plaque pathology is unclear, including whether

this clustering is a cause or an effect of plaque formation. Furthermore, it is currently unknown whether PAM cells are brain-resident microglia or peripheral monocyte-derived macrophages that have infiltrated the brain parenchyma. The difficulty in distinguishing between these two populations has limited our understanding of each of their roles in neuroinflammation, thus underscoring a need for new strategies to discern them.

In a healthy brain, microglia and macrophages are easily distinguished through microscopy by their ramified and amoeboid morphology, respectively. Alternatively, these cells can also be differentiated by flow cytometry using relative expression of cell surface markers, such as CD45. Microglia were classically defined as CD11b+, $CD45^{lo}$ and infiltrating monocytes and macrophages as CD11b+, $CD45^{hi}$ (Sedgwick et al., 2006). Other proposed 'microglia-specific' markers include Tmem119, Sall1, P2ry12 and Siglec-H, were also recently identified (F. C. Bennett et al., 2018; M. L. Bennett et al., 2016; Buttgereit et al., 2016; Haynes et al., 2006; Konishi et al., 2017). While these markers are useful in healthy brains, during neuroinflammation, such as in AD, activated microglia and peripheral macrophages alter their respective morphology and marker expression patterns, confounding their distinction. Upon activation, microglia retract their processes and adopt a more macrophage-like, rounded morphology. Activated microglia also upregulate CD45 levels, making the conventional $CD45^{lo}/CD45^{hi}$ strategy inadequate in distinguishing microglia through flow cytometry. Additionally, homeostatic microglial genes like *Tmem119* and *P2ry12* are downregulated and other markers such as *Trem2* and *Apoe* are upregulated by microglia in an inflammatory milieu (Butovsky et al., 2014; Keren-Shaul et al., 2017a).

To overcome the limitations of these markers, lineage tracing mouse models have been generated using the microglial expression of the fractalkine receptor, *Cx3cr1* (S. Jung et al., 2002).

One study crossbred the *Cx3cr1*$^{GFP/GFP}$ mice with the 5xFAD mouse model of AD and found that dying GFP positive cells contributed to Aß plaque growth by releasing previously phagocytosed Aß into the extracellular space (Baik et al., 2016). However, macrophages can also express *Cx3cr1,* thus the contribution of peripheral monocyte-derived macrophages cannot be ruled out. These questions can potentially be addressed using the inducible reporter *Cx3cr1-CreER*^{T2} (Parkhurst et al., 2013; Yona et al., 2013). While long-lived microglia will retain induced labeling after tamoxifen pulse, the short-live infiltrating macrophages will eventually be replaced by unmarked macrophages derived from unlabeled bone marrow monocytes. Thus, this labeling system can allow the distinction between these two populations in the brain. However, these genetic reporters may prove impractical or expensive in certain experimental setups, particularly when disease models are also employed, which require complex breeding.

Another strategy to genetically distinguish brain-resident microglia from peripheral bone marrow derived cells is to use bone marrow chimeras. Mice transplanted with hematopoietic stem cells (HSCs) post-irradiation can replenish all peripheral immune cell types, but not microglia (Mildner et al., 2007). Thus, transplanting HSCs from genetically distinct (e.g. GFP+) donor bone marrow can readily distinguish the peripheral immune cells from host microglia. This was performed in an AD model and revealed that the PAM cells contained peripheral macrophages (Simard et al., 2006). However, a major caveat of this approach is that robust donor HSC engraftment requires the elimination of the host blood system by high doses of irradiation, upwards of 10 Gy (or 1000 Rads). This can have long term effects on the brain environment, by activating microglia, modifying pathology and disrupting the blood brain barrier (BBB; Menzel et al., 2018). Moreover, a follow-up study from the same group and others showed that shielding the head during irradiation to reduce BBB disruption, or use of parabiosis resulted in little to no contribution of

bone marrow-derived cells to the PAM population, despite robust bone marrow engraftment and donor peripheral immune cell reconstitution (Lampron et al., 2012; Mildner et al., 2007; Wang et al., 2016). The limitations of these strategies highlight the need for antibodies against surface markers that reliably distinguish microglia from peripheral macrophages in healthy and inflamed brains, circumventing the need for bone marrow chimeras.

Here we discuss and characterize a candidate peripheral immune cell-specific marker, CD11a (*Itgal*). CD11a, along with CD18, forms the leukocyte function-associated antigen 1 (LFA1) integrin. LFA1, and thus CD11a, is expressed on all peripheral immune cells, except red blood cells and platelets (Fathman et al., 2014). LFA1 is important for immunological synapse formation as well as extravasation into tissues during infection or injury (Green et al., 2006; Lum et al., 2002; Monks et al., 1998). As microglia are brain-resident and not in circulation, we hypothesized that LFA1 would not be expressed on microglia. In support of this, a recent single-cell mapping study identified CD11a as a marker that is expressed only on immune cells in the periphery and not in microglia (Mrdjen et al., 2018). Another study also utilized CD11a, along with CD49d, to distinguish tumor-associated microglia from bone marrow-derived macrophages using flow cytometry (Bowman et al., 2016). While both of these studies suggest that CD11a is only expressed in peripheral immune cells through RNA-sequencing, we demonstrate its utility as a surface marker to distinguish microglia from peripheral immune cells through flow cytometry as well as immunofluorescence.

As many seemingly reliable markers alter their expression during inflammation (e.g. CD45, P2ry12, Tmem119), it is critical to carefully evaluate the expression patterns of any new markers in a variety of neuroinflammatory contexts. Here we show the utility of CD11a in flow cytometry to mark infiltrating peripheral cells and distinguish them from microglia in steady state,

in LPS-induced neuroinflammation, and in two different mouse models of Alzheimer's Disease. In these cases, CD11a remains highly expressed on peripheral, infiltrating immune cells and remains unexpressed in microglia. As a result, CD11a allows reliable bifurcation of microglia, which are CD11a negative, and infiltrating monocytes, which are CD11a positive, by flow cytometry and fluorescence immunohistochemistry. Additionally, our immunohistochemistry data shows that PAM cells are CD11a negative and that infiltrating myeloid cells are rare in AD brains and do not cluster around Aß plaques, implicating the PAM cells as microglia. Lastly, we also present a novel flow cytometry-based spiking method to accurately quantify changes in infiltrating immune cells in aged WT and AD mice. We provide evidence of a statistically-significant increase in microglia numbers and infiltrating T cells in female AD mice compared to their WT littermates. Taken together, our data provides new insights into the infiltration of peripheral immune cells into the brains of AD mice using CD11a.

RESULTS

CD11a is expressed on peripheral immune cells in the brain, but not on microglia

A microarray database screen of markers that are differentially expressed in peripheral immune cells and brain-resident microglia cells revealed that integrin alpha L chain, *Itgal* or *CD11a*, was not expressed in microglia, but highly expressed in all circulating immune cell types (**Figure 1.1A**). Therefore, we sought to confirm cell surface expression of CD11a in these cells via flow cytometry (**Figure 1.1B**). Cells from adult B6 mouse brains were harvested and stained for surface marker expression. In the CD11b+, $CD45^{lo}$ microglia population, we did not detect CD11a surface expression when compared to the Fluorescence Minus One (FMO) negative control.

Figure 1.1

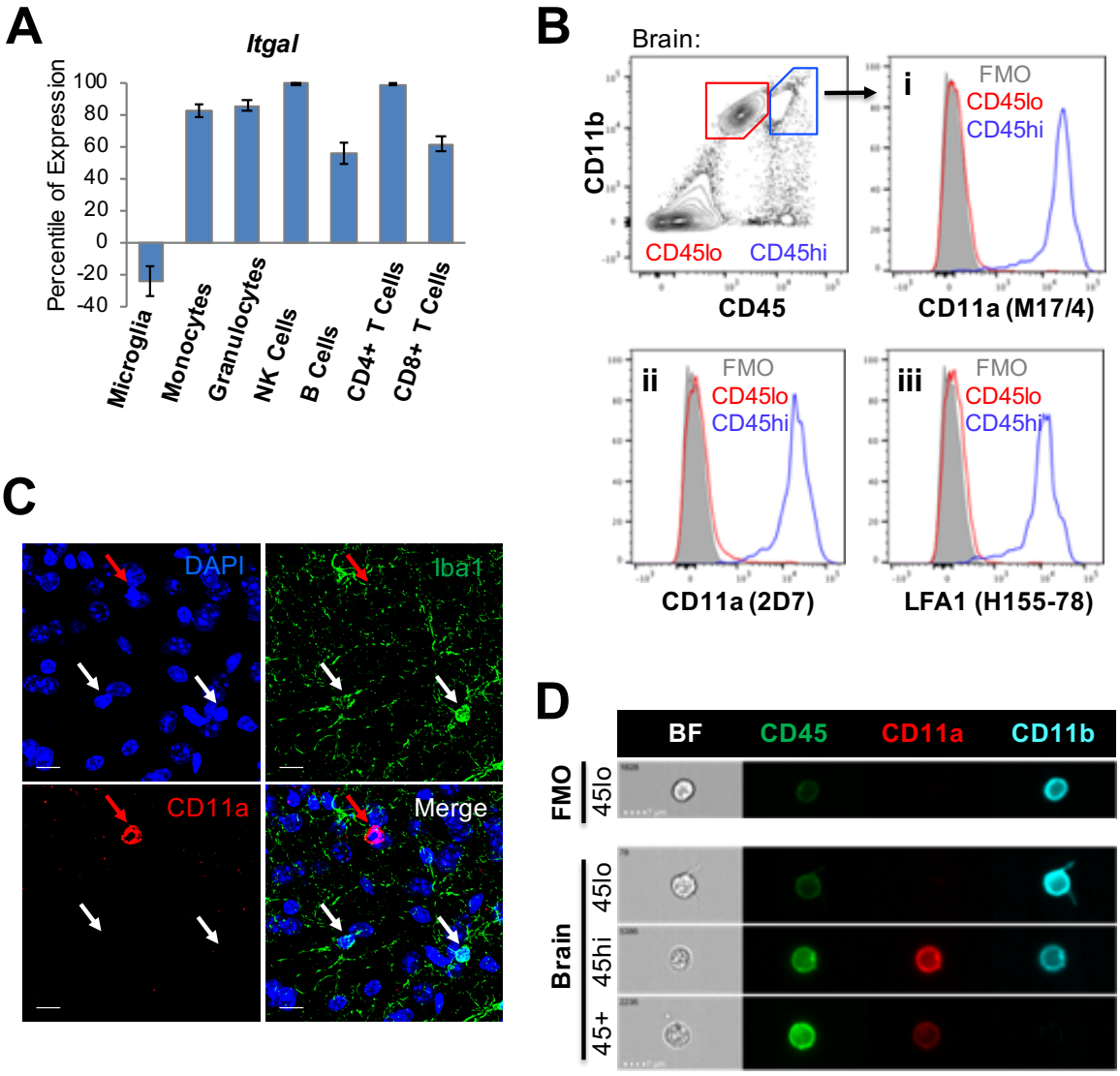
A
Itgal
Percentile of Expression
100
80
60
40
20
0
-20
-40
Microglia
Monocytes
Granulocytes
NK Cells
B Cells
CD4+ T Cells
CD8+ T Cells
B
Brain:
CD11b
CD45lo
CD45hi
CD45
i
FMO
CD45lo
CD45hi
CD11a (M17/4)
ii
FMO
CD45lo
CD45hi
CD11a (2D7)
iii
FMO
CD45lo
CD45hi
LFA1 (H155-78)
C
DAPI
Iba1
CD11a
Merge
D
BF
CD45
CD11a
CD11b
FMO
45lo
Brain
45lo
45hi
45+

Figure 1.1: CD11a is not expressed in steady-state microglia. (A) Gene expression profile of Itgal (CD11a) in microglia and peripheral hematopoietic cells. Percentile of expression is based on comparison to a reference panel of nearly 12,000 microarrays (www.gexc.riken.jp). Values below zero are considered unexpressed. (B) Flow cytometry plots of adult mouse brain cells. CD11b+ $CD45^{lo}$ microglia ("$CD45^{lo}$", red gate) and CD11b+ $CD45^{hi}$ macrophages ("CD45hi", blue gate) were analyzed for cell surface expression of CD11a using antibody clones M17/4 (i), 2D7 (ii) against CD11a, and H155-78 (iii) against LFA-1 (CD11a/CD18). Histograms show $CD45^{lo}$ microglia (red), $CD45^{hi}$ macrophages (blue), and fluorescence minus one control ("FMO", grey). (C) Immunofluorescence image of C57/B6 brain. White arrows denote representative microglia which are Iba1+ but CD11a-. The red arrow denotes an example of a CD11a+ immune cell, which is Iba1-. Images were taken at 120X, scale bars = 10μm. (D) Imaging flow cytometry of brain cells. Representative images of cells within CD11b+ CD45lo microglia ("45lo"), CD11b+ $CD45^{hi}$ macrophages ("45hi") and CD11b- CD45+ lymphocytes (45+) populations in each channel (see Figure S1C for splenocyte controls). Exact same voltage correction settings were applied to all samples

Conversely, CD11a was highly and uniformly expressed in the CD11b+, $CD45^{hi}$ population which contains primarily monocyte-derived macrophages. The CD11b- $CD45^{hi}$ population, which contains mainly lymphocytes, was also uniformly CD11a+ (data not shown). We found identical expression patterns using three distinct clones of antibodies that recognize CD11a. These include the M17/4 and 2D7 clones of the CD11a antibody, along with clone H155-78 that recognizes LFA-1, the complex of CD11a with CD18 (**Figure 1.1B, i - iii**). To test the expression of CD11a on peripheral immune cells, CD45+ splenocytes were also stained with the same antibody cocktail as the brain cells. Splenocytes of myeloid and lymphoid lineages express all three clones of CD11a at high levels (**Figure 1.2A**).

Immunofluorescence analysis of CD11a expression in fixed brain tissue was difficult to assess using all clones and required tyramide signal amplification in order to detect CD11a+ cells. After amplification, Iba1+ microglia cells in adult B6 brain did not express CD11a, but we observed rare round CD11a+ cells that are likely infiltrating lymphocytes, based on a lack of Iba1 staining (**Figure 1.1C)**. To visualize the differential expression of CD45 and CD11a in microglia (CD11b+ $CD45^{lo}$), macrophages (CD11b+ $CD45^{hi}$) and lymphoid cells (CD11b- CD45+), brain and spleen samples were also stained and analyzed on an imaging flow cytometer to obtain high resolution images of single cells. Consistent with our observations by FACS, CD11a was not detected on the surface of microglia, but readily expressed on monocytes and lymphocytes in the brain and spleen (**Figure 1.1D, 1.2B-C).**

The fractalkine receptor *Cx3cr1*, is strongly expressed by microglia in the CNS and has been crucial in studying microglia development and functions in homeostatic and neuroinflammatory conditions (Cardona et al., 2006; S. Jung et al., 2002; Mizutani et al., 2011).

Figure 1.2

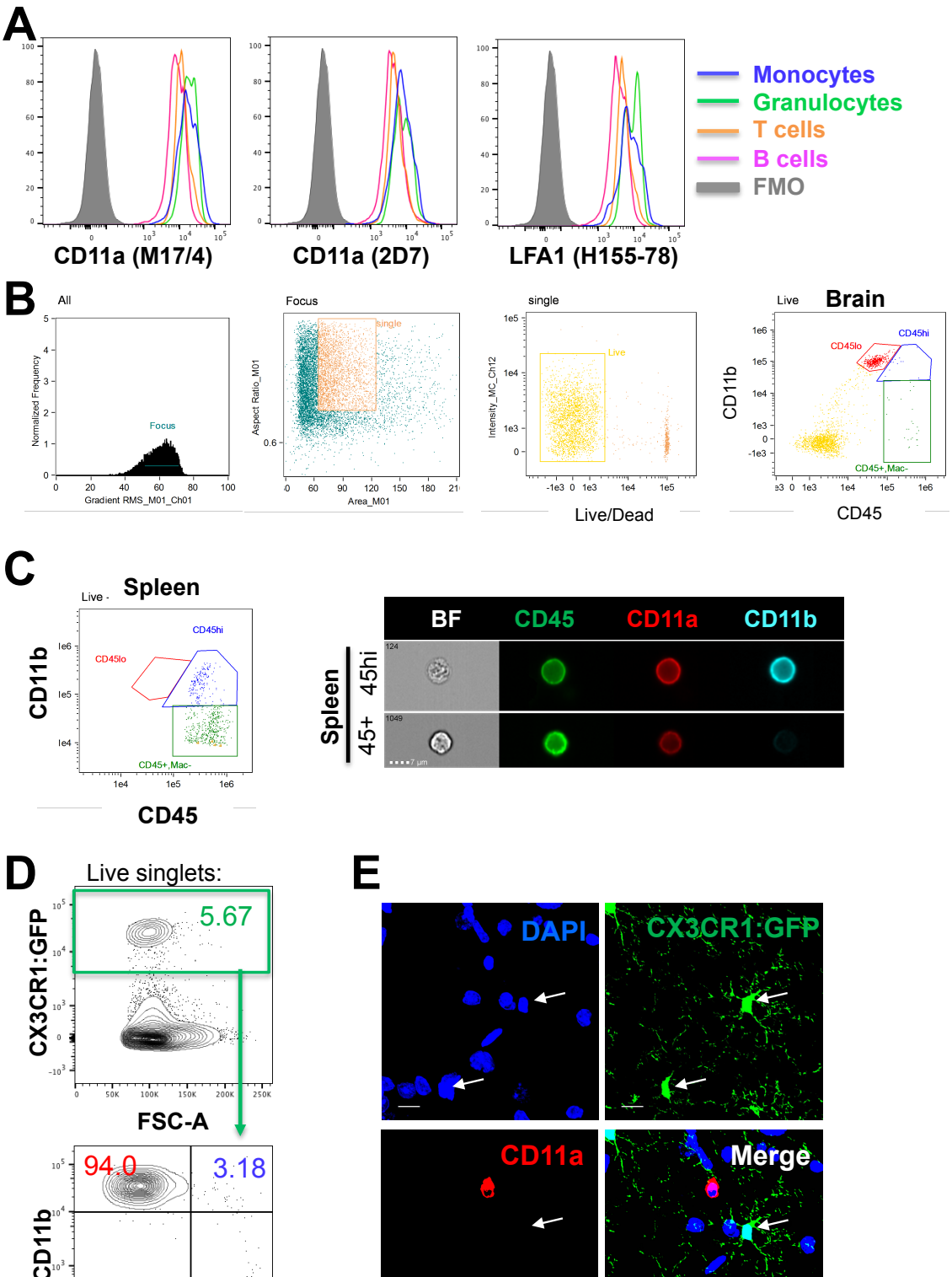
A
CD11a (M17/4)
CD11a (2D7)
LFA1 (H155-78)
Monocytes
Granulocytes
T cells
B cells
FMO
B
All
Focus
Gradient RMS_M01_Ch01
Normalized Frequency
single
Aspect Ratio_M01
Area_M01
Live
Intensity_MC_Ch12
Live/Dead
Brain
CD45lo
CD45hi
CD45+,Mac-
CD11b
CD45
C
Spleen
Live
CD45hi
CD45lo
CD45+,Mac-
CD11b
CD45
BF
CD45
CD11a
CD11b
Spleen
45hi
45+
D
Live singlets:
5.67
CX3CR1:GFP
FSC-A
94.0
3.18
1.24
1.59
CD11b
CD11a
E
DAPI
CX3CR1:GFP
CD11a
Merge

Figure 1.2: **Peripheral cells express high levels of CD11a compared to microglia.** (**A**) FACS analysis of CD45+ splenocytes. CD11b+ Gr1-monocytes (blue), CD11b+ Gr1+ granulocytes (green), CD11b- CD3+ T lymphocytes (orange), and CD11b- CD19+ B lymphocytes (magenta) express all three clones of CD11a compared to the FMO control (grey histogram). (**B**) Imaging flow cytometry dot plots and gating strategy of "CD45lo" microglia (red), "CD45hi" macrophages (blue) and "CD45+" lymphocyte populations in the brain corresponding to images in Figure 1D. (**C**) Imaging flow cytometry dot plots and corresponding images of peripheral immune cells in the spleen. Note: Voltages between brain (**B**) and spleen (**C**) samples are the same, but the scaling for the spleen plot was altered for improved visualization. (**D**) Representative flow cytometry plot of CD11a in *Cx3cr1-GFP*/+ brains. Most of the GFP+ microglia cells are CD11a negative (lower plot). (**E**) Immunofluorescence analysis of *Cx3cr1-GFP*/+; *Ccr2-RFP*/+ mice. GFP labeled microglia do not express CD11a (arrows). Rare CD11a+ (red) cells appear amoeboid in morphology and lack *Cx3cr1-GFP* expression and thus are likely not microglia. CD11a and Ccr2-RFP are detected in the same channel (Red), however, *Ccr2-RFP* is not expressed in the brain without stimulation and thus the fluorescence observed is due to CD11a and not Ccr2. Images taken at 120X magnification, scale bars = 10μm.

Thus we also compared CD11a expression in the commonly-used *Cx3cr1-GFP* reporter mice (Saederup et al., 2010). As expected, GFP-labeled cells in the brain, which consist mostly of microglia, did not express CD11a (**Figure 1.2D-E**). Together, these data show that in healthy brains, CD11a remains highly expressed in all peripheral hematopoietic cells, but remains unexpressed in brain-resident microglia. Thus, CD11a meets the requirement for an on-off marker that can clearly distinguish between microglia (off) and peripheral immune cells (on) in a homeostatic mouse brain.

Microglia and monocytes/macrophages do not alter CD11a expression in activation states.

CD45 expression levels are commonly used to distinguish microglia ($CD45^{lo}$) from infiltrating peripheral monocytes ($CD45^{hi}$) by flow cytometry. However, CD45 expression increases in microglia cells with activation in neuroinflammatory contexts (Greter et al., 2015; Sedgwick et al., 2006). To determine whether activated microglia similarly upregulate CD11a expression, we injected the inflammatory molecule lipopolysaccharide (LPS) or vehicle control intracranially into 6-8-week-old B6 mice to activate microglia. LPS is known to cause a massive inflammatory response in the brain and induces a rapid influx of infiltrating immune cells into the brain (Cazareth et al., 2014). Brains of vehicle- and LPS-treated mice were harvested 24 hours post-injection. As expected, CD45 expression slightly increased in all CD11b+ cells with LPS treatment, partially obscuring the normal separation between $CD45^{lo}$ microglia and $CD45^{hi}$ monocytes (**Figure 1.3A,** left panels). However, CD11a expression remained absent on microglia, while infiltrating monocytes highly expressed this marker (**Figure 1.3A,** middle panels). Furthermore, an influx of monocytes into LPS-injected brains further blurred the distinction between microglia and monocytes using CD45, which becomes apparent when CD11a- and

Figure 1.3

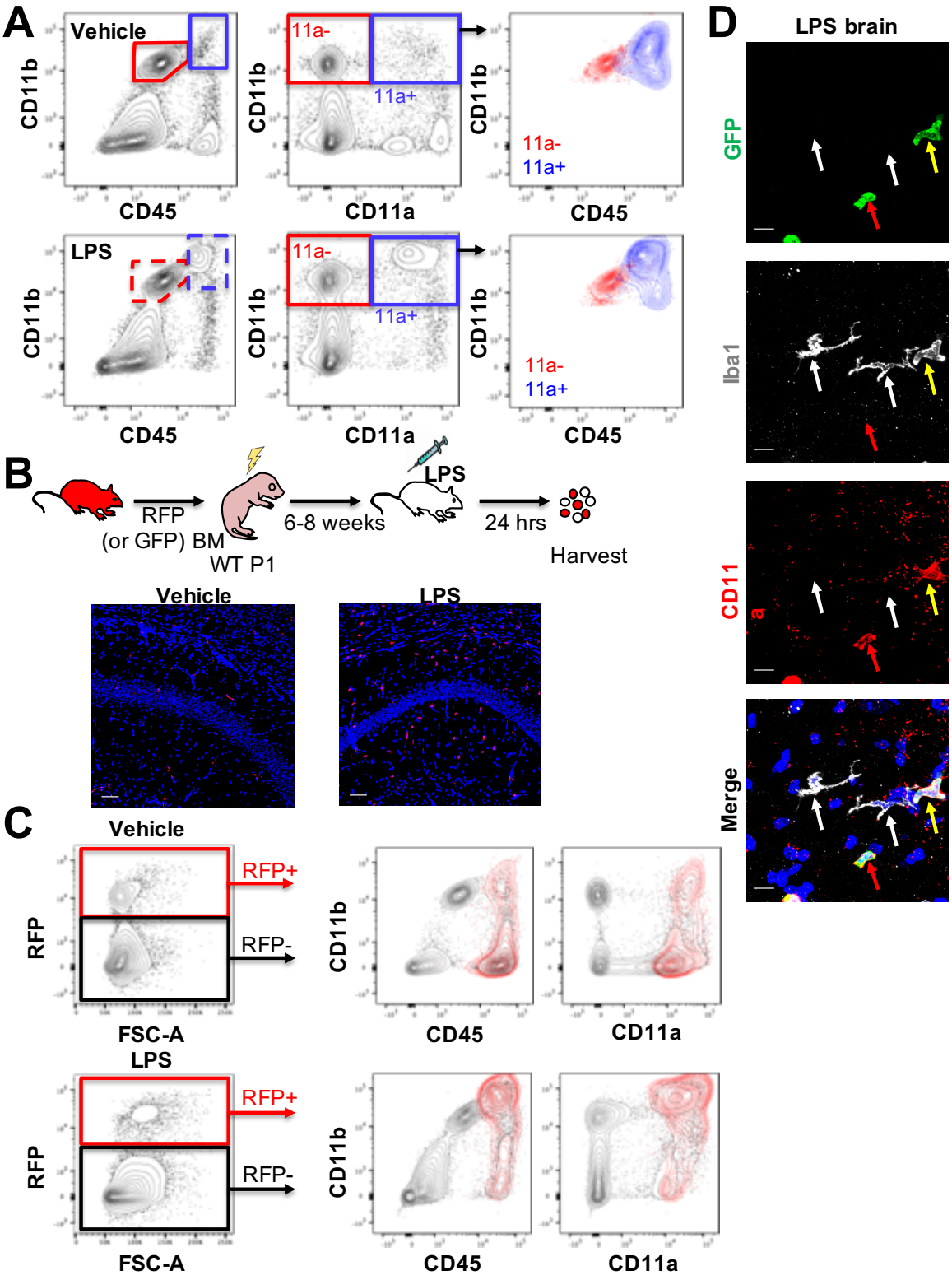
A
Vehicle
CD11b
CD45
11a-
11a+
CD11a
LPS
B
RFP
(or GFP) BM
WT P1
6-8 weeks
LPS
24 hrs
Harvest
Vehicle
LPS
C
Vehicle
RFP
RFP+
RFP-
FSC-A
CD45
CD11a
LPS
D
LPS brain
GFP
Iba1
CD11a
Merge

Figure 1.3: CD11a expression remains consistent in activated microglia and infiltrating macrophages. (A) FACS plots of the brains of C57/B6 adult mice 24 hours after intracranial injection of vehicle (top row) or 10 μg of LPS (bottom row). Leftmost plots show traditional CD11b vs CD45 gating scheme with microglia (CD11b+ $CD45^{lo}$, red gates) and macrophages (CD11b+ $CD45^{hi}$, blue gates). Middle plots show CD11b versus CD11a and revised gating for microglia (CD11b+ CD11a-, "11a-", red gate) and macrophages (CD11b+ CD11a+, "11a+", blue gate). Rightmost plots show overlays of CD11a- (red) and CD11a+ (blue) populations (from the middle plots) on CD11b vs. CD45 plots. **(B)** Schematic of transplantation of adult RFP+ bone marrow into P1 C57/B6 (WT) pups, followed by intracranial LPS (or vehicle) injection 6-8 weeks after transplant, and analysis 24 hours post-injection. 20X images of one brain lobe following vehicle (left) or LPS (right) injection showing RFP+ (red) BM-derived cells in the brain versus DAPI-stained nuclei (blue). Scale bars = 50μm. **(C)** Flow cytometry analysis of the other brain lobe 24 hours after vehicle (top row) or LPS (bottom row) injection. The leftmost plots show gating on RFP+ BM-derived donor cells versus RFP- host cells. The middle and right plots show CD11b versus CD45 (middle plots) or versus CD11a (right plots). RFP+ cells are shown in red and host cells in grey. **(D)** Representative immunofluorescence images of brain sections from LPS-treated mice after transplantation of adult GFP+ bone marrow cells into neonatal recipients (120X, scale bars = 10μm). All GFP+ infiltrating cells (green) co-stain with CD11a (red). White arrows denote Iba1+ microglia, which do not express CD11a or GFP. Red arrows indicate GFP+ cells that are CD11a+ Iba1-. Yellow arrows indicate GFP+ cells that express Iba1 as well as CD11a.

CD11a+ populations are overlaid using the conventional CD11b vs. CD45 gating strategy (**Figure 1.3A**, right panels).

It is formally possible that some infiltrating monocytes rapidly downregulate CD45 and CD11a upon infiltration and would be included in the "microglia" gate. To ensure that infiltrating monocytes and their descendent macrophages did not downregulate CD11a expression, we repeated the LPS and vehicle injection in 6-8 weeks old B6 mice that had been irradiated and transplanted as neonates with bone marrow cells from adult GFP+ or RFP+ donors (**Figure 1.3B**). This neonatal transplantation strategy allowed for effective HSC engraftment with low doses of irradiation (≤3.5 Gy) compared to the higher required dose for adult recipients (8-10 Gy). It also allowed for the blood-brain barrier to recover and the bone marrow compartment to stabilize by the time of LPS injection. 6-8 weeks post-transplant, vehicle or LPS was injected intracranially and the brains were harvested 24 hours post-injection. Fluorescent imaging of one lobe of each brain showed infiltrating RFP+ cells throughout the brain only in the LPS-treated mice (**Figure 1.3B**). Flow cytometric analysis was performed on the other lobe of the brain and showed that all donor bone-marrow derived RFP+ cells lied within the CD11a positive gate (**Figure 1.3C**). This confirms that infiltrating RFP^+ cells did not downregulate CD11a. Microglia, which are not replenished by the bone marrow, remained RFP- and CD11a-. Immunostaining of brains transplanted with GFP bone marrow cells (instead of RFP), showed $Iba1^+$ microglia remained CD11a- even after LPS-treatment, while all GFP+ cells were CD11a+, including both Iba1+ (myeloid) or Iba1- (likely lymphoid) populations (**Figure 1.3D, 1.4A-B**). Together, these data indicate that activated microglia remain CD11a negative and infiltrating immune cells remain CD11a+ in an inflammatory milieu. Thus, CD11a is a stable marker that can distinguish peripheral immune cells from brain-resident microglia.

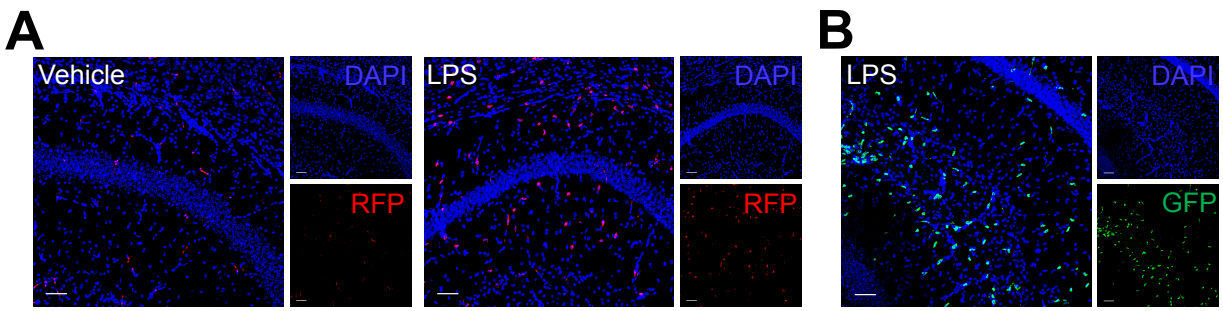

Figure 1.4: Infiltration of peripheral immune cells.
Images of Vehicle- and LPS-injected brains of transplanted mice. Infiltration of RFP+ **(A)** or GFP+ **(B)** cells is robust only in LPS-injected brains. Nuclei (blue) were stained with DAPI. All images were taken at 20X magnification. Scale bars = 50µm.

Whereas microglia in LPS- injected mice did not express CD11a, they did upregulate its expression in chronic *Toxoplasma gondii* infection, a parasite known to infect the brain and induce a strong immune reaction. Through flow cytometry analysis, microglia showed slight upregulation of CD11a in the acute stage of *T. gondii* infection (7 dpi) compared to mock-infected mice (**Figure 1.5A**). However, this shift in microglia was not detectable via immunofluorescence staining, despite tyramide amplification (**Figure 1.5B**). In contrast, during chronic infection, when the parasites are encysted in the brain, CD11a was detectable on microglia by both flow cytometry and immunofluorescence microscopy and highly upregulated in peripheral immune cells (**Figure 1.5C-E**). This finding aligns with previous reports that activated microglia and infiltrating cells express CD11a during chronic infection (Biswas et al., 2015). In this context, CD11a is comparable to CD45 as a marker. Thus, CD11a upregulation is context-dependent and must be tested in each model of neuroinflammation.

Microglia in AD model mice do not express CD11a.

In the 5xFAD mouse model of Alzheimer's disease, a tandem of two transgenes contain a total of five familial mutations in human Amyloid Precursor Protein (APP) and Presenilin-1 (PSEN1) genes. Together they cause a rapid accumulation of Aß in the brain as early as three months, with AD plaque-like pathology being observable at 4 months, and end-stage equivalent at 6 months of age (Oakley et al., 2006). Similar to activated microglia, CD45 expression in aged 5xFAD mice is upregulated in all CD11b+ cells, making it difficult to distinguish monocytes from microglia using the conventional CD11b vs CD45 gating scheme. With disease progression, it becomes increasingly unclear whether the abundant population of $CD45^{hi}$ cells are microglia or infiltrating monocytes (**Figure 1.6A**). However, these populations could still be distinguished using a CD11b

Figure 1.5

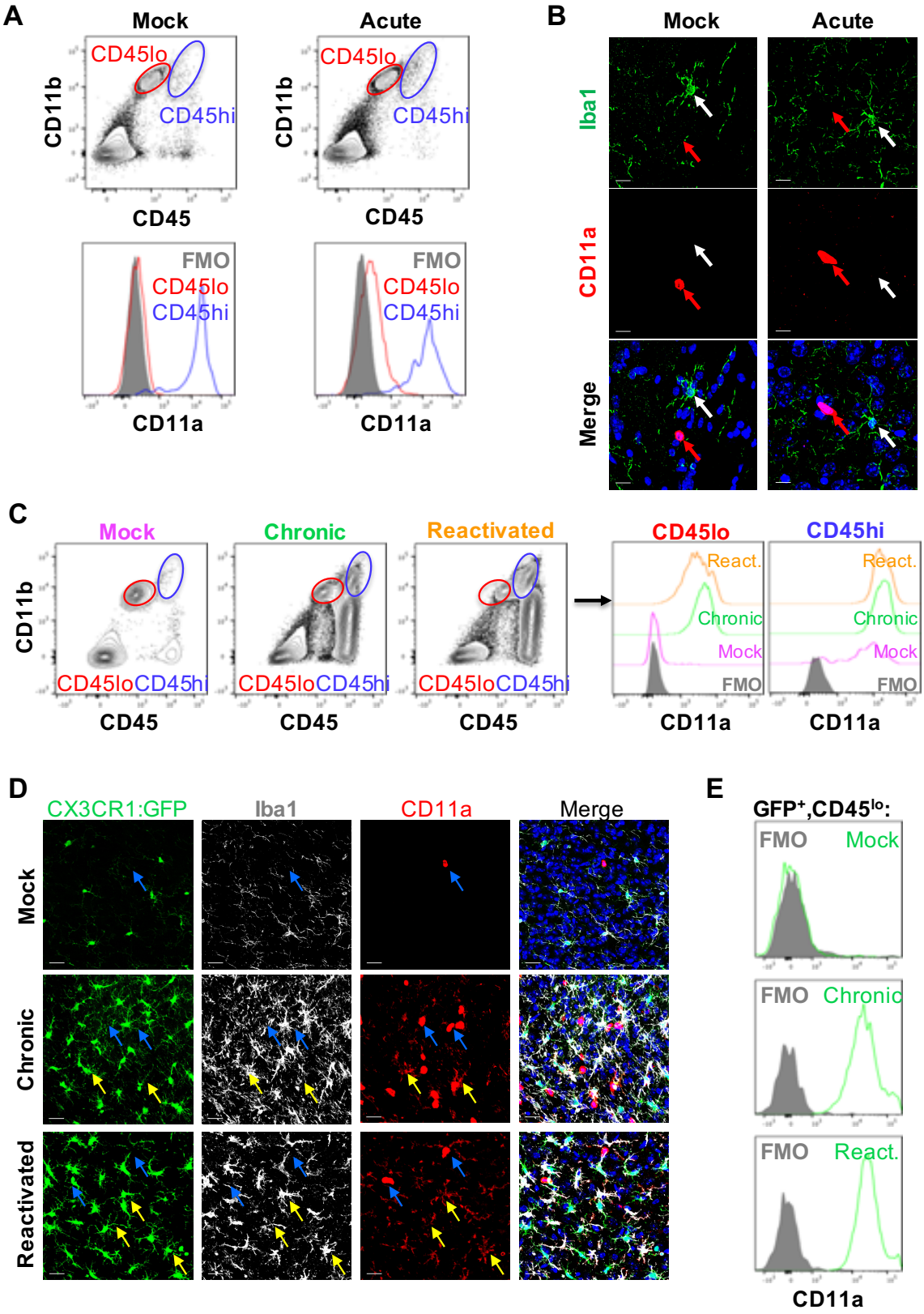
A
Mock
Acute
CD45lo
CD45hi
CD11b
CD45
FMO
CD11a
B
Mock
Acute
Iba1
CD11a
Merge
C
Mock
Chronic
Reactivated
CD45lo
CD45hi
CD45loCD45hi
CD45
React.
Chronic
Mock
FMO
CD11a
D
CX3CR1:GFP
Iba1
CD11a
Merge
Mock
Chronic
Reactivated
E
GFP+,CD45lo:
FMO
Mock
Chronic
React.
CD11a

Figure 1.5: CD11a is upregulated on microglia in Toxoplasma gondii-infected brains. (A) Representative FACS plots of mock and acute infection (7 days post infection, dpi) in B6 mice. Top panel shows traditional CD11b vs. CD45 gating scheme of microglia (CD45lo, red gates), and macrophages (CD45hi, blue gates). Lower panels show histograms of CD11a expression of cells from the "CD45lo" and "CD45hi" gates and FMO control (grey). **(B)** Representative immunofluorescence images of brains from mock and acutely infected B6 mice. Nuclei stained with DAPI (blue), Iba1 (green), and CD11a (red). CD11a upregulation in microglia (white arrows) from acute infected mice is not detectable, even with tyramide amplification. All images taken at 120X magnification, scale bars = 10 μm. **(C)** CD11b vs. CD45 FACS plots of B6 mock-infected, chronically infected (38 dpi), and chronically infected brains (38 dpi), in which reactivation of encysted parasites was induced by injection of anti-IFN-□ blocking antibody at 28 and 32 dpi. Histogram overlays of CD11a expression in microglia (CD45lo, red gates) and macrophages (CD45hi, blue gates) in mock (pink histograms), chronic (green histograms) and reactivated (orange histograms) B6 brains. **(D)** Representative immunofluorescence images of Cx3cr1-GFP/+; Ccr2-RFP/+ (double reporter) mice during mock, chronic and reactivated infection. Cx3cr1-GFP labeled microglia (green) express Iba1 and show upregulation of CD11a (yellow arrows). Peripheral cells continue to express high levels of CD11a and are GFP negative (blue arrows). Please note that CD11a and Ccr2-RFP are both detected in the same channel, but the brightness of the Ccr2-RFP is much lower and not detectable at the exposure time used. Images taken at 100X magnification, scale bars = 20μm. (E) FACS histograms of GFP+, CD45lo microglia (green histograms) show upregulation of CD11a on microglia from chronic and chronic reactivated mice compared to FMO control (grey histogram). CD11a is detected on a different channel than Ccr2-RFP here.

vs. CD11a gating strategy (**Figure 1.6B**). Using CD11a also highlighted the abundant $CD45^{hi}$ population in aged 5xFAD brains, which also upregulates CD11b but is almost entirely CD11a- (**Figure 1.6C**). Therefore, these cells likely represent microglia that have upregulated CD45, and not a massive influx of infiltrating monocytes/macrophages. We also observed a similar trend in a second independent AD transgenic model, Arc48 mice, which express a different combination of familial mutations than the 5xFAD mouse model (Cheng et al., 2004) (**Figure 1.7**). While there were slight increases in CD11a expression on microglia with age and disease progression in AD mice, a similar trend was also noticed in their WT littermates, as well as in the monocyte/macrophage populations of WT and AD mice, and the separation between CD11a- and CD11a+ populations was still distinct (**Figure 1.6B**).

Plaque-associated myeloid cells are microglia, not peripheral monocytes/macrophages.

Immunofluorescence imaging of microglia in WT and AD mice consistently showed that microglia (Iba1+) in the brain parenchyma did not express CD11a. Additionally, plaque-associated Iba1+ cells did not co-label with CD11a even at 12 months of age (**Figure 1.6D**). On rare occasions, CD11a+ cells were found near plaques, but they did not co-stain with Iba1, meaning they were not of myeloid lineage. Together, these data show that microglia in two AD mouse models, 5xFAD and Arc48, remain CD11a negative despite the increase in plaque burden with age. Moreover, peripheral myeloid cells have nominal contribution to the overall $CD45^{hi}$ population, indicating there is not a massive influx of peripheral monocytes in the AD brain.

Figure 1.6

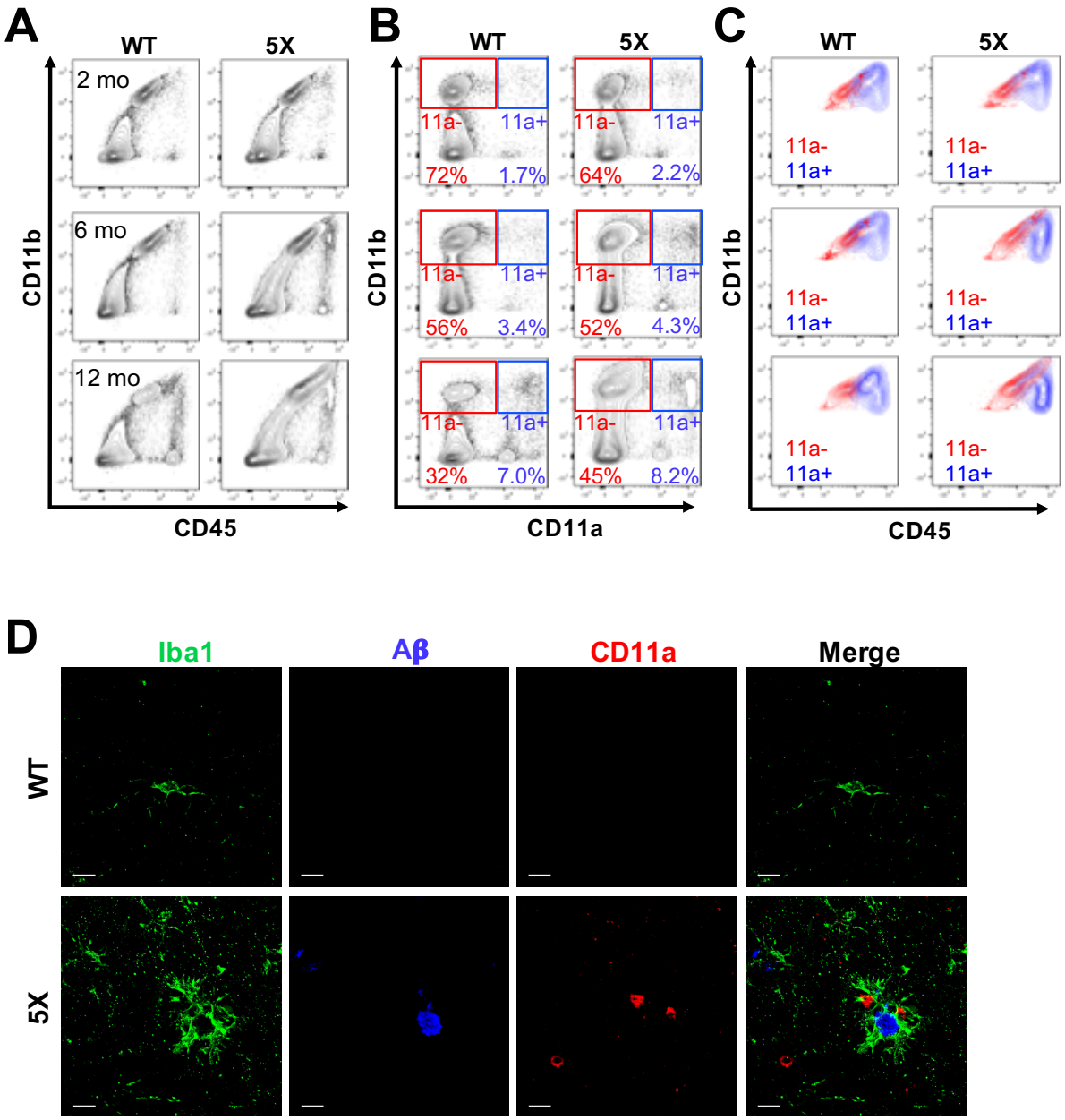
A
WT
5X
2 mo
6 mo
12 mo
CD11b
CD45
B
WT
5X
11a-
11a+
72%
1.7%
64%
2.2%
56%
3.4%
52%
4.3%
32%
7.0%
45%
8.2%
CD11b
CD11a
C
WT
5X
11a-
11a+
CD11b
CD45
D
Iba1
Aβ
CD11a
Merge
WT
5X

Figure 1.6: Microglia in 5xFAD mice do not express CD11a. (A-C) Representative FACS plots of $5xFAD^{-/-}$ (WT, left columns) and $5xFAD^{+/-}$ (5X, right columns) littermates at 2 months (top row), 6 months (middle row), and 12 months (bottom row) of age. **(A)** Traditional CD11b versus CD45 plots show increasing overlap between microglia and macrophages in 5X mice with age. **(B)** CD11b versus CD11a plots show a clear distinction between microglia (CD11b+ CD11a-, "11a-", red gate) and macrophages (CD11b+ CD11a+, "11a+", blue gate). **(C)** Traditional CD11b versus CD45 plot showing an overlay of microglia ("11a-", red) and macrophage ("11a+", blue) populations using the CD11a gating strategy from B. **(D)** Representative immunofluorescent images (120X, scale bar = 10µm) of 12-month-old WT (top) and 5X (bottom) brains. Iba1+ cells (green) surrounding beta amyloid plaques (Aß, blue) are CD11a-. Extremely rare instances of CD11a+ cells (red) found near plaques do not express Iba1.

Figure 1.7

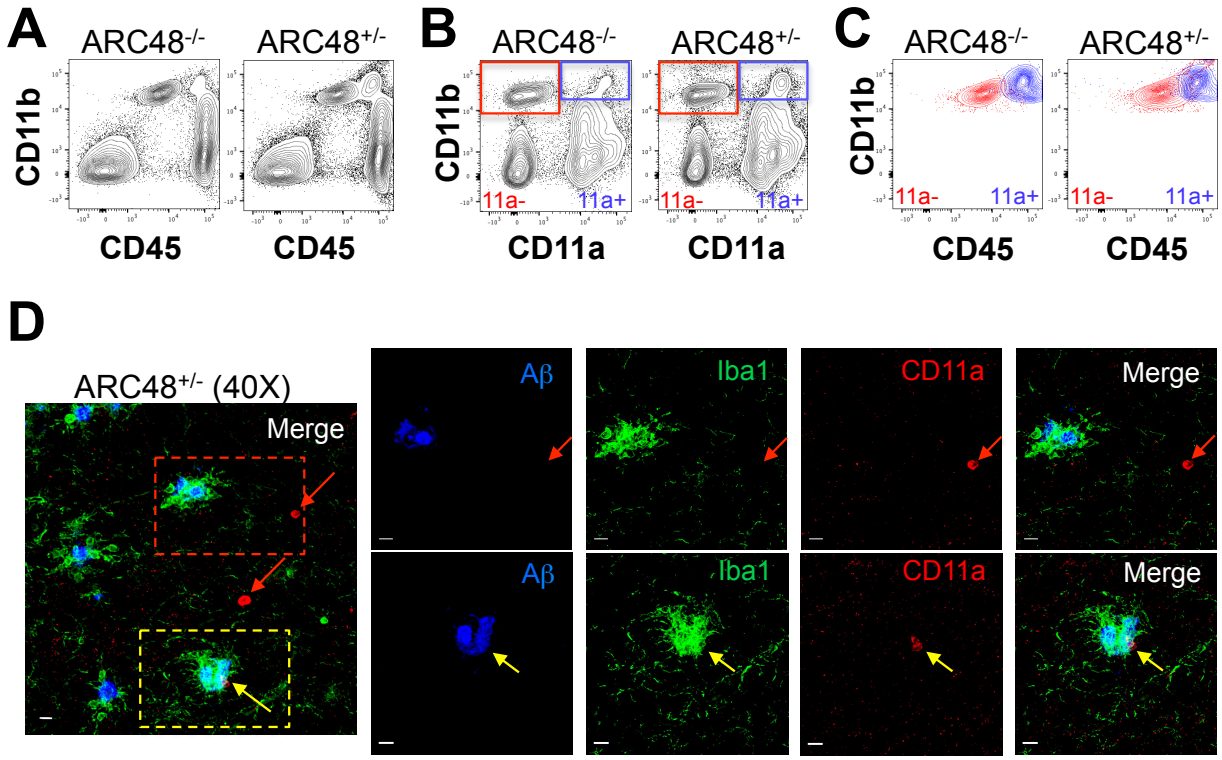
A
ARC48-/-
ARC48+/-
CD11b
CD45
CD45
B
ARC48-/-
ARC48+/-
CD11b
11a-
11a+
11a-
11a+
CD11a
CD11a
C
ARC48-/-
ARC48+/-
CD11b
11a-
11a+
11a-
11a+
CD45
CD45
D
ARC48+/- (40X)
Merge
Aβ
Iba1
CD11a
Merge
Aβ
Iba1
CD11a
Merge

Figure 1.7: Microglia in Arctic 48 model of AD also do not express CD11a.
(**A**) Representative FACS plot of CD11b vs. CD45 of 9-month-old Arc48$^{-/-}$ (WT) and Arc48$^{+/-}$ (AD) littermates. In the AD model, the separation between CD45^{hi} and CD45^{lo} populations is less distinct than the WT control. (**B**) CD11a vs. CD11b gating shows a clearer separation between CD11b+, CD11a- microglia ("11a-", red gate) and CD11b+ CD11a+ macrophages ("11a+", blue gate), similar to the 5xFAD model (Figure 3B). (**C**) 11a- (red) and 11a+ (blue) populations overlaid on CD45 vs. CD11b plot demonstrate the upregulation of both markers in AD microglia and how they confound the "CD45hi" population in the conventional gating scheme. (**D**) Representative confocal images of Aß plaques in Arc48$^{+/-}$ brain show. The left image was taken at 40X magnification and shows examples of CD11a+ cells far from plaques (red arrow) or near plaques (yellow arrow). Zoomed in images of plaques on the right were taken at 80X magnification and show the red dashed box (top row) and yellow dashed box (bottom row) from the 40X image on the left. Almost all Iba1+ cells are CD11a- microglia, with rare CD11a+ cells that are Iba1- and are likely not macrophages. All scale bars = 10μm.

Peripheral immune cells do not downregulate CD11a upon infiltration in AD brains.

Given the low amounts of $CD45^{hi}$ and CD11a+ cells observed in 12-month-old 5xFAD mice, we wanted to confirm that infiltrating monocytes/macrophages did not downregulate CD11a. To this end, we transplanted neonatal 5X and WT littermates with RFP+ bone marrow cells (**Figure 1.8A**). After 12 months of age (and 12 months post-transplantation), we harvested one lobe for flow cytometry and the other for immunofluorescence imaging. By flow cytometry, almost all RFP cells remained in the CD11a+ fraction whereas the CD11a- cells were all negative for RFP (**Figure 1.8B**). There was little evidence of robust infiltration of peripheral cells, as the percentage of RFP+ cells in the brain was low in both WT and 5X mice. Donor chimerism was high in all recipient mice, as measured by HSC chimerism in the BM (**Figure 1.8B**). Thus, the absence of RFP^+ cells in the brain was not due to low engraftment levels of RFP^+ cells. As seen in LPS-treated chimeric mice, infiltrating RFP^+ cells in 5X and WT mice did not downregulate CD11a (**Figure 1.8B**). Importantly, RFP cells maintained CD11a expression one year after transplant. Therefore, CD11a- cells in the 5X brains are unlikely to be from bone marrow-derived cells infiltrating from the periphery. This transplantation approach also allowed us to quantify the relative abundances of different immune populations (CD11b+ CD11a- microglia, CD11b+ CD11a+ myeloid cells, and CD11b- CD11a+ lymphoid cells) in 5X and WT brains (**Figure 1.8C)**. No significant difference was observed in the distribution of bone marrow-derived cells in 5X mice compared to their WT littermates. To assess whether the RFP+ cells clustered around plaques, we also imaged sections of the other lobe of these transplanted 5x mice. Observation of RFP cells was extremely rare in 5X brains as well as WT mice (**Figure 1.8D**). Thus, it is unlikely that any RFP+ cells contributed to the PAM population. Taken together, these data provide strong evidence that infiltrating cells do not downregulate CD11a and that infiltration of CD11a+ peripheral immune cells is not

Figure 1.8

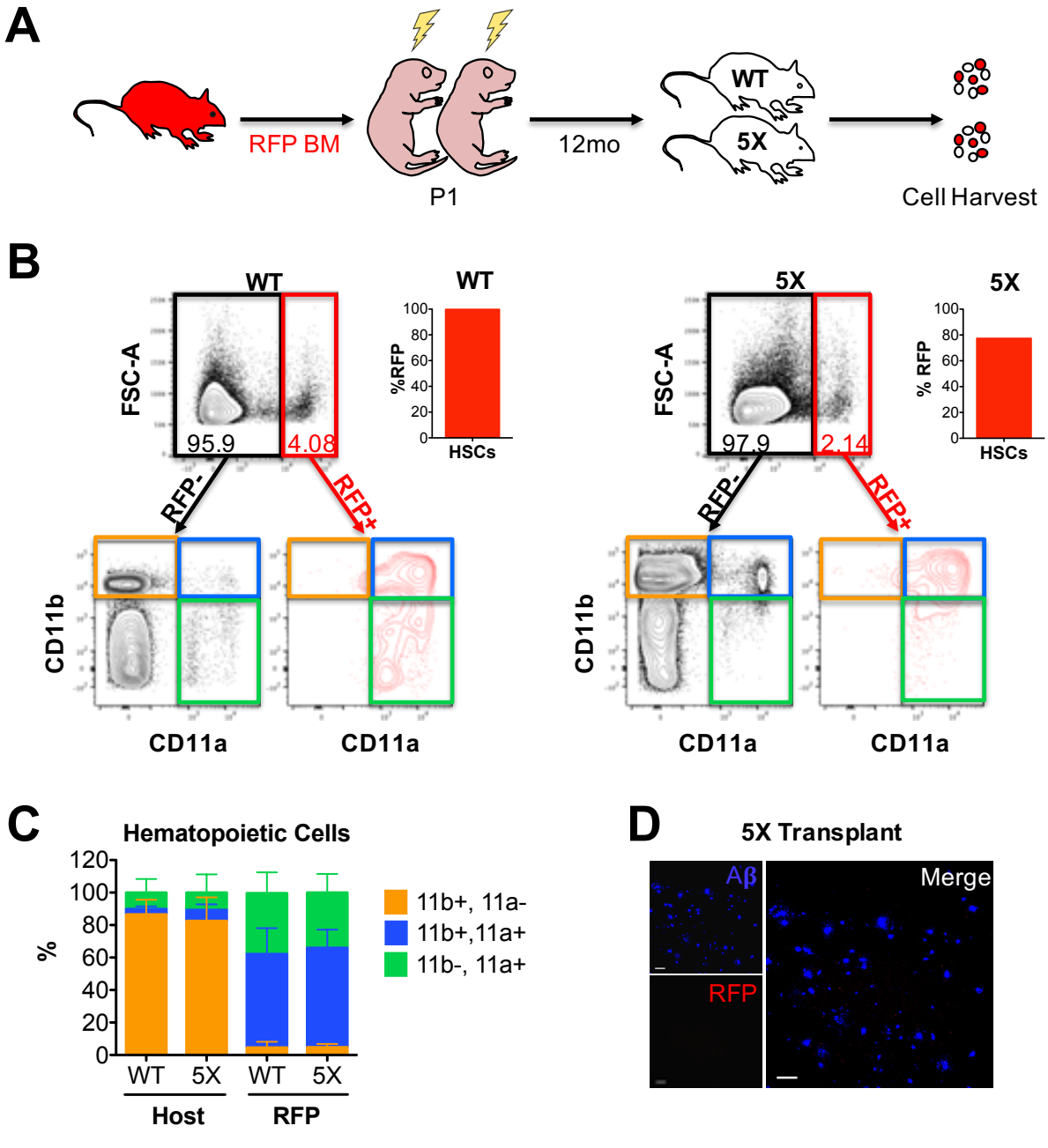
A
RFP BM
P1
12mo
WT
5X
Cell Harvest
B
WT
FSC-A
95.9
4.08
RFP-
RFP+
CD11b
CD11a
CD11a
WT
%RFP
HSCs
5X
FSC-A
97.9
2.14
RFP-
RFP+
CD11b
CD11a
CD11a
5X
% RFP
HSCs
C
Hematopoietic Cells
%
WT
5X
WT
5X
Host
RFP
11b+, 11a-
11b+,11a+
11b-, 11a+
D
5X Transplant
Aβ
RFP
Merge

Figure 1.8: Plaque-associated myeloid cells are not derived from bone marrow. (A) 5xFAD$^{-/-}$ (WT, n=4) and 5xFAD$^{+/-}$ (5X, n=4) littermates were transplanted with RFP+ bone marrow as neonates (P1), then analyzed 12 months later. **(B)** Representative flow cytometry plots of WT (left) and 5X (right) brains at 12 months of age. Total RFP- (black gate) and RFP+ (red gate) cells were analyzed for CD11b vs. CD11a expression (lower FACS plots). The bar graph (right) indicates the donor HSC chimerism in the BM of the transplanted mice at 12 months. The bottom CD11b versus CD11a plots show the distribution of immune populations in the RFP- host cells (left, black) and RFP+ BM-derived cells (right, red). Quadrants Q1 (CD11b+ CD11a-, orange quadrant) represent microglia, Q2 (CD11b+ CD11a+, blue quadrant) macrophages, and Q3 (CD11b- CD11a+, green quadrant) lymphocytes. **(C)** Bar graph showing the distribution of immune cell types in the host (left bars) and RFP+ donor (right bars) in WT and 5X brains. The sum of the three immune cell quadrants was set to 100%. Error bars are S.D. (N=4 mice each). **(D)** Representative image of the brain of a 5X mouse transplanted with RFP+ BM 12 months post-transplant show no infiltrating RFP+ cells (red). Aß plaques are shown in blue. Images taken at 20X magnification, scale bars = 50μm.

increased in AD mice compared to their wildtype littermates. This also provides further evidence that the plaque-associated myeloid cells are CD11a-, brain-resident microglia.

Fluorescence-Assisted Quantification Technique (FAQT) reveals an increase in T cell infiltration in 5xFAD females

Our transplantation approach in 5X mice did not show any major influx of peripheral immune cells (**Figure 1.8C and 1.8D**), especially compared to LPS-injected brains (**Figure 1.3B**). Given the improved distinction between microglia and peripheral immune cells that the CD11b vs. CD11a gating strategy provides, we aimed to quantify the relative number of infiltrating cells in unmanipulated, aged 5X mice compared to their wildtype littermates. However, 5X brains, which suffer from chronic inflammation, have differences in cell viability and display different properties on flow cytometry analysis than WT brains, making it difficult to quantitatively compare microglia, monocytes or lymphocytes between WT and 5X brains as a percentage of total cells in the brain. Furthermore, the final cell yield, which requires mechanical digestion and centrifugation through a Percoll gradient, is inconsistent and can lead to huge variability in the absolute numbers of cells harvested from prep to prep. Lastly, counting beads, which can be added to sample tubes to estimate absolute numbers, are depleted via Percoll gradient, and therefore cannot be added during the prep stage to accurately control for differences in prep yield.

As a solution to these issues, we developed a method called "Fluorescence-Assisted Quantification Technique" (FAQT) to spike in fluorescently labeled brain tissue during the initial harvesting step and before the Percoll gradient steps. As such, any discrepancies in yield due to preparation would equally affect the fluorescently labeled cells. As long as an equal amount of fluorescently-labeled brain tissue (i.e. one lobe each from the same brain) was added to each prep

Figure 1.9

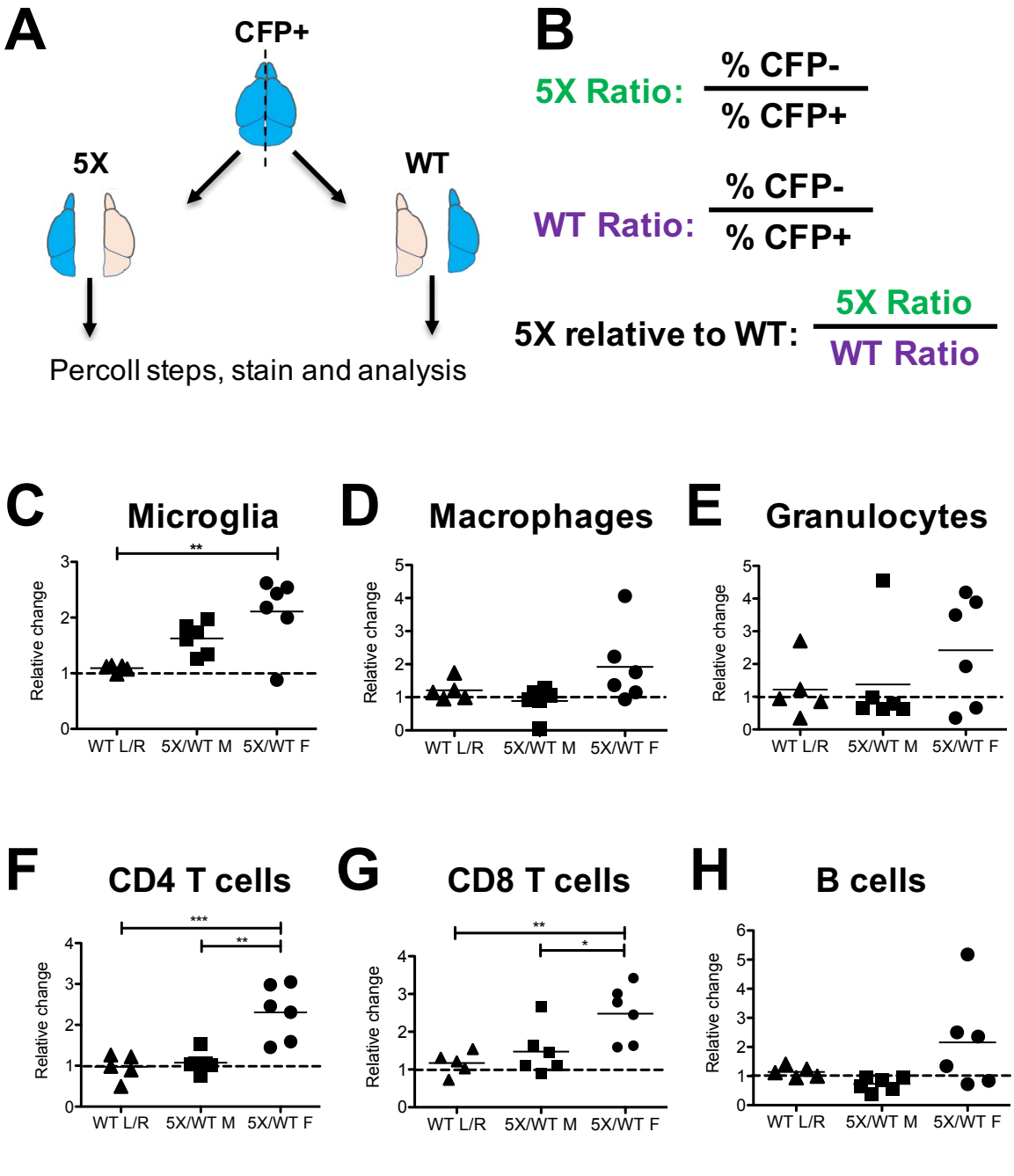
A
CFP+
5X
WT
Percoll steps, stain and analysis
B
5X Ratio: % CFP- / % CFP+
WT Ratio: % CFP- / % CFP+
5X relative to WT: 5X Ratio / WT Ratio
C
Microglia
D
Macrophages
E
Granulocytes
F
CD4 T cells
G
CD8 T cells
H
B cells
Relative change
WT L/R
5X/WT M
5X/WT F

Figure 1.9: Fluorescence-Assisted Quantification Technique (FAQT). (A) Schematic of FAQT. Fluorescent brains (e.g. CFP) are divided into lobes and mixed with one lobe from a 5X mouse and one lobe of a WT littermate, then processed and analyzed by flow cytometry. After FACS analysis, immune cell populations were each gated and then separated into CFP+ and CFP- fractions. See gating strategy for each immune cell type in **Figure S5. (B)** Quantification strategy. The ratio of CFP- to CFP+ cells was calculated for both the 5X and WT pair, then was used to calculate the ratio of 5X to WT cells (5X:WT), canceling out the CFP+ spiking cells. **(C-H)** For each immune cell population, the leftmost column shows the relative ratio of immune cells between the left and right lobes of a WT brain (WT L/R), which represents the WT lobe-to-lobe control. The 5X:WT ratio of each pair of 5X/WT lobes is plotted, showing male pairs (middle) and female pairs (right). The value is the ratio of 5X immune cells relative to WT (which is set to one and indicated by the dashed line). Statistical analysis (one-way ANOVA, Tukey's multiple comparison test) compares the three groups. Asterisks represent a p-value of <0.05.

of WT and 5X brain, the yields of brain populations could be normalized to the fluorescent control and the relative abundances of each population calculated. As illustrated in **Figure 1.9A**, we harvested a pair WT and 5X littermates, and added one lobe of each brain to separate tubes. We then harvested a CFP+ brain and separated the two lobes, then added one lobe to the WT tube and one lobe to the 5X tube, so each tube received an identical amount of fluorescent brain tissue. We then proceeded with the normal preparation and Percoll gradient. We then stained and analyzed each brain prep by flow cytometry, gated on each immune population (e.g. microglia, monocytes, T cells, B cells, granulocytes), then separated them into CFP+ and CFP- fractions (**Figure 1.10**). Thus, any variability in cell yield will be reflected in both the CFP+ and CFP- cells within the sample. We could then compare the percentage of fluorescently-labeled cells between the WT and 5X population to estimate the ratios of each population to the fluorescent control (**Figure 1.9**). If we divide the ratio of WT:CFP microglia by the ratio of 5X:CFP microglia, then we can estimate the abundance of the 5X microglia relative to its WT littermate (which is set to 1). For example, if 50% of microglia in the WT brain are CFP+ (a 1:1 WT:CFP ratio), but only 25% of microglia in the 5X brain are CFP+ (a 3:1 5X:CFP ratio), then this would suggest that the microglia in the 5X brain are three times as abundant as the WT microglia, because we added the same number of CFP+ microglia to each tube. As a control, we first performed this using only WT brains, comparing the abundance of immune populations between the left lobe and right lobe ("WT L/R"), which we assume to be equal (**Figure 1.9C-H**). The differences we observe between the left and right lobes represent the variation inherent in this system and offer a control group to the 5X:WT ratios for statistical comparisons.

We used this technique to measure the relative abundance of several immune populations between the brains of WT and 5X littermates at approximately 12 months of age. We separately

Figure 1.10

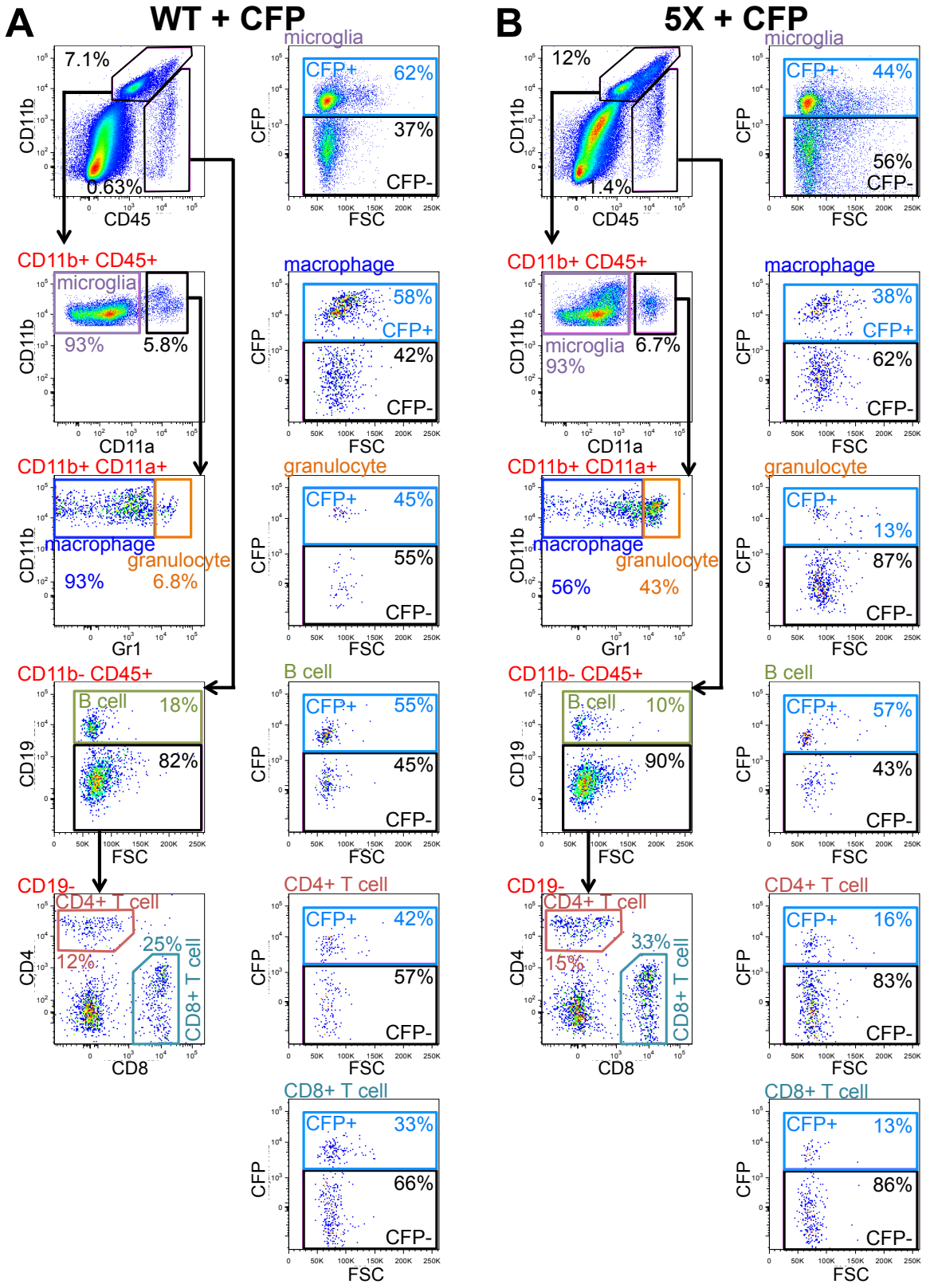
A
WT + CFP
B
5X + CFP
microglia
macrophage
granulocyte
B cell
CD4+ T cell
CD8+ T cell
CD11b+ CD45+
CD11b+ CD11a+
CD11b- CD45+
CD19-
CD11b
CD45
CD11a
Gr1
CD19
CD4
CD8
CFP
FSC
7.1%
0.63%
93%
5.8%
58%
42%
45%
55%
18%
82%
55%
45%
12%
25%
42%
57%
33%
66%
12%
1.4%
93%
6.7%
38%
62%
56%
43%
10%
90%
57%
43%
15%
33%
16%
83%
13%
86%
CFP+
CFP-

Figure 1.10: Representative gating scheme for FAQT. Representative gating used to delineate immune populations in the brain in spiking experiments for WT (**A**) and 5X (**B**) brains. The gates used for each plot are listed above each plot in red font. The left columns show the gating for each immune population and the right columns show the gating for CFP+ spiking cells and CFP- (WT or 5X) cells. The percentages of CFP+ and CFP- cells were used to calculate the ratios of WT:CFP, 5X:CFP and then 5X:WT. For example, for CD8+ T cells (bottom row), the WT:CFP ratio is 2.0 (66%/33%), the 5X:CFP ratio is 6.6 (86%/13%) and the 5X:WT ratio is 3.3 (6.6/2.0). The fluorochromes used for each antibody are as follows: CD11b (APC), CD45 (FITC), CD11a (PE), Gr1 (Alexa700), CD19 (BV421), CD4 (PECy7), CD8 (APCCy7), CFP (Amcyan). Note, microglia autofluoresce in the q605 channel, and bleeds badly into the Amcyan channel, and so a compensation correction was applied to the Amcyan channel to take this into account. The antibodies and gating used for GFP+ or RFP+ spiking experiments differed slightly from that used for CFP and are not shown.

analyzed male and female brains due to the known differences in AD pathology between the genders in this mouse model (Oakley et al., 2006; Sadleir et al., 2015). In the males, the differences between WT and 5X brains were relatively minor for most populations and were not statistically significant compared to the WT lobe-to-lobe control. In the female 5X brains, where pathology is greater, there was a significant increase in microglia, but not in macrophages or granulocytes, which were slightly elevated but not statistically significant (**Figure 1.9C-E**). Furthermore, we saw a statistically significant increase in CD4+ and CD8+ T cell populations compared to either the WT only lobe-to-lobe ratios or the male 5X:WT ratios (**Figure 1.9F-G**). B cells appeared elevated in 5X females but were not statistically significant (**Figure 1.9H**). Using CD11a allowed us to determine that a majority of the $CD45^{hi}$ cells in AD brains were in fact microglia that also upregulated CD11b. Using CD11a and FAQT, we show evidence of microglial proliferation in AD brains, with no significant infiltration of peripheral myeloid cells.

DISCUSSION

In this study, we demonstrate the utility of using CD11a as a marker to distinguish healthy, activated, and Alzheimer's disease-associated microglia from CD11a+ infiltrating peripheral immune cells. As CD11a is a negative marker for microglia, it can be combined with existing positive markers (e.g. Tmem119, P2ry12) to enhance microglia/monocyte distinction, or be used in lieu of markers such as CD45 to simplify microglia identification. When combined with just CD11b, microglia can be readily identified as CD11b+ and CD11a-. CD11a overcomes several limitations of the CD45 vs CD11b gating strategy. First, we observed no significant upregulation of CD11a by activated microglia in our LPS-induced inflammation model, which is not the case for CD45. Second, we determined that microglia in two different AD mouse models do not

upregulate CD11a, unlike CD45, even at ages with peak plaque burden. Thus, using CD11a, along with CD11b, for flow cytometry will allow isolation of microglia in the CD11a- fraction and peripheral myeloid cells in the CD11a+ fraction. While CD11a is excellent in distinguishing microglia and infiltrating myeloid cells in AD models, we showed that its expression on microglia was upregulated in the chronic stages of *Toxoplasma gondii* infection. Thus, the utility of CD11a in distinguishing microglia from peripheral myeloid populations must be tested on a case-by-case basis. The signaling events that lead to LFA1 upregulation on microglia still remain to be investigated. As LFA1 is also important for antigen presentation, it is possible that LFA1 upregulation on microglia may play a role in facilitating a T cell response in the brain, as T cell-mediated immunity is well-established for *T. gondii* infection.

Using CD11a as a marker has allowed us to address outstanding questions regarding the roles of microglia versus infiltrating monocytes in AD pathology. One such question regards the identity of the myeloid cells that surround Aß plaques. We have determined that PAM cells are CD11a-, and therefore our findings support the notion that PAM cells are microglia, rather than infiltrating monocytes recruited to plaques. While it remains formally possible that monocytes, and subsequent macrophages, recruited to plaques eventually downregulate CD11a, we saw no evidence of this in our transplantation system, despite the fact that we analyzed 5X brains one year after transplantation. Although nearly 100% of the BM-derived cells were RFP+ or GFP+, we saw no fluorescent cells clustered around the plaques through immunofluorescent staining. Additionally, all fluorescent cells we observed in the brain were CD11a+ through flow cytometry. Together, our data strongly supports the notion that PAM cells are entirely composed of microglia, and not peripheral macrophages.

Our findings align with previous studies supporting microglia as the sole players in an AD CNS. Such studies have shown no significant infiltration based on lack of BBB disruption (Bien-Ly et al., 2015). However, previous studies replacing the peripheral immune system by transplanting reporter-expressing HSCs have shown evidence of bone marrow-derived monocytes infiltrating the CNS in AD models (Mildner et al., 2007; Simard et al., 2006). However, HSC transplantation in adult mice requires high doses of irradiation, which can alter the brain environment by activating microglia and disrupting the BBB. We circumvented the artifacts of high dose irradiation by transplanting 5X and WT littermates as neonates with fluorescently labeled, ckit-enriched bone marrow cells. This approach allowed us to attain high levels of chimerism with much lower doses of irradiation (≤3.5 Gy). Additionally, it allowed substantial time for BBB recovery: 6-8 weeks for LPS experiments or one full year for AD experiments and analysis. These findings suggest that neonatal transplantation allows the BBB to remain intact during the onset and progression of the disease and that the lack of infiltration is physiologically relevant.

A second question we attempted to address using CD11a was to what extent do peripheral immune cells infiltrate the brain in AD? By analyzing CD11a expression in 5X mice, we saw little evidence of a robust infiltrating monocyte population in 5X brains compared to WT, even after one year. The abundant $CD45^{hi}$ population in 5X brains was CD11a-, suggesting they are microglia. Furthermore, in the transplantation system, these $CD45^{hi}$ cells were also RFP-, suggesting they are not BM-derived. Together, this strongly argues against a massive influx of monocytes into the brain but does not rule out mild increases or gender-specific differences in infiltrating populations.

To provide a sensitive method of quantifying the abundance of immune populations in the brain, we developed a technique called FAQT (Fluorescence-Assisted Quantification Technique). Pairs of WT and 5X brains are spiked with an equal quantity of fluorescently-labeled brain tissue, then after flow cytometry analysis, each population is normalized to the fluorescent control. As long as we can assume that the abundance of each population is consistent between the right lobe and left lobe of the fluorescent mice, the age, gender, or strain of the spiking brains is irrelevant after normalization. This makes it easy to add fluorescent brains to any brain prep to allow comparison between any two mice. This method is preferable to adding fluorescent counting beads, which would either be lost during Percoll processing if added before, or neglect sample-specific differences in cell yield if added before analysis. Using this strategy, we were able to quantify and isolate gender-specific differences in peripheral immune cell populations of all aged 5X mice relative to their WT littermates. Aged male 5X mice showed no significant increases in any cell populations. Whereas peripheral myeloid populations in the females were only mildly increased, T- lymphocyte infiltration was significantly increased in 5X female brains relative to WT as well as their male counterparts. A significant increase in T-lymphocytes supports a role for the adaptive immune system in AD, as we have previously shown using an AD mouse model that lacks an adaptive immune system (Marsh et al., 2016). Moreover, FAQT can be useful in a variety of neuroinflammatory contexts to accurately quantify infiltrating immune cell populations.

While there is strong evidence that PAM cells are CD11a negative microglia in mouse models of AD, whether this finding translates to human AD patients has yet to be determined. It is known that CD11a is expressed in peripheral human immune cells (Watanabe & Fan, 1998). A recent microglial gene-expression study found CD11a is not expressed in brain tissues resected during surgery (Gosselin et al., 2017). We are currently investigating whether human peripheral

cells infiltrate the parenchyma and cluster around Aß plaques, or whether microglia are the main players in human AD, as seen in mouse models of AD.

In this study, we have established CD11a as a stable and reliable marker to distinguish microglia and peripheral myeloid populations in the brain. This commercially available marker is inexpensive and widely available in a variety of fluorochromes. For immunofluorescent staining of fixed brain sections, we highly recommend tyramide signal amplification to greatly improve signal intensity. While CD11a expression must be validated for each neuroinflammatory context prior to its use, we find that in many contexts (e.g. LPS, 5xFAD, Arc48), but not all (e.g. Toxoplasma infection), CD11a dramatically improves the ability to distinguish microglia from other infiltrating immune cell types. Therefore, we contend this marker should be included in the neuroimmunologist's standard toolkit.

MATERIALS AND METHODS

Mice. C57BL/6J (B6; stock no. 00664, JAX) strain was used for healthy, wild-type mouse experiments. 5xFAD (MMRRC stock no. 034848, JAX) heterozygous males were crossed with C57BL/6J females to obtain AD and WT littermates. CFP mice (*Rosa26*$^{ECFP/ECFP}$, aka TM5; Ueno et al., 2006) were donated by Dr. Irving Weissman (Stanford University). RFP mice (*Rosa26*$^{mTmG/mTmG}$, aka mT/mG, stock no., 007576, JAX, (Muzumdar et al., 2007)) were generated by Dr. Liqun Luo (Stanford University) and donated by Dr. Weissman. GFP mice (*Rosa26*$^{mG/mG}$) mice were created at UC Irvine by crossing *Rosa26*$^{mTmG/mTmG}$ with a Cre strain that is expressed in the male germline (Lyve1-Cre; Pham et al., 2010). The mT/mG reporter will delete the mTomato expression cassette and express mGFP upon Cre-mediated excision. The progeny was further bred to remove Lyve1-Cre and create *Rosa26*$^{mG/mG}$ homozygous mice that were used. *Cx3cr1*$^{+/GFP}$;*Ccr2*$^{+/RFP}$ double reporter mice (Saederup et al., 2010) were provided by Dr. Melissa Lodoen (UC Irvine). Arc48$^{+/-}$ (AD) and Arc48$^{-/-}$ (WT) littermates were a donation from Dr. Andrea Tenner (UC Irvine). All animal procedures were approved by the International Animal Care and Use Committee and University Laboratory Animal Resources of University of California, Irvine.

Microarray analysis of Itgal expression in immune populations. Microarrays (Mouse 430 2.0) of mouse hematopoietic populations were downloaded and processed from the Gene Expression Commons (GEXC, gexc.riken.jp) database (Seita et al., 2012). The microglia microarrays were downloaded from the Gene Expression Omnibus database (Experiment: GSE29949, Arrays: GSM741192, GSM741193, and GSM741194 (Nayak et al., 2012) and processed by the GEXC. *Itgal* expression (probeset 1435560_at) was compared using the Gene Expression Activity tool, which compares the Normalized Signal Intensity of each microarray and reports it as a percentile of expression relative to a reference panel of 11,939 microarrays. For each probeset, the StepMiner

algorithm analyzes the expression pattern across all microarrays of the reference panel and defines the cutoff between positive (high) and negative (low) expression, which is set as 0%.

Isolation of microglia and monocytes from brains. Mice were euthanized with Euthasol® prior to intracardial perfusion of the circulating blood with ice-cold PBS (Hyclone™, GE Healthcare Life Sciences). Brains and spleens were immediately extracted and placed in 10% FBS in HBSS on ice. Microglial cells were isolated as described (Ford et al., 1995, and Carson et al., 1998) without enzymatic digestion. Briefly, one lobe of the brains was mechanically dissociated with manual chopping, passed through a 23G needle and sequentially forced through a 70µm filter mesh. Myelin was removed using a discontinuous layer 1.03/1.088 g/ml Percoll gradient in HBSS. Mononuclear cells were isolated from the interface, as well as the 1.03g/ml Percoll fraction after the floating myelin disk was aspirated.

Flow cytometry. Dissociated brains or spleens were analyzed on a BD LSR II Flow Cytometer (BD Biosciences), BD FACS Aria II Cell Sorter (BD Biosciences), or a BD Fortessa X20 cytometer. Data were analyzed with FlowJo software (TreeStar). Single-cell imaging flow cytometry was performed on Amnis ImageStreamX® Mark II Imaging Flow Cytometer (EMD Millipore) and data analysis was performed on the IDEAS® software.

Immunofluorescence staining and microscopy. The second lobe of each mouse brain and spleen was drop-fixed in fresh 4% paraformaldehyde immediately after extraction and incubated at 4°C for 12-24 hours. Tissues were stored in 0.05% Sodium Azide in PBS (PBSN) or immersed in 30% sucrose for 24 hours prior to cutting. Floating 40µm sections of frozen brain or spleen tissue were cut on a sliding, freezing microtome (Leica SM 2010R) and stored in 24-well plates in PBSN till further use. For immunofluorescence staining, sections were washed with PBS and treated with AmyloGlo® (Biosensis) to stain ß-Amyloid plaques. Sections were blocked with 10% goat serum

in PBS (blocking buffer) prior to staining with primary antibodies. Primary antibodies were added to sections in blocking buffer and incubated at 4°C overnight. Secondary antibodies were diluted in PBS only and added to sections and incubated for one hour at room temperature. *Tyramide Signal Amplification (TSA)*: CD11a antibody (Clone 2D7, BD Biosciences Cat# 553118) signal amplification was performed using the TSA kit (Invitrogen, #B40933) and manufacturer's protocol. Tissue sections were mounted on charged glass slides with mounting media with or without DAPI. Microscopic analysis was performed on an Olympus FV3000 confocal microscope. It should be noted that brain tissues from each mouse and its controls were mounted on the same slide, imaged with identical microscope settings, treated with identical post-processing in *Adobe Photoshop CS4* to ensure reliable comparisons.

Antibodies. See ***Table 1*** for a full list of antibodies used for flow cytometry (FACS) and Immunofluorescence (IF) imaging. *Technical note*: While all three CD11a antibody clones appeared equally robust by flow cytometry, the 2D7 clone (BD Biosciences, Catalog# 553118) worked best for immunostaining when combined with TSA (described above), though the M17/4 clone was almost as effective.

Intracranial LPS injections. 10µg Lipopolysaccharide (LPS) from *E. coli* 011: B4 strain (Sigma-Aldrich, L4391) was diluted in 30µl sterile PBS and administered intracranially. The injection procedure for is as follows: Isoflurane (4%/min) mixed with oxygen (1L/min) were delivered to animals via an induction chamber. LPS or vehicle (PBS only) was injected into the right hemisphere of the brain using a 26-gauge needle inserted approximately 1 mm directly through the skull i.e. a hole is not drilled through the skull. Vehicle or LPS are generally delivered into ventricles by this method. Animals were analyzed 24 hours post-injection. Unpaired transplanted

5xFAD$^{-/-}$ (WT) littermates with robust chimerism (as described above) were used for these experiments at 6 to 8 weeks of age.

Toxoplasma gondii infection. Type II GFP-expressing *Prugniaud* tachyzoites (Kim et al., 2007) were maintained by serial passage in human foreskin fibroblasts. For infection, parasites were lysed out of host cells by syringe passage and diluted in sterile PBS. C57BL/6 mice or *Cx3cr1*$^{+/GFP}$;*Ccr2*$^{+/RFP}$ double reporter mice were infected by intraperitoneal injection of 200 tachyzoites. Mice were perfused with PBS intracardially and brains removed and fixed in 4% paraformaldehyde at 7 days post-infection for acute infection timepoints. To induce reactivation of latent infection, mice were injected I.P. with 2mg anti-interferon gamma or IgG control antibody (Bioxcell) at 28- and 32-days post infection (dpi). At 38 dpi, mice were perfused and brains were analyzed as described above.

Bone Marrow transplantation in neonatal mice. To generate 5xFAD mice with labeled peripheral immune cells, fluorescently-labeled BM (GFP, RFP or CFP) was transplanted into neonatal (postnatal day 1, P1) 5xFAD$^{+/-}$ (5X) and 5xFAD$^{-/-}$ (WT) littermates. P1 5X and WT littermates were given ≤3.5 Gy (350 Rads) dose of X-ray irradiation (XRAD 320, Precision X-ray). Donor bone marrow was first ckit-enriched by staining with microbead-conjugated ckit antibodies (Miltenyi) and enriched using the positive selection ("possel") setting on an autoMACS (Miltenyi). Each pup was given up to 200,000 ckit+ BM cells from RFP mice via facial vein injection. Pups were placed back with the mother, who was fed an antibiotic chow of Trimethoprim Sulfa (Uniprim, Envigo). After weaning, the recipients were switched to regular chow and genotyped with ear or tail snips. Chimerism was measured through tail vein bleeds at 5 weeks of age and immediately before harvest and confirmed by BM HSC analysis upon tissue harvesting. 5X and WT recipients with similar levels of donor chimerism were paired for comparison.

Fluorescence-Assisted Quantification Technique (FAQT): To quantify relative numbers of immune cell populations in wildtype (WT) and 5xFAD (5X) brains, fluorescently labeled brains were added to each brain sample immediately after harvest and prior to processing. Specifically, each WT sample contained one lobe of a WT brain and one lobe of a fluorescent reporter brain (GFP, RFP, or CFP). The 5X sample was prepared similarly with the remaining lobe of the same fluorescent reporter brain. Thus, each WT and 5X sample pair received equal amounts (one lobe each) of fluorescently labeled brain tissue added to it. The samples were then processed for single cell suspension and myelin removal as described above. During FACS analysis, each cell population was sub-divided into fluorescent or non-fluorescent gates (for example, CFP+ and CFP-). Assuming that each brain sample received an equal number of fluorescent brain cells, the frequency of WT versus 5X populations could then be normalized to one another by comparing to the frequency of that population in the fluorescent cells. To do this, the individual ratios of 5X and WT cell populations in the final sample were obtained by first dividing percentages of CFP- cells (5X or WT) by CFP+ cells, producing the ratios of 5X: CFP and WT: CFP cells, respectively. Next, to obtain the relative changes in diseased mice, the 5X:CFP ratio of each cell population was divided by the WT:CFP ratio. No difference in immune cell populations between WT or 5X mice would result in a relative change of one. To gauge the baseline sensitivity of this method, right and left lobes of WT mice (WT lobe-to-lobe) were processed and analyzed as described above and used as the control group for statistical comparison.

Statistical Analysis. Statistical analysis was performed with GraphPad Prism 5 software (La Jolla, CA).

Table 1		
Antigen, clone (host), fluorochrome	Vendor	Application
CD11a, M17/4 (rat, anti-mouse), PE	Biolegend	FACS
CD11a, 2D7 (rat, anti-mouse), PE	BD Biosciences	FACS
LFA1, H155-78 (rat, anti-mouse), PE	Biolegend	FACS
CD45, 30-F11 (rat, anti-mouse), FITC or APCCy7	Biolegend	FACS
CD11b, M1/70 (rat, anti-mouse), APC	Biolegend	FACS
CD3, 17A2 (rat, anti-mouse), PerCP-eFluor 710	eBioscience	FACS
Gr1, RB6-8C5 (rat, anti-mouse), AF700 or BV605	Biolegend	FACS
CD19, 6D5 (rat, anti-mouse), BV421	Biolegend	FACS
Amylo-Glo RTD, Amyloid Plaque Stain	Biosensis	IF
IgG, Biotinylated (goat, anti-rat)	Vector Labs	IF
AF555 Tyramide SuperBoost kit, Streptavidin	Life Technologies	IF
Iba1 (rabbit, anti-mouse), unconjugated	Wako	IF
CD11a, 2D7 (rat, anti-mouse), unconjugated	BD Biosciences	IF
Goat, Anti-Rabbit, Alexa Fluor 488	Life Technologies	IF
Goat, Anti-Rabbit, Alexa Fluor 647	Life Technologies	IF

CHAPTER 2: CD11A EXPRESSION IN TISSUE RESIDENT MACROPHAGES

Introduction

Tissue resident macrophages (trMacs) are a part of the mononuclear phagocyte system as described by Van Furth and group (van Furth et al., 1972). They were initially thought to be constantly replenished by the bone marrow (BM) derived monocytes, like other members of the mononuclear phagocyte system. Other studies also discovered macrophage and dendritic cells progenitors in the BM that replace adult trMacs of lung called Alveolar macrophages (AVM), after irradiation (Fogg et al., 2006; Naik et al., 2007; Onai et al., 2007). Contradicting studies in Langerhans cells (LC) in the skin and microglia (MG) in the brain did not follow this dogma, and were radio-resistant (Ajami et al., 2007; Ginhoux et al., 2010a; Merad et al., 2002; Mildner et al., 2007). In parabiosis studies, LC, MG and AVMs of two mice showed no evidence of mixing, unlike blood and other tissue macrophage populations (Ajami et al., 2007; Epelman et al., 2014; Guilliams et al., 2013; Hashimoto et al., 2013; Jakubzick et al., 2013). The developmental relationship between BM macrophages and trMacs during homeostasis remains of long-standing interest in developmental hematopoiesis.

Determining the exact origin of trMacs is challenging because hematopoiesis occurs in waves, and in multiple tissues within the embryo body as well as in extra embryonic tissues that are no longer present after birth (Orkin & Zon, 2008). This issue also plagues those interested in the embryonic origins of HSCs and will be explored in Chapter 3. However, a plethora of subsequent research has indicated that most trMacs are derived from erytho-myeloid progenitors (EMPs) originate the embryonic yolk sac at embryonic day (e)7.5 (Ginhoux et al., 2010b; Gomez-Perdiguero et al., 2015; Sheng et al., 2015; Yona et al., 2013). These cells mainly give rise to macrophages that give rise to the second wave of "transient definitive" EMP at e8.5 (Hoeffel et

al., 2015). These EMPs seed various tissues including the fetal liver and are capable of generating a broader range of myeloid cells as well as definitive, enucleated red blood cells and FL monocytes. From e11.5 onwards, the FL becomes the major site of hematopoiesis, including for developing and mature HSCs. The presence of these waves has mystified whether the early EMPs (at e7.5), the late EMPs (e8.5) or the FL monocytes (which peak at e12.5) are the true predecessors of trMacs (Gomez Perdiguero et al., 2015b; G Hoeffel, Chen, Lavin, Low, & Almeida, 2015; Sheng et al., 2015). Is it the same for all tissue? What is the relative contribution of BM-derived monocytes to the trMacs during homeostatic conditions? These questions have spurred three different models (**Figure 2.1**) (Ginhoux & Guilliams, 2016).

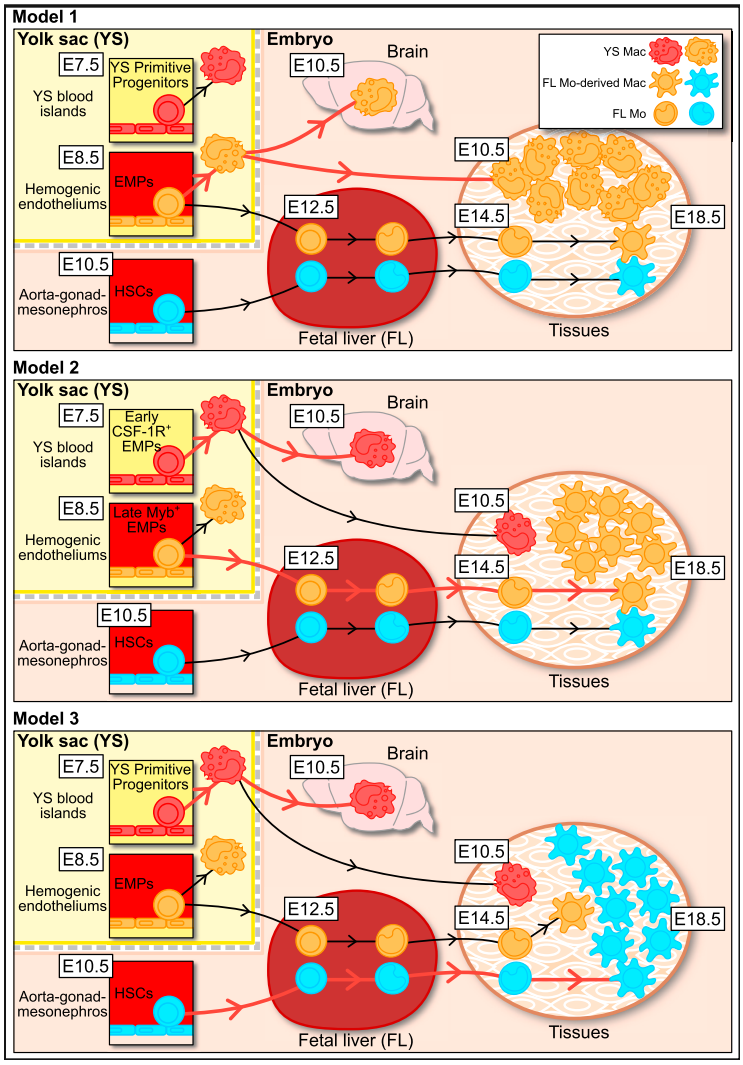

Figure 2.1: Models of trMAC development. Model 1 (top) asserts that EMPs that arise at e8.5 seed the brain, and are precursors to microglia, whearas the contribution of FL monocytes is unlikely. Model 2 (middle panel) shows that microglia come solely from the earlier EMPs that arise at e7.5, whereas other trMacs arise predominantly from e8.5 EMPs, with little contribution from FL monocytes. Model 3 (bottom panel) proposes that most trMacs come from FL monocytes, except microglia. Red lines indicate major path of development, black lines indicate little to no likelihood of possible path of origin. *Image adapted from Ginhoux & Giulliams, 2016.*

Altogether, it has been established that most trMacs arise from HSC-independent EMPS through two major programs. First, early EMPS (e7.5) give rise to YS macrophages without a monocyte intermediate. These are the precursors for microglia (Ajami et al., 2007; Gomez-Perdiguero et al., 2015b). Second, e8.5 EMPs give rise to FL monocytes around e12.5, which give rise to most other trMacs (Sheng et al., 2015). Thus model 3 (**Figure 2.1)** has been established as the current dogma in the field. However, the role of BM-derived macrophage population during inflammation, injury or cancers in tissue repair and return to homeostasis remains elusive. High resolution markers that can distinguish the embryonic-derived, nascent trMacs form infiltrating BM macrophages can help address this issue.

Langerhans Cells (LCs)

Langerhans cells are the skin's first line of defense. LCs are known to migrate to the lymph nodes to present antigen under homeostatic conditions, unlike other trMacs which are generally non-migratory (Doebel et al., 2017). Moreover, LCs are also known as epidermal dendritic cells as they typically express CD11c and are able to activate T cells. Thus, in inflammatory contexts, it becomes difficult to differentiate between these two populations (Wu et al., 2016). However, LCs are maintained by local proliferation in a differentiated state, like conventional trMacs (Chorro et al., 2009; Ghigo et al., 2013; Kierdorf et al., 2013a). LC are typically characterized by their expression of Langerin (CD207) (Valladeau et al., 2000). However, Langerin is not uniquely expressed by LCs in the skin, it is also expressed by dermal dendritic cells. It is also known that LCs are radioresistant, however, during inflammation, multiple studies have shown infiltration of peripheral myeloid populations into the dermis, which mystifies the role of nascent LCs (Merad et al., 2008). Thus, reliable markers that remain on or off in BM-derived myeloid populations would help decipher LC- specific roles in inflammatory contexts in the skin.

Kupffer Cells (KCs)

Kupffer cells reside in the hepatic sinusoid and main innate immune cells of the liver. They make the largest fraction of tissue macrophages in the body. They server as the first line of defense against endotoxins, bacteria derived from the gastrointestinal tract. Additionally, KCs are play roles in the adaptive immune system in recognizing DAMPs, PAMPs by expressing TLRs (Naito et al., 2004). As antigen presenting cells (APCs), they bridge the innate and adaptive immune systems in the liver (Kolios, Valatas, & Kouroumalis, 2006). KCs are made of diverse macrophage precursors, both pro-and anti-inflammatory (Mantovani et al., 2013). Thus, in clinical settings such as liver transplants, the specificity of immune responses depends on amount of replacement from BM populations (Klein et al., 2007). Mixed evidence has been presented in terms of the ontogeny of KCs. Ginhoux and colleagues have shown that KCs are populated by EMPs before birth, while others have shown that BM-derived cells can also differentiate into KCs (Ginhoux & Jung, 2014; Klein et al., 2007). Therefore, markers that distinguish BM-derived KCs can demarcate the specific function recruited cells play in transplantation, cirrhosis and other inflammatory contexts.

Alveolar Macrophages (AVMs)

AVMs are the most abundant innate immune cells in the lung and allocated along the luminal surface of the alveolar space. They are the first line of defense against pathogens and pollutants and help initiate immune responses. Their main local function involves the clearance of surfactant, lubricates the lungs. The ontogeny of AVMs is different from other tissue resident cousins, as the alveolar niche does not exist until birth (Gibbings et al., 2017; Joshi, Walter, & Misharin, 2018). The first breath of a newborn is what establishes the first niche for this immobile AVMs. Therefore, EMPs and FL monocytes may populate the lung during embryogenesis, but the true source of AVMs remains elusive. Fate mapping studies have shown that AVM populations

proliferate locally without contribution from BM populations (Hashimoto et al., 2013; Sheng et al., 2015; Yona et al., 2013). However, it is still possible that during postnatal lung growth, as embryonic macrophages seed the newly forming alveoli, the empty niche is then occupied by BM monocytes (Rodero et al., 2015; Westphalen et al., 2014). Thus, markers that can distinguish BM derived AVM population can help delineate functional consequence these cells may have during inflammation or injury.

In Chapter 1, we established CD11a as a marker that can distinguish microglia from peripheral BM derived cells in steady state and inflammatory contexts (Shukla et al., 2018). In this short chapter, we explore the expression pattern of CD11a in lung AVMs, epidermal LCs as well as liver KCs.

PRILIMINARY RESULTS

To determine whether trMac populations, besides microglia, LC, KC, and AVM were harvest from steady-state Lyve1$^{Cre/+}$; R26$^{mTmG/+}$ mice. This is a yolk-sac specific mouse reporter that begins labeling YS endothelial cells at e9.5, as well as hematopoietic cells within the embryo (Pham et al., 2010). This reporter has been previously reported to mark yolk sac definitive hematopoiesis but bypasses primitive erythropoiesis. This system labels 40% of all EMPs in the YS at e9.5. This reporter also labels a third of all HSCs in adult mice. (Lee et al., 2016). To determine adult trMac populations expressed CD11a, we harvest LCs, KCs, and AVMs from 3-month-old mice. KCs and AVMs were defined as CD45+, Ly6C-, Ly6G-, F4/80+ and CD206+. Indeed, 97.3% of KCs we CD11a- (**Figure 2.2A,** left panel). However, AVM had bimodal expression of this marker (**Figure 2.2A,** right panel). Langerhans cells were defined as CD45+, F4/80+, CD207+. In the LC compartment, 97.6% of cells were CD11a- (**Figure 2.2B**). Thus, LCs and KCs , but not AVMs, can be distinguished from BM-derived cells using CD11a.

Figure 2.2

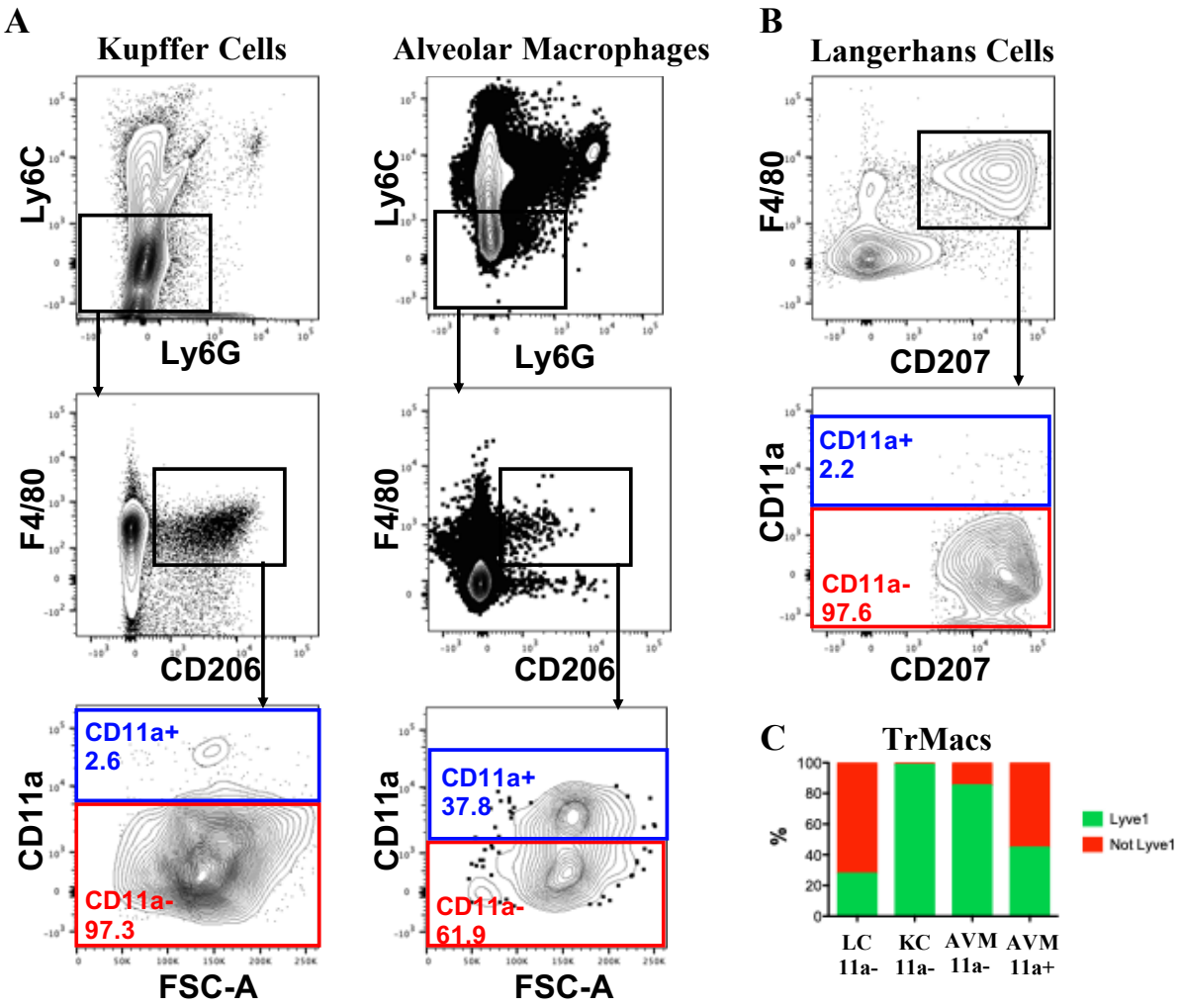
A
Kupffer Cells
Alveolar Macrophages
B
Langerhans Cells
Ly6C
Ly6G
F4/80
CD206
CD11a
FSC-A
CD207
CD11a+
2.6
CD11a-
97.3
CD11a+
37.8
CD11a-
61.9
CD11a+
2.2
CD11a-
97.6
C
TrMacs
%
Lyve1
Not Lyve1
LC
11a-
KC
11a-
AVM
11a-
AVM
11a+

Figure 2.2: CD11a is not expressed in steady state Kupffer or Langerhans cells, while its expression is bimodal in Alveolar macrophages. (A) Representative plots of CD45+, live cells isolated from liver (left panel) and lung (right panel). KCs and AVMs (Ly6C-, Ly6G-, F4/80+ and CD206+) were further gated on for CD11a expression (CD11a-, red gate; CD11a+, blue gate). (B) Representative plots of CD45+, live cells isolated from the epidermis. LCs were defined as F4/80+, CD207+ and were further gated on for CD11a expression as stated above. (C) Bargraphs show trMac populations that are Lyve1-derived (green) and others (red). On CD11a- KC and LCs were shown as they represent a majority of the cell population. Both, CD11a- and CD11a+ fraction of AVMs are depicted. BM HSCs are approximately 30% labeled (data not shown).

To determine whether the YS specific reporter could ascertain the source of these trMac populations were also analyzed for CD11a expression. As has been previously reported, approximately 30% of all peripheral blood cells are Lyve1-derived and labeled by this reporter (Lee et al., 2016). Within the trMac populations, we analyzed that CD11a- cells only for LC and KC, as they represented a majority of the population. Interestingly, these two populations had very different labeling outcomes. LC labeling matched that of peripheral blood monocytes, and EMPs at about 30%, however, KC were almost entirely Lyve1-derived (**Figure 2.2C**). Moreover, the CD11a+ and CD11a- AVM fractions also had very different labeling. The CD11a- fraction was nearly 90% Lyve1 derived, whereas the CD11a+ represented only 50% Lyve1-derived cells (**Figure 2.2C**). Overall, CD11a is not expressed in microglia, Langerhans cells and Kupffer cells, but is expressed in some alveolar macrophages.

Most markers alter expression during inflammation. Thus, it is imperative to determine whether CD11a expression patterns are sustained after immune challenge. One way to demarcate BM-derived cells is using bone marrow chimeras. Here, we use WT mice that were transplanted with GFP bone marrow (**Figure 2.3A**). In this system, all BM-derived cells will be GFP+, which can help us analyze whether these cells also continue to express CD11a. TrMac populations were analyzed one year after transplantation. As expected, LC in these mice remained CD11a- (**Figure 2B**, top left bargraph). We also observed that some CD207+ cells were CD11a+, however, many of these cells were also GFP+, indicating that they are bone marrow derived (**Figure 2.3B,** bottom left bargraph). Though further analysis is required, some CD11a+ cells were not GFP+. These cells may account for dermal dendritic cells and host bone-marrow derived macrophages that may be present in the epidermis.

Figure2.3

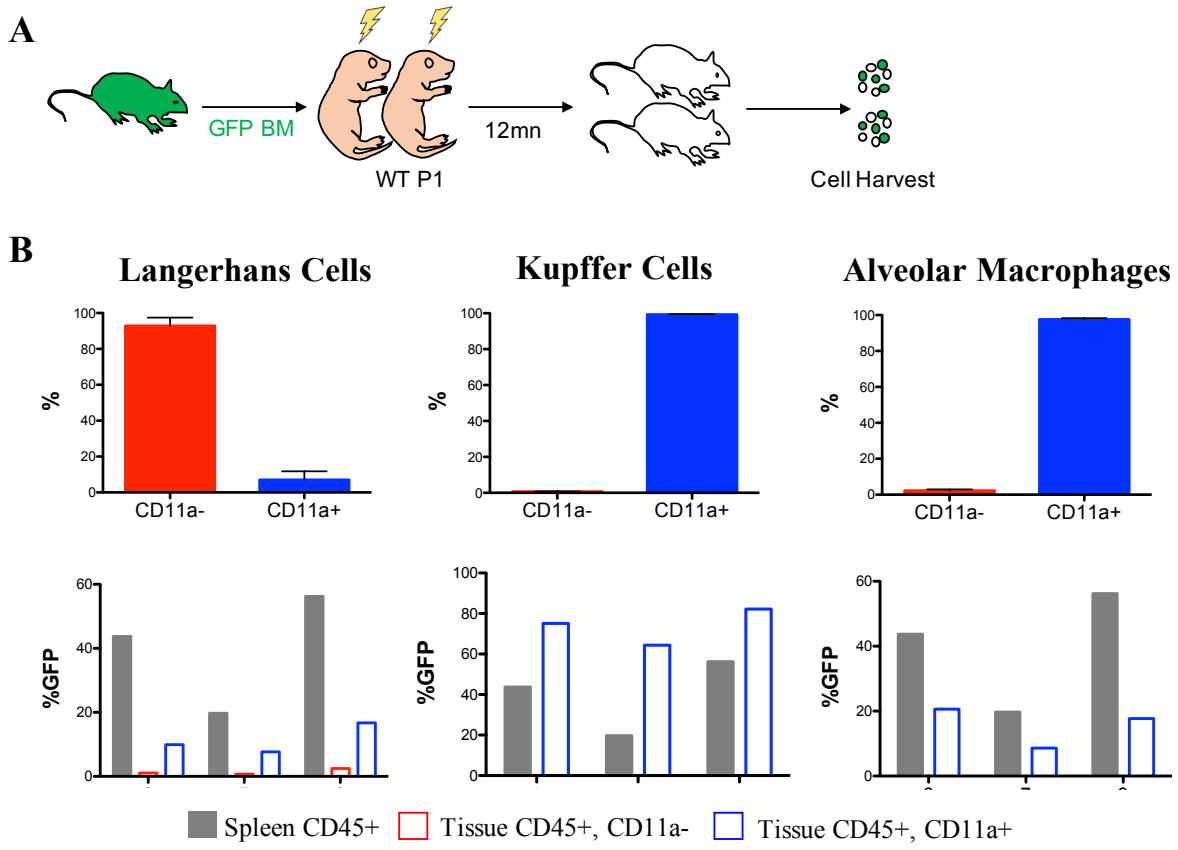

Figure2.3: CD11a can distinguish bone marrow derived cells after irradiation. (A) Schematic of neonatal transplantation. Ckit+ GFP BM was transplanted into irradiated newborn WT mice. Tissues were harvested one year after transplant. (B) CD11a expression in trMacs (top panels, n=3 mice) and percentage of GFP chimerism (bottom panels, 3 individual mice shown) in spleen (grey bars) to display peripheral chimerism, CD11a- fraction (red bargraph, where applicable) and CD11a+ fraction (blue bargraph).

Surprisingly, all KCs were CD11a+ (**Figure 2.3B,** top middle bargraph). Additionally, most of these cells were also GFP+, BM-derived cells (**Figure 2.3B,** bottom middle bargraph). Thus, it is likely that KC are not resistant to irradiation, and we completely replace by bone marrow-derived cells. AVM were also mostly CD11a+ (**Figure 2.3B,** top right bargraph), but were not as highly replenished by the bone-marrow (bottom right bargraph). Thus, CD11a expression is reliable for radioresistant trMacs, like Langerhans cells and microglia. While depleted Kupffer cells are replenished by bone-marrow derived cells, the alveolar macrophages may be repopulated by an alternative source.

DISCUSSION

Langerhans cells remain CD11a-, despite possible activation due to irradiation. Activation in severe inflammatory contexts and disease models has yet to be confirmed. In regards to their ontogeny, and inducible Lyve1 system can perhaps be more informative. Inducing Lyve1 labeling after e11.5, when its expression in FL peaks can help target trMacs that are exclusively derived from FL monocytes. Additionally, inducing Lyve1 labeling when its expression first begins in the YS at e9.5, can help trace trMac populations that are derived from EMPs that emerge at e8.5. While CD11a may be useful in distinguishing LCs during steady-state conditions, the presence of few CD11a+ cells may also indicate low BM replacement. It has been shown that LC are radioresistant (Merad et al., 2002). However, despite irradiation, the level of CD11a+ cells only increase from 2% in steady-state to <10% in chimeric mice. Moreover, it is also possible that increased numbers dendritic cells are also included in this CD11a+ populations, given the low levels GFP chimerism in this population. Together, it can also be concluded that BM-derived cells have a relatively low contribution in the total Langerhans cell compartment.

Kupffer cells were mostly CD11a- in steady state conditions. After irradiation, they were mostly CD11a+. However, given the percentage of GFP chimerism, it can be concluded that host KCs did not survive irradiation and the niche was filled by GFP+ bone-marrow derived cells. Lyve1 labeling within KC compartment corroborates existing data that most KCs are derived by FL monocytes (Guillaume Hoeffel et al., 2015; Sheng et al., 2015), that were then irradiated due to irradiation at birth. Thus, CD11a expression must be further examined in non-irradiated mice that have been challenged, such as with LPS.

Trends of CD11a expression in alveolar macrophages were most complex. Under steady state conditions, CD11a+ and CD11a- AVMs were found. This may fit the paradigm where fetal derived, possibly CD11a-, AVMs migrate towards developing alveoli and BM derived monocytes are recruited to fill the empty niche in the existing ones (Joshi et al., 2018; Rodero et al., 2015; Westphalen et al., 2014). Lyve1 labeling in the CD11a+ AVMs was comparable to HSC labeling, which further supports this model. Therefore, further fate mapping analysis is required to determine the exact source(s) of AVMs. Like KCs, all AVMs were CD11a+ after irradiation. Interestingly, their GFP chimerism was not as high as peripheral chimerism. This can have two possible explanations. First, the putative nascent AVMs (CD11a- fraction) upregulates CD11a expression after irradiation. Or, second, it is possible that there is another host-derived source that repopulates these cells, which is not BM-derived. Follow up analysis of AVMs at different stages of lung development may help address this question. If embryonic derived AVMs are constantly migrating toward younger alveoli, analysis in aged mice should show diminishing CD11a- fraction of AVMS.

In this preliminary analysis, we have shown an incredible range of CD11a expression within trMac population in steady state and in chimeric mice. Thus, further analysis in steady-state

as well as inflammation contexts is necessary. Each trMac population must be carefully manipulated to gain insight into their patterns of CD11a expression. It is possible, that a complete picture of CD11a expression may reveal clues about the source of each of these populations. More importantly, however, CD11a can be an effective tool to study the contribution of BM-derived cells in steady-state and inflammatory contexts within each tissue.

MATERIALS AND METHODS

Lyve1$^{Cre/Cre}$ (Pham et al., 2010) mice were mated with Rosa26$^{mTmG/mTmG}$ (Muzumdar et al., 2007) and harvest at 3 months of age.

Epidermal cell harvest. Mice were shaved fully on their backs and sprayed Spray the shaved region with 70% ethanol. Back skin was cut without penetrating the peritoneum. Fat that connecting the skin to the peritoneum was removed at this time. Skin was pinned epidermis side down and excess fat from dermis was removed using a razor blade. Skin was cut into smaller pieces and treat topically with 5mls of 0.25% Trypsin without EDTA. This was incubated at 37° for 1 hour without CO_2 (in a bacterial incubator). Trypsin was deactivated, epidermal cells were scrapped off, washed and stained for FACS analysis.

Liver and Lung harvest. Liver and lung were harvests, cut into smaller pieces, and placed in 70μm cell strainer. The strainer with tissue was places in a 6-well plate. 5mls of harvest media (5mg/ml Collagenase IV, 10U.ml DNase II, RPMI) were pipetted into each well. Tissues were incubated for 37° for 30 minutes without CO_2 (in a bacterial incubator). After incubation, tissues were passed through the strainer using a plunger of a 3ml syringe. Media with cells was transferred to 15ml conical tube containing FACs buffer and spun at 1000 rpm for 15 minutes. Tissues were washed with PBS only and spun again. Supernatant was decanted and resuspended

in 40% Percoll. Cells were than overlay on 70% Percoll layer to for percoll gradient. Cells were spun at 2500rpm for 30mins without brakes. Cells were extracted from the interface with that contains mononuclear cells and resuspended in FACS buffer. Cells were washed once more in FACS buffer and stained for FACS analysis.

Bone Marrow transplantation in neonatal mice. To generate chimeric mice with labeled peripheral immune cells, fluorescently-labeled BM (GFP) was transplanted into neonatal (postnatal day 1, P1) C57BL6/J mice that were given ≤3.5 Gy (350 Rads) dose of X-ray irradiation (XRAD 320, Precision X-ray). Donor bone marrow was first ckit-enriched by staining with microbead-conjugated ckit antibodies (Miltenyi) and enriched using the positive selection ("possel") setting on an autoMACS (Miltenyi). Each pup was given up to 200,000 ckit+ BM cells from GFP mice via facial vein injection. Pups were placed back with the mother, who was fed an antibiotic chow of Trimethoprim Sulfa (Uniprim, Envigo). After weaning, the recipients were switched to regular chow and genotyped with ear or tail snips. Chimerism was measured through tail vein bleeds at 5 weeks of age and immediately before harvest and confirmed by splenocyte analysis upon tissue harvesting.

CHAPTER 3: EXTRA-EMBRYONIC MESODERM-DERIVED HEMATOPOIETIC STEM CELLS

INTRODUCTION

The mechanisms of hematopoietic stem cells (HSCs) emergence during development, including which tissues produce the first HSCs in the embryo, remain contentious in the field. HSCs. There is general consensus in the field that the first blood cells appear in the yolk sac (YS) around embryonic day 7.0 (e7.0). However, these cells are a part of the "primitive" hematopoietic wave and lack characteristics such as engraftability, multipotency and the ability to self-renew over a lifetime. These are the defining characteristics of HSCs, which arise during the definitive hematopoietic wave around e11.5, from embryonic precursors, or pre-HSCs. Pre-HSCs can be found in the aorta-gonad-mesonephros (AGM), the fetal liver (FL), as well as the YS and placenta starting at e10.5 (Taoudi et al., 2008). However, circulation begins at e8.5. Thus, the origin of these HSC predecessors remains unclear as they are in circulation.

While there is robust evidence suggesting that pre-HSCs emerge *de novo* from the ventral wall of the dorsal aorta in the AGM, it relies on the transplantation of *ex vivo* tissues explants of the dorsal aorta (J. Bertrand et al., 2010; Cumano et al., 2001). Other studies include evidence of time-lapse imaging of the dorsal aorta in zebrafish embryos and mouse dorsal aorta sections cultured *in vitro* (J. Bertrand et al., 2010; J.-C. Boisset et al., 2010; Kissa & Herbomel, 2010). This phenomenon of endothelial to hematopoietic transition (EHT) is attributed to specialized group endothelial cells called hemogenic endothelium. More recently, transplantation of cultured pre-circulation embryos, where YS has been removed, also attributed definitive HSC activity to embryonic sources like AGM (Ganuza et al., 2018). However, *in vivo* evidence also suggests that HSCs and their precursors originate in extraembryonic sources, like YS and PL, which are no longer present at birth. Lineage tracing studies using a tamoxifen-inducible *Runx1-CreER* reporter

showed HSC labeling, where Cre induction took place when *Runx1* was expressed only in the YS (Samokhvalov et al., 2007). However, *Runx1* is expressed in all hematopoietic cells, which can confound conclusions if tamoxifen lingers when *Runx1* turns on within the embryo proper. Evidence for the placenta as the site for HSC development has also been presented (Lee et al., 2016; Lee et al., 2010; Mikkola et al., 2005; Ottersbach & Dzierzak, 2005). Additionally, in *Ncx1* knockout embryos that lack circulation and die at e10.5, all hematopoietic cells are found in the YS and PL (Lux et al., 2008; Rhodes et al., 2008). Thus, concluding whether the yolk sac and other extra-embryonic tissues give rise to adult HSCs has been difficult.

However, the field generally agrees that YS can give rise to some definitive hematopoietic populations. Definitive, erythro-myeloid progenitors (EMPs) are required for the sustenance of the developing embryos until fully mature HSCs can take over the total hematopoietic output in the mouse. EMPs originate in the YS at e8.5 in a myb-independent manner, a transcription factor that is required for HSC development (Gomez Perdiguero et al., 2015a; Guillaume Hoeffel et al., 2015; McGrath et al., 2015; Schulz et al., 2012). Unlike definitive HSCs, EMPs are not engraftable in the adult, they do show transient erythroid potential (McGrath et al., 2015). However, most tissue-resident macrophages, such as microglia in the brain and Langerhans cells in the epidermis are derived from EMPs (Ginhoux et al., 2010; Gomez-Perdiguero et al., 2015; Gomez-Perdiguero et al., 2015; Sheng et al., 2015). Thus, the exact contribution of tissues like the yolk sac and the placenta in definitive hematopoietic cells, especially pre-HSCs and HSCs must be established.

A tamoxifen-inducible *HoxB6-CreER* reporter can address whether any HSCs are derived from extra-embryonic mesoderm (EEM) in tissues like the yolk sac, placenta as well as the vitelline vessels (Nguyen et al., 2009). *HoxB6* is a homeobox gene that is expressed in all of mesoderm, thus a *HoxB6-Cre* reporter has been previously shown to label all blood cells (Zovein et al., 2010).

However, *HoxB6* is first expressed in the EEM at e7.5. Its expression in the embryonic mesoderm (EM) starts at e8.5 (Lowe et al., 2000). This window, where *HoxB6* expression is localized to the EEM, can be utilized to trace hematopoietic stem cells in the adult that arose there.

Through timed and paired mating, as well as the use of active metabolite of tamoxifen, 4-hydroxytamoxifen (4OHT), we show that extra-embryonic sources do contribute to primitive and definitive hematopoietic cells. At timepoints of 4OHT injection when labeling is restricted to the yolk sac and placenta within the embryos, we see HSC labeling in the adult counterparts. These HoxB6- derived HSCs consistently give rise to all lineages of adult blood cells, are long lived, and have similar engraftability and lineage potential upon transplantation as their non HoxB6-derived counterparts. Additionally, our data also indicates that EMPs and tissue resident macrophages are not HoxB6-derived. Thus, *HoxB6-CreER* reporter provides evidence for extra-embryonic sources of hematopoietic stem cells.

RESULTS

HoxB6 is expressed in the extra-embryonic mesoderm tissues before embryonic mesoderm.

Pregnant females from HoxB6 and mTmG crosses were injected with single 4OHT injections to induce Cre expression while HoxB6 expression is on. Embryos were always harvested at e10.5 for flow cytometry and immunohistochemistry (**Figure 3.1A**). In t6.5 and t7.0 embryos, where tamoxifen is injected at e6.5 and e7.0, respectively, GFP labeling is only observed in tissues of the EEM, namely YS, PL, umbilical as well as the vitelline arteries (**Figure 3.1B** left panel**, 3.2A, 3.2B** left panel**).** There is no visible GFP in the body of t7.5 embryos (**Figure 3.2C**). GFP labeling in the embryo body is observed in the isthmic organizer (head region), and limb and tail buds of t8.5 embryos (**Figure 3.1B** right panel**, S1B** right panel). The presence of GFP within the

Figure 3.1

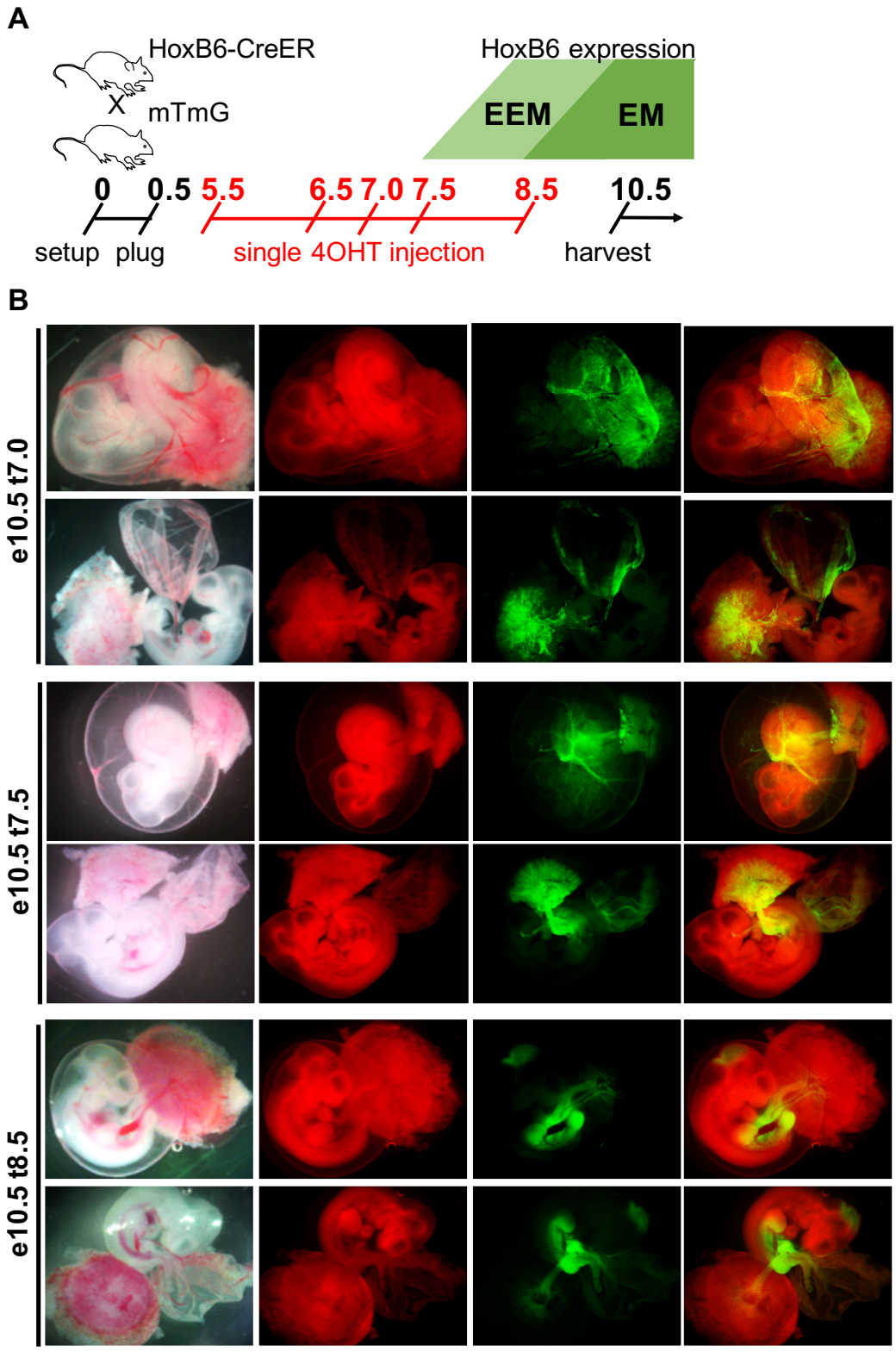
A
HoxB6-CreER
X
mTmG
HoxB6 expression
EEM
EM
0
0.5
5.5
6.5
7.0
7.5
8.5
10.5
setup
plug
single 4OHT injection
harvest
B
e10.5 t7.0
e10.5 t7.5
e10.5 t8.5

Figure 3.1: HoxB6 expression in EEM precedes EM. (A) Schematic of timed breeding strategy, Cre induction using single 4OHT injections at various timepoints, and harvest at embryonic day 10.5. (B) Dissecting scope images of e10.5 embryos injected with 4OHT at e7.0 (top) and e7.5 (middle) and e8.5 (bottom). At t7.0 labeling is restricted to EEM tissues like YS, PL, umbilical artery (not shown) and vitteline artery (VV). At t7.5 both vitelline vessels are labeled, placental and yolk sac labeling peaks at this timepoint. At t8.5 labelling of EM within limb buds and head, in addition to both umbilical vessels and vitelline vessels is observed. Diminished labeling is seen in the PL and YS.

embryo was also ascertained using sagittal sections. No labeling is seen within or near the dorsal aorta of t7.0 embryos (**Figure 3.1C left**), whereas extensive labeling is observed near the dorsal aorta (DA), from forelimb bud to tail bud regions of the t8.5 embryo (**Figure 3.1C** right panel**, 3.2D**). Immunofluorescence staining of YS and AGM also revealed that only CD31+ endothelial cells in the YS are labeled at t7.0 embryos, and no labeling is seen within the endothelial cells of the DA (**Figure 3.1D,** top two panels). In t8.5 embryos, CD31+ cells within YS and AGM are robustly labeled with GFP (**Figure 3.1D,** bottom two panels). Thus, with early injections (t6.5 and t7.0) we can achieve labeling exclusively within tissues of the EEM. While t7.5 injections result in some labeling of endothelial cells in the AGM, it also robustly labels all EEM tissues as well. In t8.5 embryos, robust labeling was observed within EM, including in the AGM.

HoxB6 labels endothelial cells and definitive hematopoietic populations.

To quantify the amount of labeling within each tissue, the YS, PLU, VV, AGM and FL were dissected as described above and analyzed using flow cytometry. We quantified each embryonic population by absolute cell number per embryo for determining the abundance of each cell type in each tissue as well as percentage of GFP cells to determine overall labeling of each population by the reporter. GFP+ endothelial cells (**Figure 3.3A,** Ter119-, CD43+, CD144+, CD31+; ECs), which may include hemogenic endothelium, were most abundant in YS and PLU in t6.5, t7.0 and t7.5 by absolute cell count estimates per embryo (**Figure 3.3B** left panels, **3.4A)**. Overall labeling in ECs was significantly higher within YS and PLU in t6.5 and t7.0 embryos compared to AGM and FL, where little to no labeling was detected (**Figure 3.3B** right panels, **3.4A**). Together, the absolute cell numbers of GFP+ EC indicate that the YS and PLU are

Figure 3.2

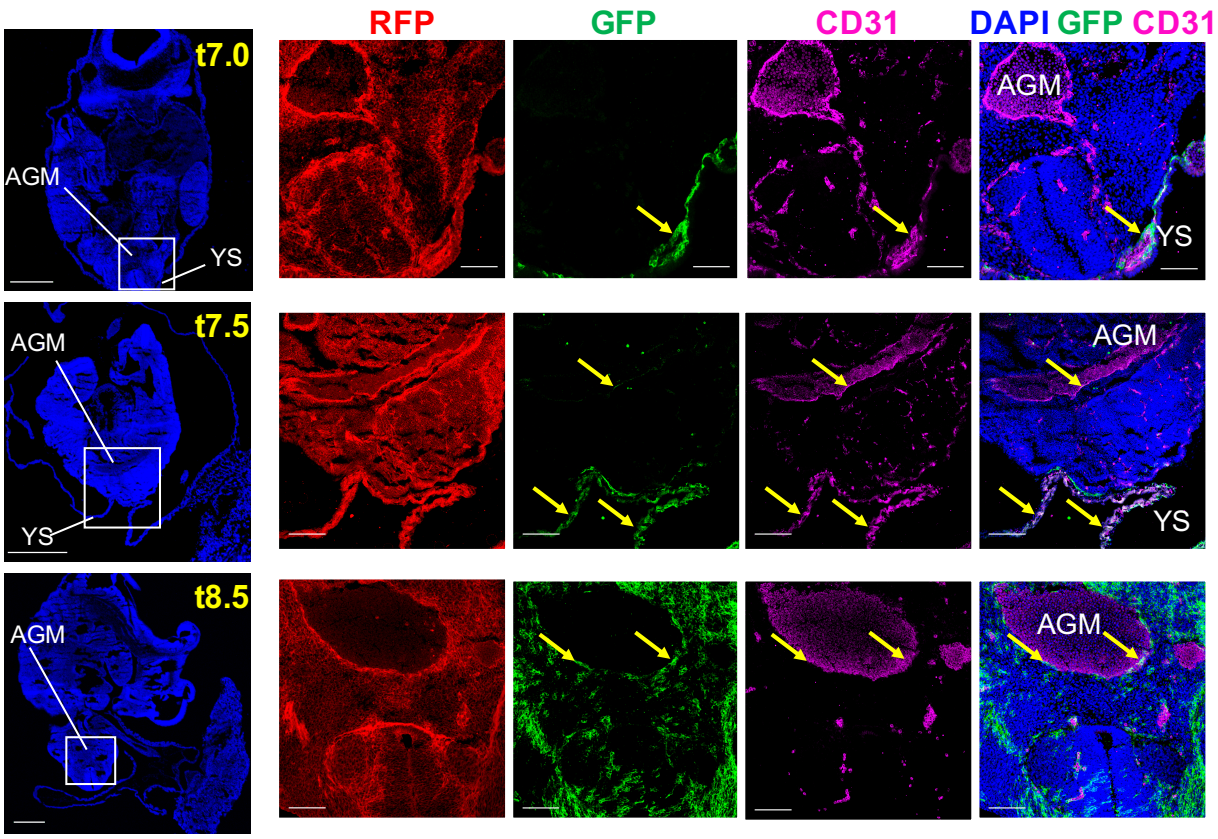

Figure 3.2: Immunofluorescence images reveal EEM specific labeling prior to e7.5. DAPI images of transverse or sagittal sections of whole embryos at t7.0 (top row), t7.5 (middle row), t8.5 (bottom row). GFP labeling within CD31+ endothelial cells (yellow arrows) begins in the YS at t7.0 (top row). Labelling within the AGM begins at t7.5 (middle row), and peaks at t8.5 (bottom row). For DAPI only images scale bar =1000µm. All other scale bars = 200µm.

labeled in this system, with a decline in YS labeling in t8.5 embryos (**Figure 3.3E** left panel). This data also indicates that labeling is restricted EEM tissues t6.5, t7.0 and t7.5 embryos.

Next, we examined primitive hematopoietic cells, which originate in yolk sac blood islands at e7.5. Primitive red blood cells (pRBCs) were differentiated from maternal blood cells using Ter119 expression and higher forward scatter (**Figure 3.4E,** top panel, red gates). GFP+ pRBCs were highly abundant in YS and PLU in all cases (**Figure 3.4E,** middle panel) with highest labeling in t7.0 embryos (**Figure 3.4E,** bottom panel).

We also examined whether definitive hematopoietic populations were also labeled in this system. GFP+ hematopoietic cells (Ter119-, CD43+, CD144+/-) were present at significantly higher levels in the YS and PL in t7.0 and t7.5 embryos. This trend is consistent with the higher level of endothelial cell labeling in these embryos. The labeling of these circulating cells was expectedly consistent within all tissues at all timepoints (**Figure 3.3C, 3.4B**). Within the hematopoietic compartment, we putative hematopoietic precursors of HSCs, defined as Ter119-, CD43+, Ckit+, Sca1+, CD144+, CD11a- (Karimzadeh et al, 2019 unpublished data), which we call $11a^-$ KLS. In all cases, $11a^-$ KLS cells most abundant in the YS and PL (**Figure 3.3D, 3.4C** left panels. Moreover, in t7.0 embryos, the percentage of $11a^-$ KLS cells in PL significantly higher. GFP- labeled HCs and $11a^-$ KLS cells are also most abundant in the YS and PLU (**Figure 3.3E,** middle. right panels). Additionally, the number of labeled HCs and $11a^-$ KLS cells also declines in t8.5 embryos, indicating that HoxB6 reliably labels hematopoietic cells that originate in the EEM.

Figure 3.3

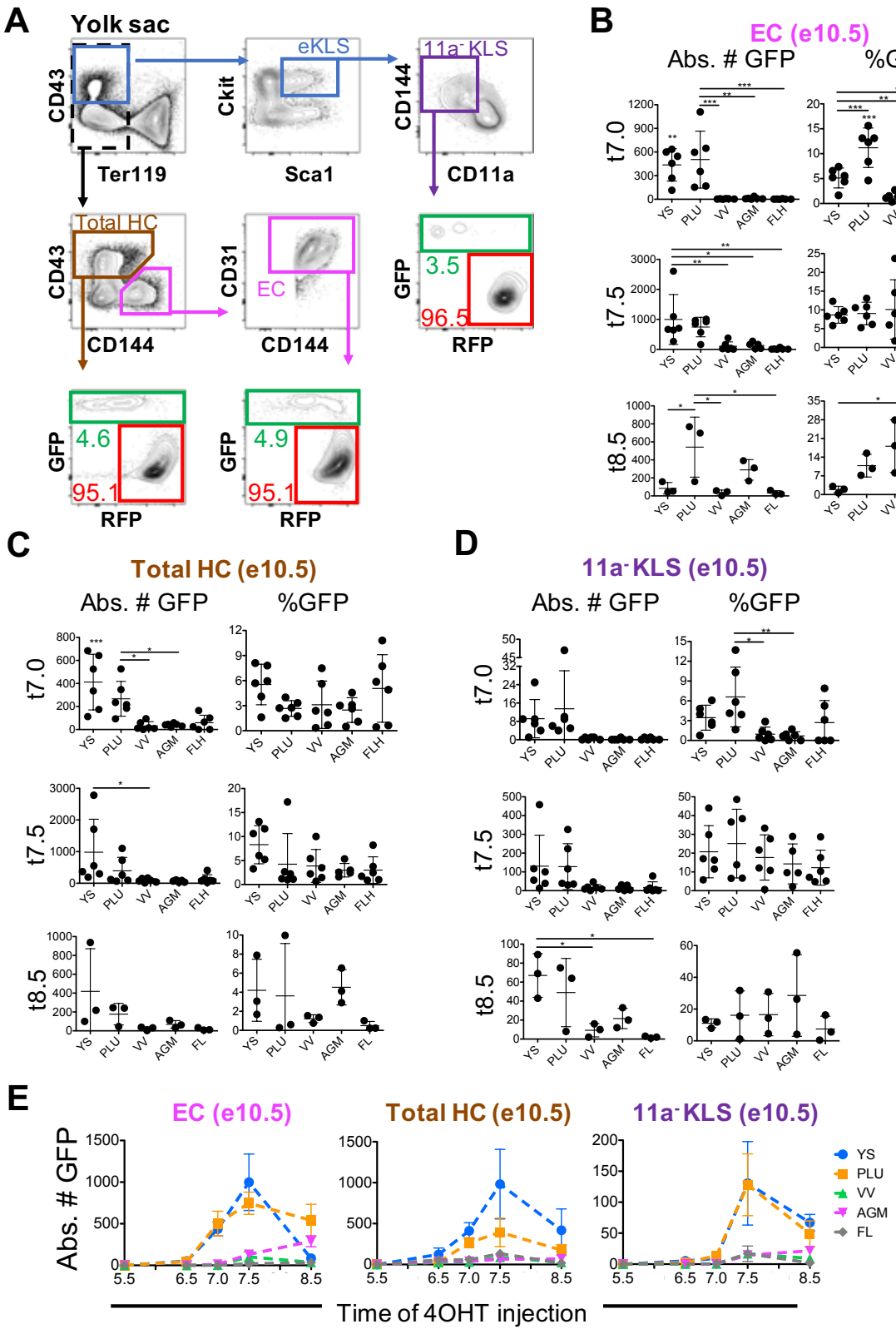
A
Yolk sac
CD43
Ter119
Ckit
eKLS
Sca1
CD144
11a-KLS
CD11a
Total HC
CD43
CD144
CD31
EC
CD144
GFP
3.5
96.5
RFP
GFP
4.6
95.1
RFP
GFP
4.9
95.1
RFP
B
EC (e10.5)
Abs. # GFP
%GFP
t7.0
t7.5
t8.5
YS
PLU
VV
AGM
FLH
FL
C
Total HC (e10.5)
Abs. # GFP
%GFP
t7.0
t7.5
t8.5
YS
PLU
VV
AGM
FLH
FL
D
11a-KLS (e10.5)
Abs. # GFP
%GFP
t7.0
t7.5
t8.5
YS
PLU
VV
AGM
FLH
FL
E
EC (e10.5)
Total HC (e10.5)
11a-KLS (e10.5)
Abs. # GFP
5.5
6.5
7.0
7.5
8.5
Time of 4OHT injection
YS
PLU
VV
AGM
FL

Figure 3.3: EEM-specific labeling is achieved in e10.5t7.0 embryos. (A) Representative flow cytometry gating strategy of endothelial and hematopoietic populations in the yolk sac at e10.5. (B) GFP+ Endothelial cell (EC; $Ter119^-$, $CD43^-$, $CD144^+$, $CD31^+$) labeling in all tissues after Cre induction at e7.0 (top row), e7.5 (middle) and e8.5 (bottom row) with single injections of 4OHT. GFP+ ECs are present in higher numbers (left column) in EEM tissue like YS and PL after e7.0 and e7.5 inductions. Absolute number (bottom left) and overall percentage of GFP+ ECs increases in the AGM at t8.5. Asterisk above any one tissue indicates similar degree of significance compared to AGM and FL (for example, absolute cell number of GFP+ ECs YS at t7.0 is significant than AGM and FL, $p < 0.005$ for each) (C) GFP+ total hematopoietic cells (HC; $Ter119^-$, $CD43^+$) are prevalent in EEM tissues at all time points. (D) GFP+ embryonic precursors of HSCs ($11a^-$KLS; $CD43^+$, $Ter119^-$, $cKit^+$, $Sca1^+$). Most labeled cells are within EEM tissues. (B-D) Statistical significance was determined with one-way ANOVA and Tukey's post test comparison. (E) Absolute cells numbers of labelled EC, Total HC, and $11a^-$KLS populations are shown for all timepoints of Cre induction with single 4OHT injections. No labeling is observed at t5.5 injections anywhere within the embryo. Few labeled hematopoietic cells are found only in YS and PL at t6.5. EC labeling is restricted to YS and PL at t7.0 indicating exclusive EEM labeling. Labeling of ECs within the AGM begins at t7.5 and surpasses YS labeling at t8.5.

HoxB6 labels all adult blood lineages as well as long-term hematopoietic stem cells.

To examine whether HoxB6 derived cells contribute to adult hematopoiesis, HoxB6$^{Cre/+}$; R26$^{mTmG/+}$ mice were allowed to be born after single 4OHT injections (**Figure 3.5A**). Mice were bled every 4 weeks to determine the amount of labeling in PBMCs. In t7.0 mice, where labeling is restricted to EEM in embryos (**Figure 3.1B, 3.1D**), two percent of all blood lineages were labeled consistently for 12 weeks (**Figure 3B**). Regardless of the time point of 4OHT injections, no lineage bias was observed in the GFP+ blood cells, with a maximum of 40% of peripheral blood being labeled starting at t7.5 (**Figure 3.5C, 3.4B**).

The lack of lineage bias and consistent levels of labeling for twelve weeks pointed to the presence of long-term hematopoietic stem cells (HSCs). Thus, we examined the bone marrow compartment to quantify whether HSCs, defined as CD27+, Ckit+, Sca1+, CD150+, CD34- cells, were GFP+ (**Figure 3.5D**). Indeed, labeling of HSCs begins in t6.5, t7.0 and peaks in t7.5, similar to the peripheral blood levels (**Figure 3.5E**). Together, these data provide a strong argument that HoxB6 derived HSCs originated in the tissue of EEM, like the placenta and the yolk sac.

EEM-derived HSCs are self-renewing and engraftable, like those derived from AGM.

In addition to being multipotent, bona fide HSCs are also capable to homing to the bone marrow niche upon transplantation. To compare the engraftability of HoxB6-derived HSCs with other HSCs, whole bone marrow from HoxB6$^{Cre/+}$; R26$^{mTmG/+}$ mice was transplanted into irradiated C57BL/6J adult mice (**Figure 3.6A**). Recipients were bled every four weeks for a twelve-week period to ensure engraftment, long term self-renewal and multipotential of transplanted HSCs. HoxB6-derived cells were represented in all blood lineages and at normal distributions even at 12 weeks (**Figure 3.6B**). This data strongly indicated that HoxB6 derived HSCs were self-renewing

Figure 3.4

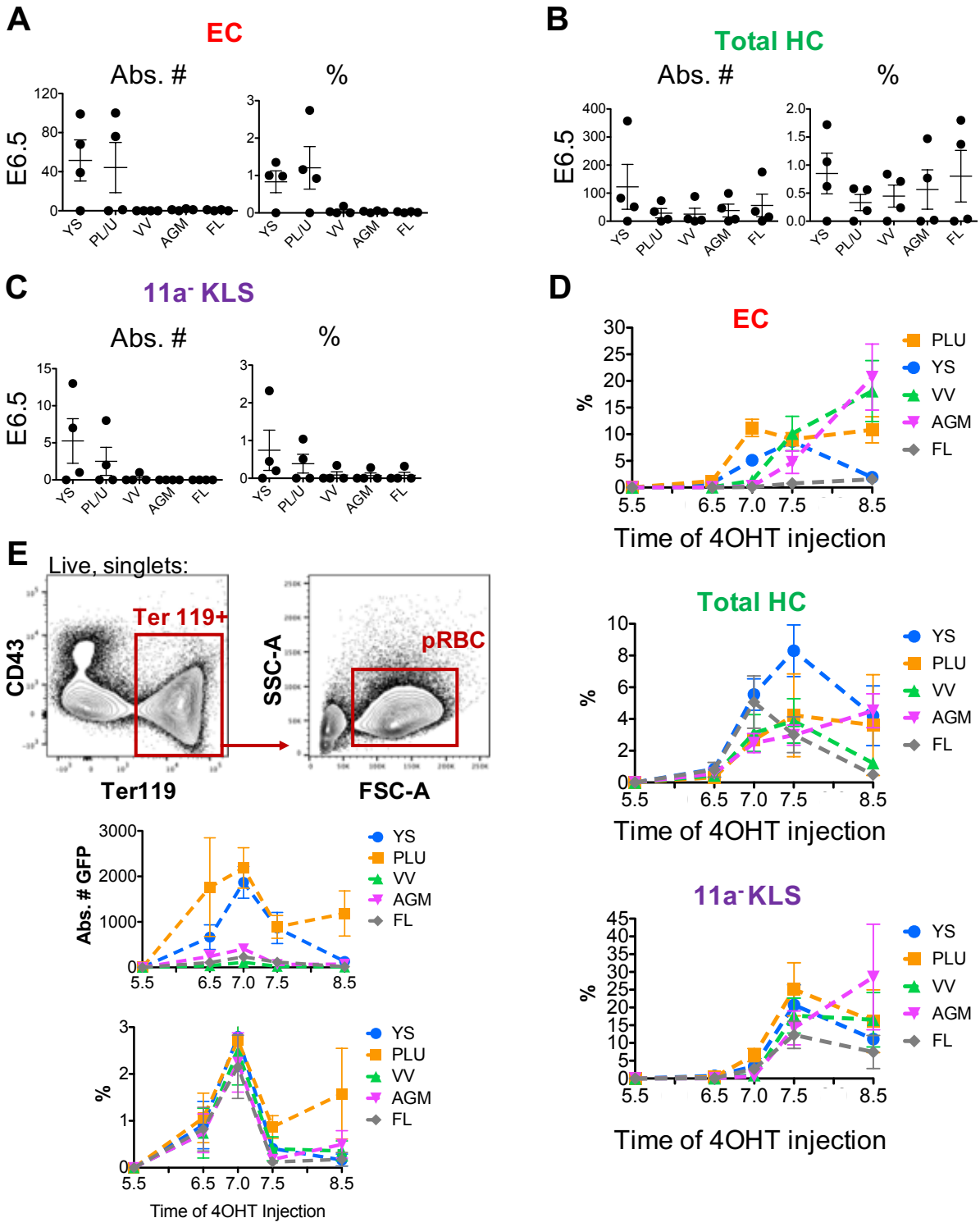
A
EC
Abs. #
%
E6.5
YS
PL/U
VV
AGM
FL
B
Total HC
C
11a- KLS
D
PLU
Time of 4OHT injection
E
Live, singlets:
Ter 119+
CD43
Ter119
SSC-A
pRBC
FSC-A
Abs. # GFP
Time of 4OHT Injection

Figure 3.4: HoxB6 labels primitive RBCs and definitive hematopoietic progenitors. Absolute cell number per embryo percentage (right) of EC (A), total HCs (B) and CD11a^{-}KLS cells (C) labeling in e10.5t6.5 embryos (n=4 independent litters and experiments). (D) Percentage labeling of embryonic tissues over time. (E) Labeling of Primitive RBCs (pRBCs), defined as CD43-,Ter119+ gated based on size (representative FAC plots, top), absolute number of GFP+ pRBCs middle graph, and percentage (bottom graph) over time.

Figure 3.5

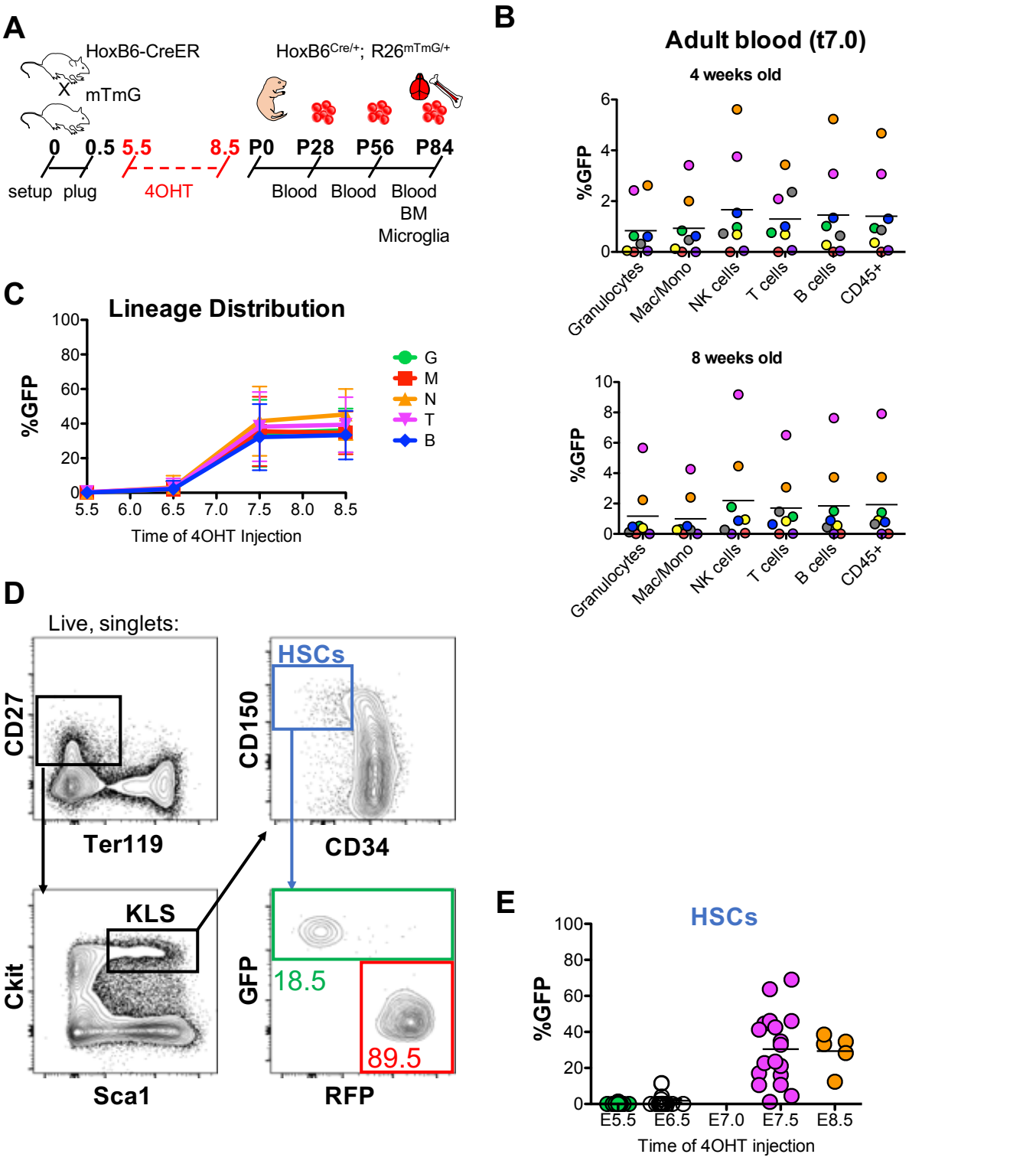
A
HoxB6-CreER
X
mTmG
HoxB6Cre/+; R26mTmG/+
0
0.5
5.5
8.5
P0
P28
P56
P84
setup
plug
4OHT
Blood
Blood
Blood
BM
Microglia
B
Adult blood (t7.0)
4 weeks old
%GFP
Granulocytes
Mac/Mono
NK cells
T cells
B cells
CD45+
8 weeks old
C
Lineage Distribution
%GFP
Time of 4OHT Injection
G
M
N
T
B
D
Live, singlets:
CD27
Ter119
HSCs
CD150
CD34
KLS
Ckit
Sca1
GFP
RFP
18.5
89.5
E
HSCs
%GFP
E5.5
E6.5
E7.0
E7.5
E8.5
Time of 4OHT injection

Figure 3.5: HoxB6 labels all adult blood lineages and HSCs. (A) Schematic of breeding strategy, Cre induction and tissue harvest in adults. Peripheral was blood collected every 4weeks after birth. Blood, bone marrow, and microglia were collected at 12weeks of age. (B) All blood lineages are consistently labeled at 4, 8, and 12 weeks of age at t7.5 injections. (C) No lineage bias in adult blood is observed at any time of 4OHT injection. Labeling of adult blood cells begins at t7.0. (D) Representative gating strategy for flow cytometric analysis. HSCs in whole bone marrow are defined as $CD27^{+}$, $Ter119^{-}$, $Ckit^{+}$, $Sca1^{+}$, $CD150^{+}$, $CD34^{-}$. (E) HSC labeling at each timepoint of 4OHT injection. No labeling is observed at t5.5 (n=23 mice, 3 litters). HSC labeling begins at t6.5 (n=20 mice, 4 litters). At t7.0 (n=) HSCs labeling becomes prevalent and peaks at t7.5 (n=18 mice, 3 litters) and t8.5 (n= 5 mice, 1 litter).

and engraftable. Indeed, the recipient GFP and RFP chimerism reflected the donor GFP labeling (**Figure 3.6C**). No significant increases or decreases were observed in percentage of GFP and RFP HSCs in recipients when compared to donor HSC labeling (**Figure 3.6D**). Thus, HoxB6-derived HSCs are multipotent, long-term self-renewing, engraftable and functionally identical to non-HoxB6 derived HSCs.

Most erythromyeloid progenitors and microglia are not HoxB6 derived.

Definitive erythromyeloid progenitors (EMPs) are thought to originate in the YS, seed embryonic tissues, and give rise to tissue resident macrophages in the adult (Sheng et al., 2015). EMP development in the YS is distinct from primitive hematopoiesis as well as independent from HSC precursors (Gomez-Perdiguero et al., 2015; McGrath et al., 2015). Thus, we examined whether EMPs (Ter119-, CD43+, Ckit+, $CD41^{lo}$, FCγR+) labeled within our system. In all cases GFP+ EMPs were most abundant in the YS, fitting the dogma that they originated there (**Figure 3.7A**). Peak labeling of EMPs was observed in t7.5 embryos. Lack of EMP labeling in t8.5 embryos suggests that EMPs no long express HoxB6.

Given the transient labeling in EMPs, we predicted that t7.5 adult mice would have robust labeling in YS-derived tissue resident macrophages. To test this, we harvested microglia (CD11b+, $CD45^{lo}$) from adult t7.5 $HoxB6^{Cre/+}$; $R26^{mTmG/+}$ mice at 12 weeks of age. Interestingly, microglia showed very low amount of GFP labeling compared to peripheral macrophages (CD11b+, $CD45^{hi}$) isolated brains of these mice ((**Figure 3.7B**). In fact, in t7.5 mice, which showed peak peripheral blood and HSC labeling, only about 5% of microglia were HoxB6-derived (**Figure 3.7C)**. In t7.5 and t8.5 mice, microglial labeling was approximately 10% or less than that of peripheral macrophages or HSCs in the same mice (**Figure 3.7D**). Thus, most cells in the hematopoietic wave

Figure 3.6

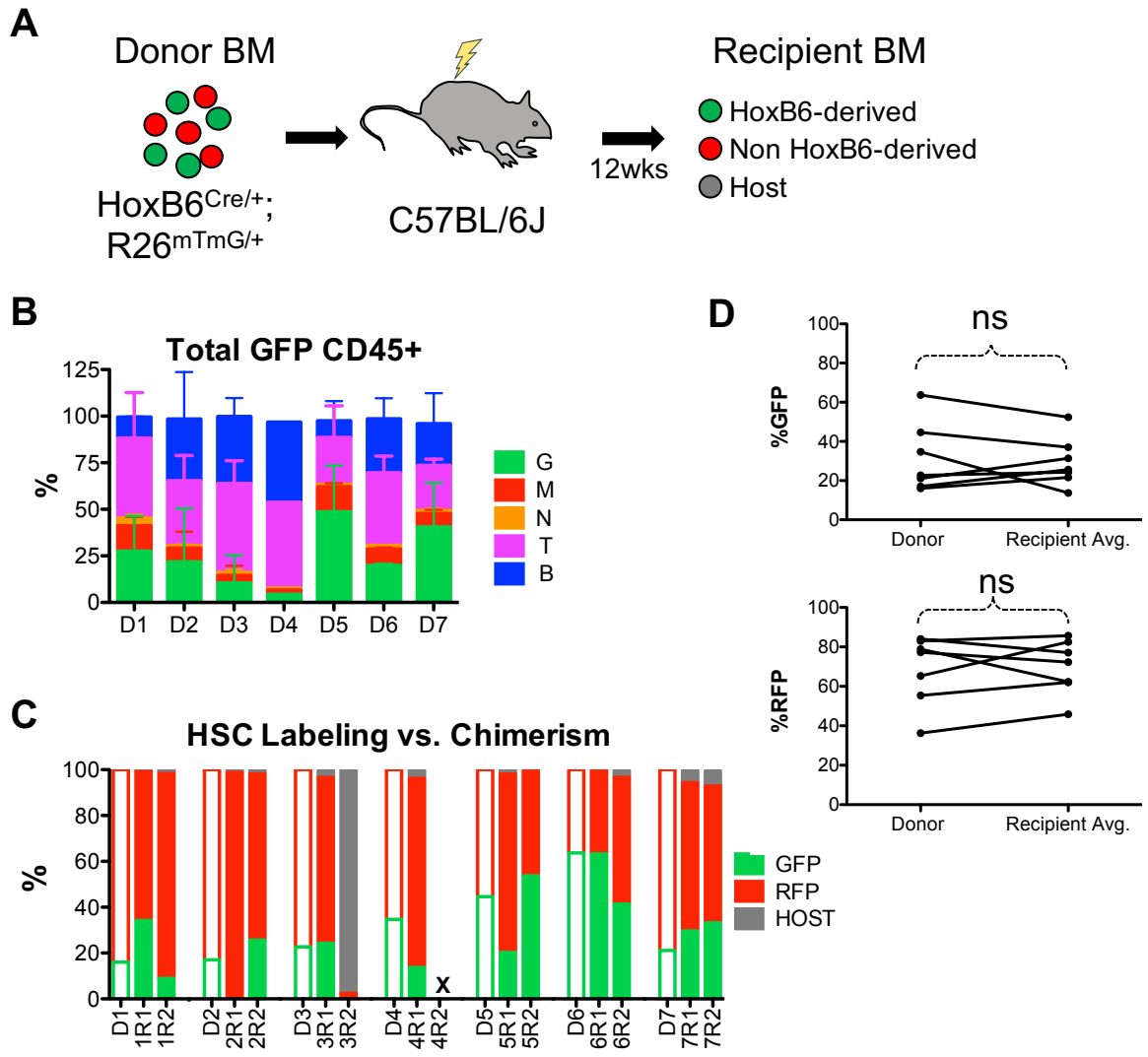

Figure 3.6: HoxB6-derived HSCs are self-renewing, multipotent and engraftable like non-HoxB6 derived HSCs. (A) Schematic of transplantation strategy and lineage reconstitution in recipient. (B) Lineage distribution in recipients 12weeks after transplantation shows reconstitution of all lineages in total GFP+, CD45+ cells. (C) Representative comparison between recipient GFP HSC chimerism 12 weeks after transplant. GFP chimerism in recipients (n=2 per donor) reflects levels of GFP labeling in donor (n=7). X indicates failed transplant (1/14). (D) Long term self-renewal of GFP HSCs shown by a lack of significant decrease in GFP (top) and increase in RFP (bottom) levels in the recipients compared to the donor. (B-D) Data includes donors(n=7) and recipients (n=14) from two independent litters which received 4OHT at e7.5 and independent transplant experiments.

Figure 3.7

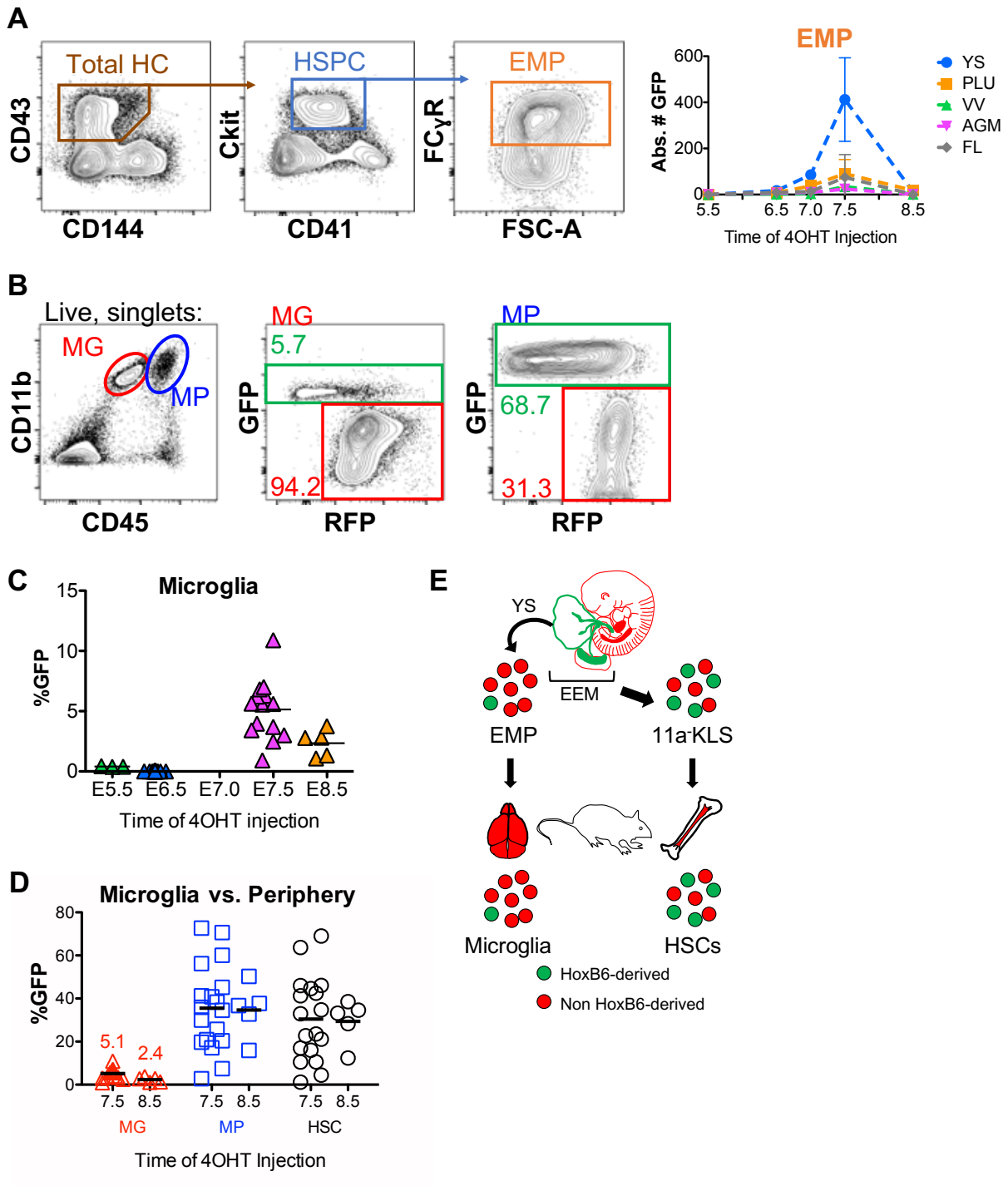
A
Total HC
HSPC
EMP
CD43
Ckit
FCγR
CD144
CD41
FSC-A
EMP
Abs. # GFP
600
400
200
0
5.5
6.5 7.0 7.5
8.5
Time of 4OHT Injection
YS
PLU
VV
AGM
FL
B
Live, singlets:
MG
MP
CD11b
CD45
MG
5.7
GFP
94.2
RFP
MP
68.7
GFP
31.3
RFP
C
Microglia
%GFP
15
10
5
0
E5.5 E6.5 E7.0 E7.5 E8.5
Time of 4OHT injection
D
Microglia vs. Periphery
%GFP
80
60
40
20
0
5.1
2.4
7.5 8.5 7.5 8.5 7.5 8.5
MG
MP
HSC
Time of 4OHT Injection
E
YS
EEM
EMP
11a-KLS
Microglia
HSCs
HoxB6-derived
Non HoxB6-derived

Figure 3.7: Most erythro-myeloid progenitors are not HoxB6-derived. (A) Schematic representation of divergence of EMP from other HoxB6-derived mesodermal cells EEM. (B) Representative flow cytometry plots and gating strategy for EMPs ($Ter119^{-}$, $CD43^{+}$, $CD144^{+/-}$, $Ckit^{+}$, $CD41^{lo}$, $FC\gamma R^{+}$) in e10.5 embryos. (C) Absolute number of GFP+ EMPs in each tissue from t5.5 to t8.5 embryos. EMPs were most abundant in the YS at all timepoints (D) Representative gating scheme for HoxB6-derived microglia ($CD11b^{+}$, $CD45^{lo}$; red gate) and peripheral macrophages ($CD11b^{+}$, $CD45^{hi}$; blue gate). (E) Labeling in microglial population from litters induced with 4OHT at different timepoints. (F) Labeling of microglia (red triangles) , peripheral macrophages in the brain (blue squares), and HSCs (grey circles) at t7.5 and t8.5. Microglial labeling was on approximately10% of that of the peripheral populations.

that is responsible for EMP development, are not HoxB6-derived, despite their YS origin (**Figure 3.7E**). This modal further proves the notion that EMPs development independently from the embryonic precursors that give rise to adult HSCs.

DISCUSSION

The AGM is thought to be the ultimate source of definitive pre-HSCs (J. Bertrand et al., 2010; Cumano et al., 2001; Ganuza et al., 2018). The vitelline arteries, which we consider as part of the EEM here, have also been shown to contain hemogenic endothelium cells (Zovein et al., 2010). In other studies, the placenta has also been attributed as a site a site for HSC development (Gekas et al., 2005; Lee et al., 2016; Mikkola et al., 2005). However, the YS is typically considered to be a source of only primitive bloods cells, and definitive erythromyeloid progenitors (Cumano et al., 2001; Sheng et al., 2015). Our data support the idea that definitive precursors of HSCs arise in multiple hematopoietic sites, including the yolk sac and the placenta.

Through tightly controlled mating and induction of Cre using 4OHT, we were able to obtain EEM- specific reporter labeling in t7.0 embryos. Our *in vivo*, non-invasive model demonstrates the abundance of labeled pre-HSCs and total hematopoietic cells in YS and PL, while there is no evidence of endothelial cell labeling within the AGM or fetal level through flow cytometry or imaging of sectioned embryos. Thus, any GFP hemogenic endothelial cells (HECs), which gave rise to Pre-HSCs and subsequently adult HSCs observed in t7.0 mice, are like located in the YS or the placenta.

Our assertion of EEM-specific labeling relied on endothelial cell labeling observed in the embryos, because hematopoietic cells are in circulation and their location is not indicative of their origin. However, for each analysis, absolute cell number per embryo was determined to identify

the tissues in which each population was most abundant. Total GFP hematopoietic cells as well as 11a^{-}KLS Pre-HSCs were significantly more abundant in YS and placenta compared to the AGM not just in t6.5 and t7.0 embryos, but also in t7.5 embryos. Given this disparity and the extensive labeling of ECs in these tissues within these embryos, it can be concluded that some of these cells may have freshly emerged from HECs and have yet to enter circulation. However, it is also possible that higher number of hematopoietic cells is due to the fact that the YS and placenta are highly vascularized. Regardless, labeled endothelial cells were most abundant in EEM tissues, especially in t6.5 and t7.0 embryos. The percentage for GFP+ endothelial cells in t7.0 embryos was also significantly higher in YS and placenta, which further demonstrated that the labeling was restricted to these EEM tissues.

Our lineage tracing experiments were also carried out in adult mice. Adult blood cell labeling is first observed after Cre induction as early as e6.5 (in t6.5 adults). GFP labeling peaks at t7.5 indicating that HoxB6 is likely expressed in AGM mesoderm during this time, in addition to EEM. In all cases, percentage of labeling was consistent across all blood lineages, indicating the presence of labeled HSCs. Indeed, as seen in the embryos, HSC labeling is also first observed in t6.5 adults, albeit at very low levels. However, these HoxB6-derived HSCs are exhibit all characteristics of true HSCs. They are multipotent, as myeloid and lymphoid blood cells in HoxB6$^{Cre/+}$;R26$^{mTmG/+}$ adults are equally labeled. These lineages are consistently labeled for 12 weeks, indicating that the HSCs self-renew long term. Finally, these HSCs also replenish all blood lineages upon transplantation, and are as engraftable as their non-HoxB6 derived counterparts. Together, our results suggest that some HSCs do originate in the extra-embryonic tissues, and are comparable to those that originate in the AGM.

The HoxB6 system has also confirmed previous studies that the developmental branch of EMPs that originate in the YS is distinct from that of HSCs that arise there (Guillaume Hoeffel et al., 2015; Schulz et al., 2012) . EMPs are responsible for seeding developing tissues, and are considered the primary source of tissue resident macrophages, such as microglia (Ginhoux et al., 2010; Gomez-Perdiguero et al., 2015; Kierdorf et al., 2013a). Interestingly, though the YS was extensively labeled in t7.0, t7.0 and especially in t7.5 embryos, microglia labeling was not nearly as extensive in their adult counterparts of these mice. Peak microglia labeling was observed in t7.5 and t8.5 adults, but it was roughly 10% of peripheral macrophages or HSCs labeling in these mice. One of the reasons behind low microglial label can be that EMPs are simply not HoxB6-derived. HoxB6 is either not expressed or is expressed for a very short period of time in EMPs or the developmental precursors that give rise to microglia. Studies have also suggested that in other tissue resident macrophages like liver Kupffer cells and Langerhans cells in the skin, fetal liver (FL)-derived precursor may be replaces the original YS-derived cells that seeded tissues (Guillaume Hoeffel et al., 2012; van de Laar et al., 2016; Yona et al., 2013). In all cases in the HoxB6 system, endothelial cells in the FL had little to no labeling, by absolute cells count as well as percentage of GFP cells. The low amount of microglia labeling can also be explained if these FL-derived cells do emerge directly from HECs in the FL, and then replace the YS-derived cells seeded in the brain. This finding would be novel, but further study is required to distinguish these FL-derived precursors from YS-derived EMPs.

Overall, our study provides evidence that extra-embryonic sources of HSC exist, but does not negate the contribution of AGM as a prominent site of HSC development. Future studies will focus on determining whether the EEM derived HSCs come from the placenta, as has been previously reported (Gekas et al., 2005; Lee et al., 2016), or whether the YS has any contributions.

While transplantation of separated EEM tissues can be used to deduce this as has been previously reported (Karimzadeh et al., 2019 unpublished data), a lineage tracing system that can distinguish placenta-derived from yolk sac-derived and vitelline vessel-derived hematopoietic cells, would be most certainly identify the extra embryonic source of hematopoietic stem cells.

METHODS

Mice: homozygous HoxB6-CreER, aka HoxB6 (Nguyen et al., 2009) with *Rosa26*$^{mTmG/mTmG}$, aka mTmG, stock no., 007576, JAX (Muzumdar et al., 2007). C57BL/6J (B6; stock no. 00664, JAX) adult mice were used for transplantation.

Timed pregnancies and embryo collection: Hox and mTmG mice were placed in the same cage for mating after 6pm, at the beginning of the 12-hr dark cycle. Females were examined for post-coital plugs and separated from males the following morning. Noon on the day of the post-coital plug was counted as embryonic day 0.5 (i.e. e0.5). Plugged females were injected with 1mg of 4-hydroxytamoxifen (4OHT; Millipore Sigma, CAT# 579002-5mg) was dissolved in corn oil with 10% absolute ethanol. Briefly, 5mg vial of 4OHT was reconstituted with 100µl of ethanol by vortexing for 5mins at room temperature. The mix was then added to 900µl of corn oil and sonicated (60Hz) at room temperature for 45 mins (Branson 2510). 200µl were administered to each female via an intraperitoneal injection. All plugged females sacrificed on e10.5 for embryonic analysis or litters we allowed to be born. E10.5 embryos were staged according to 30-36 somite pair count. Tissue labeling was examined using a dissecting microscope (Nikon SMZ1500).

Immunofluorescence staining and microscopy: Embryos were also dropped and incubated 4% paraformaldehyde immediately after dissection and incubated at 4°C for 12-24 hours. Embryos

were then transferred to 30% sucrose for cryopreservation and embedded in OCT. 20 micron transverse and sagittal cryostat sections (Leica CM1850) were obtained on 0.3% Gelatin-coated slides. Slides were incubated with primary antibodies overnight at 4°C and for 1 hour at room temperature with the secondary antibodies in a humidified chamber. Slides were imaged an Olympus FV3000 confocal microscope

Embryo tissue harvest and flow cytometry: For flow cytometry analysis, embryos were dissected and Yolk sac (YS), Vitelline vessels (VV), Placenta and Umbilical vessels (PLU), Fetal liver (FL), Aorta-gonad-mesonephros (AGM) were collected in separate Eppendorf tubes. For AGM dissection, tail region below the lower limb bud, head region above the upper limb buds, as well as all four limb buds themselves were removed. FL was collected and the remaining tissue which contains the dorsal aorta (DA) is collected as "AGM". Tissues from 4-5 embryos were pooled for analysis. Here we consider YS, PLU and VV tissues containing the extra-embryonic mesoderm (EEM), while AGM and FL are characterized as embryonic mesoderm (EM). Tissues were dissociated with 1mg/ml Collagenase type IV (Gibco; REF 17104-019) for 30 minutes in a 37°C water bath. Dissociated cells were then washed with 2% FBS in PBS and stained for analysis. Absolute cell numbers per embryo equivalence (ee) were determined by adding 10,000 Count Bright cell counting beads (Invitrogen; REF C36950) to the sample before acquisition on the cytometer. Cells in each population were normalized based on the number of beads acquired in the sample and divided by the number of embryos pooled for analysis. Statistical analysis was performed with GraphPad Prism 5 software (La Jolla, CA).

Antibodies. See ***Table 2*** for a full list of antibodies used for flow cytometry (FACS) and Immunofluorescence (IF) imaging.

Table 2

Antigen, clone, fluorochrome	Vendor	Purpose
CD11a, M17/4, Biotin, PE	Biolegend	FACS
CD117, 2B8, BV421	Biolegend	FACS
CD27, LG.3A10, APC/Cy7	Biolegend	FACS
CD45, 30-F11, BV785, 7PE, APC/Cy7	Biolegend	FACS
CD16/32,93 , BV510	Biolegend	FACS
CD3, 390, PerCP-eFluor 710	eBiosciences	FACS
Sca1, D7, PECy7	Biolegend	FACS
Ter119, Ter119, PECy5	Biolegend	FACS
CD41, MWReg30, Alexa Fluor780	eBiosciences	FACS
CD150, TC15-12F12.2, PE	Biolegend	FACS
Gr1, RB6-8C5, BV605	Biolegend	FACS
NK1.1, PK136, APC	Biolegend	FACS
CD19, 6D5, BV421	Biolegend	FACS
VE-Cadherin, BV13, Biotin, APC	Biolegend	FACS
CD34, RAM34, eFluor 660	Invitrogen	FACS
CD43, S7, APC	BD Biosciences	FACS
CD11b, M1/70 (rat, anti-mouse), APC	Biolegend	FACS
CD3, 17A2 (rat, anti-mouse), PerCP-eFluor 710	eBiosciences	FACS
Streptavidin, Anti-rat, Q dot 605	Life Technologies	FACS
Goat, Anti-Rabbit, Alexa Fluor 488	Life Technologies	IF
Rabbit Anti-GFP, Polyclonal, unconjugated	Abcam	IF
CD31, Mec13.3, Alexa Fluor 647	Biolegend	IF

CHAPTER 4: DISCUSSION AND FUTURE STUDIES

Alzheimer's Disease

In Chapter 1, we have tackled two very important challenges in the field of Alzheimer's Disease and neuroimmunology at large. First, we have provided strong evidence that CD11a is a reliable marker for bone-marrow derived cells. Lack of CD11a expression on microglia can help us differentiate between tissue-resident microglia and infiltrating immune cells. This marker overcomes the pitfalls of other markers, such as CD45, Tmem119, P2ry12, etc, which alter their expression patterns upon microglia activation (Butovsky et al., 2014; Keren-Shaul et al., 2017b). CD11a remains stably "OFF" in microglia under steady-state, LPS- induced inflammation as well as in Alzheimer's Disease. Using this marker, we have demonstrated that the myeloid cells that cluster around Aß plaques in various mouse models of AD are microglia (**Figure 4.1**). Our findings and other reports have conclusively shown that microglia are the sole myeloid players in AD (Bien-Ly et al., 2015; Shukla et al., 2018). Thus, future research can focus on rejuvenating the potential of microglia to clear these plaques.

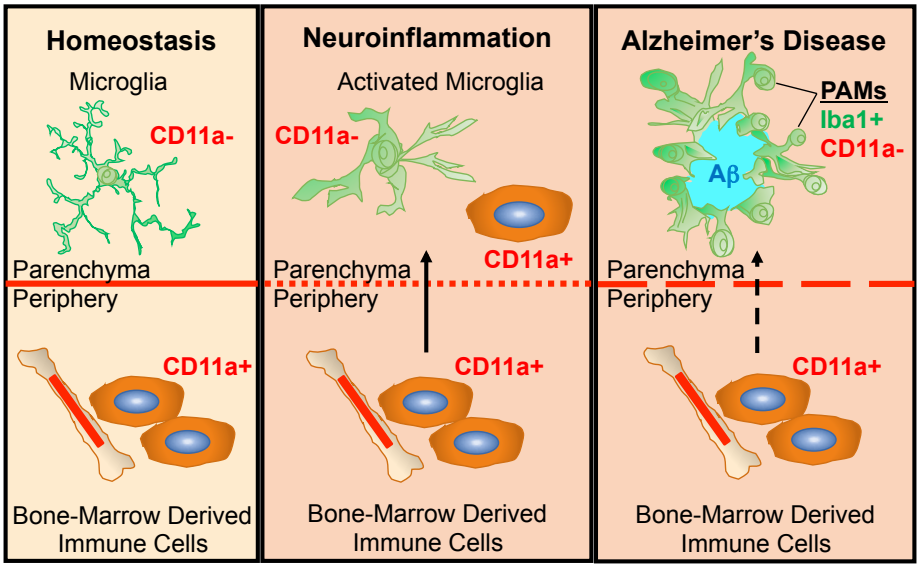

Figure 4.1: Model of peripheral cell infiltration in neuroinflammation

Secondly, we have introduced a novel method of quantifying peripheral cell infiltration. Researchers have long focused on the integrity of the blood brain in AD. Previous reports have demonstrated the lack of any significant BBB breakdown in AD (Bien-Ly et al., 2015; Marsh et al., 2016; Simard et al., 2006). However, the exact level of peripheral cell infiltration through other avenues, such as choroid plexus, has always been unclear in AD. This further mystified the precise role of microglia in AD. Here, we have demonstrated a two-fold increase in microglial numbers in AD mice compared to their WT littermates. We also identified significant increases in T lymphocytes, especially in female 5X mice. The FAQT method can be useful in any neuroinflammatory context where cell yields can vary from prep to prep and counting beads are lost due to percoll gradients.

Breaking (Blood-Brain) Barriers

It is worth exploring whether increased infiltration of other myeloid cells may ameliorate plaque burden. One way to induce infiltration is by disrupting the BBB via irradiation. Irradiation studies have indeed been conducted on AD mice before (Mildner et al., 2007; Simard et al., 2006), but with lethal doses and changes in plaque burden were not examined. In fact, infiltration of peripheral cells due to *T.gondii* infection was neuroprotective in AD (Jung et al., 2012). However, toxoplasmosis as a treatment to mitigate AD is not translatable. However, low doses of irradiation to permeate the BBB may prove to be more clinically relevant. This must first be confirmed in mouse models, of course. Future work may propose a regimen of neonatal doses of irradiation every two-four weeks from P1 to six months of age in 5X and WT littermates. However, irradiation must be restricted to the head to spare the host hematopoietic compartment.

Another approach to is increase the phagocytic potential of microglia. Microglia in the brain are in an inhibitory milieu. This is because neurons express high levels of macrophage inhibitory molecules such as CD47 (Chavarría & Cárdenas, 2013; Koning et al., 2007). CD47 signaling produces a "Don't eat me" signal on neurons as it binds to its ligand SIRP1-α. Inhibiting this suppression of microglia by intracranial injection of anti-CD47 antibodies in one lobe of AD mice, may rejuvenating local microglia to phagocytose more plaques. While there are foreseeable side-effects with this approach, anti-CD47 therapy has been beneficial in many clinical contexts (Chao et al., 2010; Koning et al., 2007; X. Zhou et al., 2014).

In addition to modulating the function of microglia, one the most obvious avenues for this work is to determine whether CD11a can distinguish microglia in humans as well. Flow cytometric analysis of human fetal microglia (CD45lo, red gate and histogram) indicated that CD11a is not expressed (**Figure 4.2**). However, CD45hi cells (blue gates and histograms) isolated with the brain tissue expressed hCD11a at high levels, similar to the mouse. Further analysis of adult microglia is required to determine whether CD11a is stably expressed throughout the lifetime.

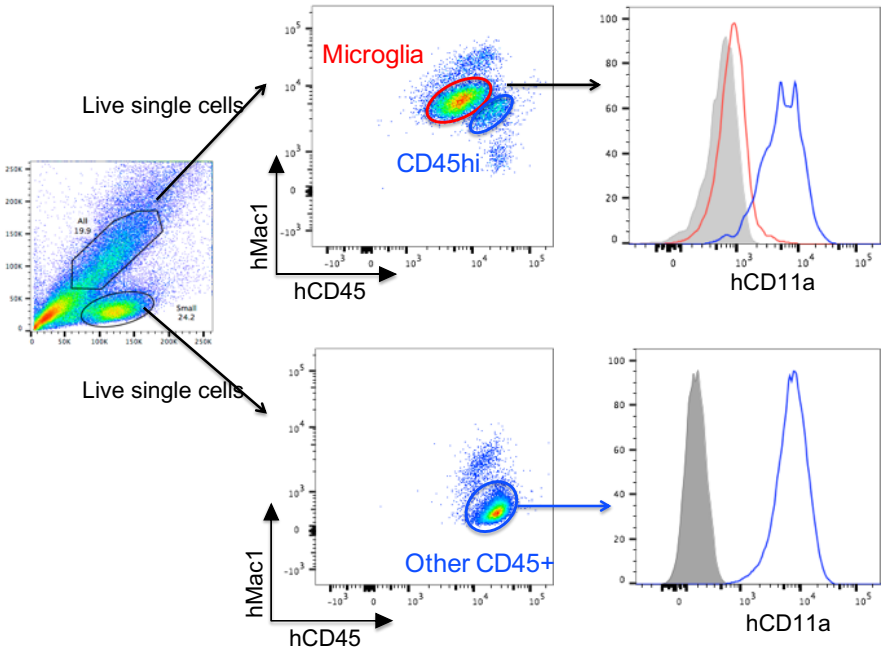

Figure 4.2: Human fetal microglia do not express CD11a

Source(s) of Tissue-Resident Macrophages

In Chapter 2, we explore whether CD11a is "OFF" in all trMac populations. Microglia and Langerhans cells are the only two radio-resistant trMacs, and likely remain CD11a- in most cases. This may suggest a developmental commonality between these two trMac populations, as implied in model 1 (**Figure 2.1**). Kupffer cells, while they were CD11a- in steady-state conditions, were completely CD11a+ after irradiation. This may simply be the result of BM-derived cell replacement of the nascent KCs, as their GFP chimerism was surprisingly high. Alveolar macrophages were heterogeneous in terms of CD11a expression and the GFP chimerism of CD11a+ cells was also relatively low. These data imply that trMacs may have multiple embryonic as well as adult source, thus CD11a may not be a universal distinguisher of trMacs. Well-studied lineage tracing systems like Lyve1, along with CD11a, can help determine the levels of BM contribution. However, as described in Chapter 2, an inducible Lyve1-driven Cre system would be most ideal in determining the source(s) of different trMac populations.

CD11a marker expression patterns on different trMacs can suggest developmental relationships between these cell types, especially in regard to their precursor cell populations and mapping their ontogeny. The challenge of understanding which signals cause bone-marrow derived monocytes to replace trMacs can be surmounted using CD11a to distinguish at least microglia and Langerhans cells from infiltrating monocytes-derived macrophages. Whether adult derived macrophages can replace all trMac populations, except microglia, remains an open question. If so, can these BM -derived cells recapitulate all the functions of nascent trMac populations also has important clinical implications. Modeling trMacs *in vitro* using induced pluripotent stem cells by providing cultured macrophages with tissue specific cues may help address some of these questions and help translate these findings to therapy.

The Origin of Hematopoietic Stem Cells

The notion of HSCs being derived from extraembryonic mesoderm, especially that in the YS, has been constantly challenged (Bruijn & Speck, 2000; Stremmel et al., 2018). In Chapter 3, we have shown an abundance of 11a^{-}KLS, pre-HSCs in the YS and PL by absolute cell number per embryos as well as percentages in our HoxB6 lineage tracing system. No evidence of endothelial cell labeling within the AGM or fetal liver was detected prior to Cre induction at e7.5. Yet, we found that HSC labeling began, albeit at low levels, starting from t6.5 mice. This lineage system provides a tight window of tamoxifen-inducible initial labeling, exclusively in the EEM. Thus, any labeling in the adult hematopoietic cells indicates that they were derived from an extraembryonic precursor, according to our model (**Figure 4.3**).

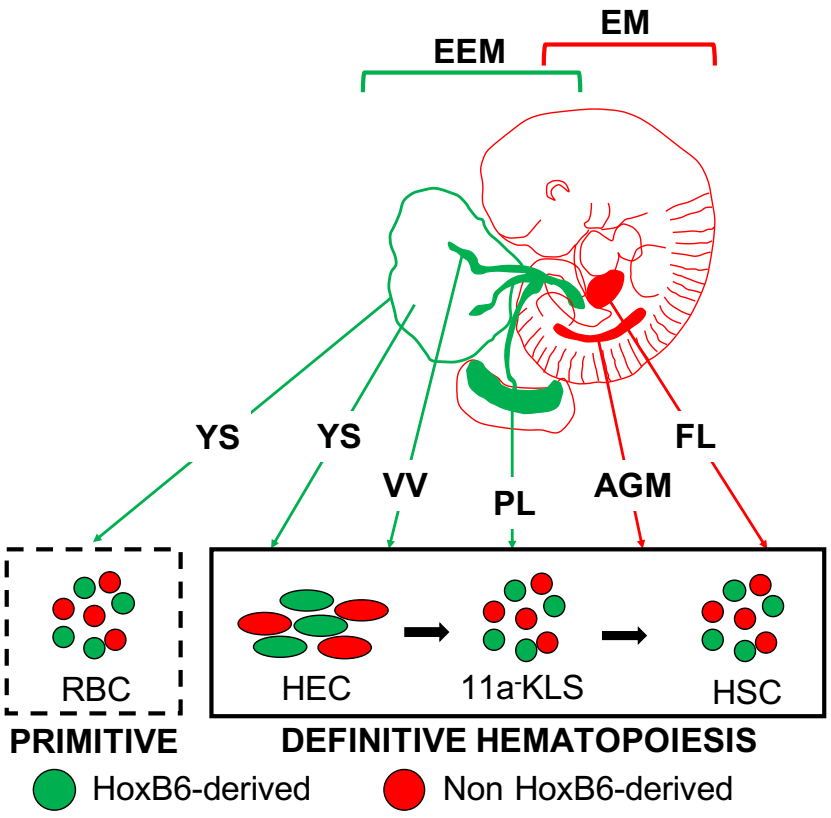

Figure 4.3: HoxB6 labels extra-embryonic mesoderm derived HSCs

Final Remarks: Our work in Alzheimer's Disease has conclusively resolved that plaque associated myeloid cells are microglia. It has provided an important immunological tool to distinguish microglia and Langerhans cells in steady-state and inflammatory conditions. Thus, future work can now focus on the specific roles of these trMacs and bone marrow derived cells play in different disease contexts. Additionally, we have delineated the extra-embryonic origins of hematopoietic stem cells. This work highlights the importance of studying the molecular mechanisms that are responsible for hematopoiesis outside the embryo. Whether it is tissue-resident macrophages or hematopoietic stem cells, extra-embryonic sites of hematopoiesis should not be neglected.

REFERENCES

A-Gonzalez, N., Quintana, J. A., García-Silva, S., Mazariegos, M., González de la Aleja, A., Nicolás-Ávila, J. A., … Hidalgo, A. (2017). Phagocytosis imprints heterogeneity in tissue-resident macrophages. *The Journal of Experimental Medicine*. https://doi.org/10.1084/jem.20161375

Abbott, N. J., Patabendige, A. A. K., Dolman, D. E. M., Yusof, S. R., & Begley, D. J. (2010). Structure and function of the blood-brain barrier. *Neurobiology of Disease*. https://doi.org/10.1016/j.nbd.2009.07.030

Abram, C. L., & Lowell, C. A. (2009). The ins and outs of leukocyte integrin signaling. *Annual Review of Immunology*. https://doi.org/10.1146/annurev.immunol.021908.132554

Ahmed, H. H., Abdel Raouf, E. R., Rashed, L. A., & Aglan, H. A. (2016). New approaches in the horizon for treatment of Alzhimer's disease. *Der Pharmacia Lettre*.

Ajami, B., Bennett, J. L., Krieger, C., Tetzlaff, W., & Rossi, F. M. V. (2007). Local self-renewal can sustain CNS microglia maintenance and function throughout adult life. *Nature Neuroscience*. https://doi.org/10.1038/nn2014

Alliot, F., Lecain, E., Grima, B., & Pessac, B. (2006). Microglial progenitors with a high proliferative potential in the embryonic and adult mouse brain. *Proceedings of the National Academy of Sciences*. https://doi.org/10.1073/pnas.88.4.1541

Alliot, Francoise, Godin, I., & Pessac, B. (1999). Microglia derive from progenitors, originating from the yolk sac, and which proliferate in the brain. *Developmental Brain Research*. https://doi.org/10.1016/S0165-3806(99)00113-3

Álvarez-Errico, D., Vento-Tormo, R., Sieweke, M., & Ballestar, E. (2015). Epigenetic control of myeloid cell differentiation, identity and function. *Nature Reviews. Immunology*. https://doi.org/10.1038/nri3777

Alzheimer's Association. (2019). Alzheimer's 2019 Facts and Figures, *501*(c), 2019.

Alzheimer, A. (1907). Über eine eigenartige Erkrankung der Hirnrinde. *Allgemeine Zeitschrift Für Psychiatrie Und Psychisch-Gerichtliche Medizin*. https://doi.org/10.1002/ca.980080612

Amit, I., Winter, D. R., & Jung, S. (2016). The role of the local environment and epigenetics in shaping macrophage identity and their effect on tissue homeostasis. *Nature Immunology*. https://doi.org/10.1038/ni.3325

Antas, V. I., Al-Drees, M. A., Prudence, A. J. A., Sugiyama, D., & Fraser, S. T. (2013). Hemogenic endothelium: a vessel for blood production. *The International Journal of Biochemistry & Cell Biology*, *45*(3), 692–695. https://doi.org/10.1016/j.biocel.2012.12.013

Baik, S. H., Kang, S., Son, S. M., & Mook-Jung, I. (2016). Microglia contributes to plaque growth by cell death due to uptake of amyloid β in the brain of Alzheimer's disease mouse model. *GLIA*. https://doi.org/10.1002/glia.23074

Batsivari, A., Rybtsov, S., Souilhol, C., Binagui-Casas, A., Hills, D., Zhao, S., … Medvinsky, A. (2017). Understanding Hematopoietic Stem Cell Development through Functional Correlation of Their Proliferative Status with the Intra-aortic Cluster Architecture. *Stem Cell Reports*. https://doi.org/10.1016/j.stemcr.2017.04.003

Bennett, F. C., Bennett, M. L., Yaqoob, F., Mulinyawe, S. B., Grant, G. A., Hayden Gephart, M., … Barres, B. A. (2018). A Combination of Ontogeny and CNS Environment Establishes Microglial Identity. *Neuron*. https://doi.org/10.1016/j.neuron.2018.05.014

Bennett, M. L., Bennett, F. C., Liddelow, S. A., Ajami, B., Zamanian, J. L., Fernhoff, N. B., … Barres, B. A. (2016). New tools for studying microglia in the mouse and human CNS.

Proceedings of the National Academy of Sciences, *113*(12), E1738–E1746. https://doi.org/10.1073/pnas.1525528113

Bertrand, J., Chi, N., Santoso, B., & Teng, S. (2010). Haematopoietic stem cells derive directly from aortic endothelium during development. *Nature*. Retrieved from http://www.nature.com/nature/journal/v464/n7285/abs/nature08738.html

Bertrand, J. Y., Giroux, S., Golub, R., Klaine, M., Jalil, A., Boucontet, L., … Cumano, A. (2004). Characterization of purified intraembryonic hematopoietic stem cells as a tool to define their site of origin. *Proceedings of the National Academy of Sciences*. https://doi.org/10.1073/pnas.0402270102

Bien-Ly, N., Boswell, C. A., Jeet, S., Beach, T. G., Hoyte, K., Luk, W., … Watts, R. J. (2015). Lack of Widespread BBB Disruption in Alzheimer's Disease Models: Focus on Therapeutic Antibodies. *Neuron*. https://doi.org/10.1016/j.neuron.2015.09.036

Biswas, A., Bruder, D., Wolf, S. A., Jeron, A., Mack, M., Heimesaat, M. M., & Dunay, I. R. (2015). Ly6Chigh Monocytes Control Cerebral Toxoplasmosis. *Journal of Immunology (Baltimore, Md. : 1950)*, *194*(7), 3223–3235. https://doi.org/10.4049/jimmunol.1402037

Boisset, J.-C., van Cappellen, W., Andrieu-Soler, C., Galjart, N., Dzierzak, E., & Robin, C. (2010). In vivo imaging of haematopoietic cells emerging from the mouse aortic endothelium. *Nature*, *464*(7285), 116–120. https://doi.org/10.1038/nature08764

Boisset, J., & Cappellen, W. van. (2010). In vivo imaging of haematopoietic cells emerging from the mouse aortic endothelium. *Nature*. Retrieved from http://www.nature.com/nature/journal/v464/n7285/full/nature08764.html

Bowman, R. L., Klemm, F., Akkari, L., Pyonteck, S. M., Sevenich, L., Quail, D. F., … Joyce, J. A. (2016). Macrophage Ontogeny Underlies Differences in Tumor-Specific Education in Brain Malignancies. *Cell Reports*. https://doi.org/10.1016/j.celrep.2016.10.052

Bradshaw, E. M., Chibnik, L. B., Keenan, B. T., Ottoboni, L., Raj, T., Tang, A., … De Jager, P. L. (2013). CD33 Alzheimer's disease locus: Altered monocyte function and amyloid biology. *Nature Neuroscience*. https://doi.org/10.1038/nn.3435

Bruijn, M. de, & Speck, N. (2000). Definitive hematopoietic stem cells first develop within the major arterial regions of the mouse embryo. *The EMBO* ..... Retrieved from http://emboj.embopress.org/content/19/11/2465.abstract

Butovsky, O., Jedrychowski, M. P., Moore, C. S., Cialic, R., Lanser, A. J., Gabriely, G., … Weiner, H. L. (2014). Identification of a unique TGF-β-dependent molecular and functional signature in microglia. *Nature Neuroscience*. https://doi.org/10.1038/nn.3599

Buttgereit, A., Lelios, I., Yu, X., Vrohlings, M., Krakoski, N. R., Gautier, E. L., … Greter, M. (2016). Sall1 is a transcriptional regulator defining microglia identity and function. *Nature Immunology*, *17*(12), 1397–1406. https://doi.org/10.1038/ni.3585

Canter, R. G., Penney, J., & Tsai, L. H. (2016). The road to restoring neural circuits for the treatment of Alzheimer's disease. *Nature*. https://doi.org/10.1038/nature20412

Cardona, A. E., Pioro, E. P., Sasse, M. E., Kostenko, V., Cardona, S. M., Dijkstra, I. M., … Ransohoff, R. M. (2006). Control of microglial neurotoxicity by the fractalkine receptor. *Nature Neuroscience*. https://doi.org/10.1038/nn1715

Carter, J., & Lippa, C. (2005). β-Amyloid, Neuronal Death and Alzheimers Disease. *Current Molecular Medicine*. https://doi.org/10.2174/1566524013363177

Cazareth, J., Guyon, A., Heurteaux, C., Chabry, J., & Petit-Paitel, A. (2014). Molecular and cellular neuroinflammatory status of mouse brain after systemic lipopolysaccharide challenge: Importance of CCR2/CCL2 signaling. *Journal of Neuroinflammation*.

https://doi.org/10.1186/1742-2094-11-132
Chao, M. P., Alizadeh, A. A., Tang, C., Myklebust, J. H., Varghese, B., Gill, S., … Majeti, R. (2010). Anti-CD47 Antibody Synergizes with Rituximab to Promote Phagocytosis and Eradicate Non-Hodgkin Lymphoma. *Cell*. https://doi.org/10.1016/j.cell.2010.07.044
Chavarría, A., & Cárdenas, G. (2013). Neuronal influence behind the central nervous system regulation of the immune cells. *Frontiers in Integrative Neuroscience*. https://doi.org/10.3389/fnint.2013.00064
Cheng, I. H., Palop, J. J., Esposito, L. A., Bien-Ly, N., Yan, F., & Mucke, L. (2004). Aggressive amyloidosis in mice expressing human amyloid peptides with the Arctic mutation. *Nature Medicine*. https://doi.org/10.1038/nm1123
Chorro, L., Sarde, A., Li, M., Woollard, K. J., Chambon, P., Malissen, B., … Geissmann, F. (2009). Langerhans cell (LC) proliferation mediates neonatal development, homeostasis, and inflammation-associated expansion of the epidermal LC network. *The Journal of Experimental Medicine*. https://doi.org/10.1084/jem.20091586
Ciau-Uitz, A., Monteiro, R., Kirmizitas, A., & Patient, R. (2014). Developmental hematopoiesis: Ontogeny, genetic programming and conservation. *Experimental Hematology*. https://doi.org/10.1016/j.exphem.2014.06.001
Citron, M. (2010). Alzheimer's disease: Strategies for disease modification. *Nature Reviews Drug Discovery*. https://doi.org/10.1038/nrd2896
Cumano, A., Dieterlen-Lievre, F., & Godin, I. (1996). Lymphoid potential, probed before circulation in mouse, is restricted to caudal intraembryonic splanchnopleura. *Cell*. https://doi.org/10.1016/S0092-8674(00)80166-X
Cumano, A., Ferraz, J. C., Klaine, M., Di Santo, J. P., & Godin, I. (2001). Intraembryonic, but not yolk sac hematopoietic precursors, isolated before circulation, provide long-term multilineage reconstitution. *Immunity*. https://doi.org/10.1016/S1074-7613(01)00190-X
D'Mello, C., Le, T., & Swain, M. G. (2009). Cerebral Microglia Recruit Monocytes into the Brain in Response to Tumor Necrosis Factor Signaling during Peripheral Organ Inflammation. *Journal of Neuroscience*. https://doi.org/10.1523/JNEUROSCI.3567-08.2009
Daneman, R. (2012). The blood-brain barrier in health and disease. *Annals of Neurology*. https://doi.org/10.1002/ana.23648
De Calignon, A., Polydoro, M., Suárez-Calvet, M., William, C., Adamowicz, D. H., Kopeikina, K. J., … Hyman, B. T. (2012). Propagation of Tau Pathology in a Model of Early Alzheimer's Disease. *Neuron*. https://doi.org/10.1016/j.neuron.2011.11.033
DeKosky, S. T., & Scheff, S. W. (1990). Synapse loss in frontal cortex biopsies in Alzheimer's disease: Correlation with cognitive severity. *Annals of Neurology*. https://doi.org/10.1002/ana.410270502
Ditadi, A., Sturgeon, C. M., Tober, J., Awong, G., Kennedy, M., Yzaguirre, A. D., … Keller, G. (2015). Human definitive haemogenic endothelium and arterial vascular endothelium represent distinct lineages. *Nature Cell Biology*, *17*(5), 580–591. https://doi.org/10.1038/ncb3161
Doebel, T., Voisin, B., & Nagao, K. (2017). Langerhans Cells – The Macrophage in Dendritic Cell Clothing. *Trends in Immunology*. https://doi.org/10.1016/j.it.2017.06.008
Elmore, M. R. P., Najafi, A. R., Koike, M. A., Dagher, N. N., Spangenberg, E. E., Rice, R. A., … Green, K. N. (2014). Colony-stimulating factor 1 receptor signaling is necessary for microglia viability, unmasking a microglia progenitor cell in the adult brain. *Neuron*. https://doi.org/10.1016/j.neuron.2014.02.040

Epelman, S., Lavine, K. J., & Randolph, G. J. (2014). Origin and Functions of Tissue Macrophages. *Immunity*. https://doi.org/10.1016/j.immuni.2014.06.013

Fathman, J. W., Fernhoff, N. B., Seita, J., Chao, C., Scarfone, V. M., Weissman, I. L., & Inlay, M. A. (2014). Upregulation of CD11A on hematopoietic stem cells denotes the loss of long-term reconstitution potential. *Stem Cell Reports*. https://doi.org/10.1016/j.stemcr.2014.09.007

Ferkowicz, M. J., & Yoder, M. C. (2005). Blood island formation: Longstanding observations and modern interpretations. *Experimental Hematology*. https://doi.org/10.1016/j.exphem.2005.06.006

Fogg, D. K., Sibon, C., Miled, C., Jung, S., Aucouturier, P., Littman, D. R., … Geissmann, F. (2006). A clonogenic bone harrow progenitor specific for macrophages and dendritic cells. *Science*. https://doi.org/10.1126/science.1117729

Galea, I., Bernardes-Silva, M., Forse, P. A., van Rooijen, N., Liblau, R. S., & Perry, V. H. (2007). An antigen-specific pathway for CD8 T cells across the blood-brain barrier. *The Journal of Experimental Medicine*. https://doi.org/10.1084/jem.20070064

Ganuza, M., Chabot, A., Tang, X., Bi, W., Natarajan, S., Carter, R., … McKinney-Freeman, S. (2018). Murine hematopoietic stem cell activity is derived from pre-circulation embryos but not yolk sacs. *Nature Communications*, *9*(1), 5405. https://doi.org/10.1038/s41467-018-07769-8

Gekas, C., Dieterlen-Lièvre, F., Orkin, S. H., & Mikkola, H. K. A. (2005). The placenta is a niche for hematopoietic stem cells. *Developmental Cell*. https://doi.org/10.1016/j.devcel.2004.12.016

Ghigo, C., Mondor, I., Jorquera, A., Nowak, J., Wienert, S., Zahner, S. P., … Bajénoff, M. (2013). Multicolor fate mapping of Langerhans cell homeostasis. *The Journal of Experimental Medicine*. https://doi.org/10.1084/jem.20130403

Ghosh, S., Chackerian, A. A., Parker, C. M., Ballantyne, C. M., & Behar, S. M. (2014). The LFA-1 Adhesion Molecule Is Required for Protective Immunity during Pulmonary Mycobacterium tuberculosis Infection. *The Journal of Immunology*. https://doi.org/10.4049/jimmunol.176.8.4914

Gibbings, S. L., Thomas, S. M., Atif, S. M., McCubbrey, A. L., Desch, A. N., Danhorn, T., … Jakubzick, C. V. (2017). Three unique interstitial macrophages in the murine lung at steady state. *American Journal of Respiratory Cell and Molecular Biology*. https://doi.org/10.1165/rcmb.2016-0361OC

Ginhoux, F., Greter, M., Leboeuf, M., Nandi, S., See, P., Gokhan, S., … Merad, M. (2010a). Fate mapping analysis reveals that adult microglia derive from primitive macrophages. *Science (New York, N.Y.)*, *330*(6005), 841–845. https://doi.org/10.1126/science.1194637

Ginhoux, F., Greter, M., Leboeuf, M., Nandi, S., See, P., Gokhan, S., … Merad, M. (2010b). Fate mapping analysis reveals that adult microglia derive from primitive macrophages. *Science*. https://doi.org/10.1126/science.1194637

Ginhoux, F., & Guilliams, M. (2016). Tissue-Resident Macrophage Ontogeny and Homeostasis. *Immunity*. https://doi.org/10.1016/j.immuni.2016.02.024

Ginhoux, F., & Jung, S. (2014). Monocytes and macrophages: Developmental pathways and tissue homeostasis. *Nature Reviews Immunology*. https://doi.org/10.1038/nri3671

Ginhoux, F., Lim, S., Hoeffel, G., Low, D., & Huber, T. (2013). Origin and differentiation of microglia. *Frontiers in Cellular Neuroscience*. https://doi.org/10.3389/fncel.2013.00045

Ginhoux, F., & Merad, M. (2010). Ontogeny and homeostasis of Langerhans cells. *Immunology*

and Cell Biology. https://doi.org/10.1038/icb.2010.38
Godwin, J. W., Pinto, A. R., & Rosenthal, N. A. (2013). Macrophages are required for adult salamander limb regeneration. *Proceedings of the National Academy of Sciences*. https://doi.org/10.1073/pnas.1300290110
Goldeck, D., Larbi, A., Pellicanó, M., Alam, I., Zerr, I., Schmidt, C., … Pawelec, G. (2013). Enhanced Chemokine Receptor Expression on Leukocytes of Patients with Alzheimer's Disease. *PLoS ONE*. https://doi.org/10.1371/journal.pone.0066664
Goldmann, T., Wieghofer, P., Joana, M., Jordão, C., Prutek, F., Hagemeyer, N., … Prinz, M. (2016). Origin , fate and dynamics of macrophages at central nervous system interfaces, (August 2015). https://doi.org/10.1038/ni.3423
Gomez Perdiguero, E., Klapproth, K., Schulz, C., Busch, K., de Bruijn, M., Rodewald, H.-R., & Geissmann, F. (2015). The Origin of Tissue-Resident Macrophages: When an Erythro-myeloid Progenitor Is an Erythro-myeloid Progenitor. *Immunity*. https://doi.org/10.1016/j.immuni.2015.11.022
Gomez Perdiguero, E., Klapproth, K., Schulz, C., Busch, K., Azzoni, E., Crozet, L., … Rodewald, H. R. (2015b). Tissue-resident macrophages originate from yolk-sac-derived erythro-myeloid progenitors. *Nature*, *518*(7540), 547–551. https://doi.org/10.1038/nature13989
Gosselin, D., Skola, D., Coufal, N. G., Holtman, I. R., Schlachetzki, J. C. M., Sajti, E., … Glass, C. K. (2017). An environment-dependent transcriptional network specifies human microglia identity. *Science*. https://doi.org/10.1126/science.aal3222
Grakoui, A., Bromley, S. K., Sumen, C., Davis, M. M., Shaw, A. S., Allen, P. M., & Dustin, M. L. (1999). The immunological synapse: A molecular machine controlling T cell activation. *Science*. https://doi.org/10.1126/science.285.5425.221
Green, C. E., Schaff, U. Y., Sarantos, M. R., Lum, A. F. H., Staunton, D. E., & Simon, S. I. (2006). Dynamic shifts in LFA-1 affinity regulate neutrophil rolling, arrest, and transmigration on inflamed endothelium. *Blood*. https://doi.org/10.1182/blood-2005-06-2303
Greter, M., Heppner, F. L., Lemos, M. P., Odermatt, B. M., Goebels, N., Laufer, T., … Becher, B. (2005). Dendritic cells permit immune invasion of the CNS in an animal model of multiple sclerosis. *Nature Medicine*. https://doi.org/10.1038/nm1197
Greter, M., Lelios, I., & Croxford, A. L. (2015). Microglia versus myeloid cell nomenclature during brain inflammation. *Frontiers in Immunology*. https://doi.org/10.3389/fimmu.2015.00249
Griciuc, A., Serrano-Pozo, A., Parrado, A. R., Lesinski, A. N., Asselin, C. N., Mullin, K., … Tanzi, R. E. (2013). Alzheimer's disease risk gene cd33 inhibits microglial uptake of amyloid beta. *Neuron*. https://doi.org/10.1016/j.neuron.2013.04.014
Guerreiro, R., Wojtas, A., Bras, J., Carrasquillo, M., Rogaeva, E., Majounie, E., … Hardy, J. (2012). TREM2 Variants in Alzheimer's Disease . *New England Journal of Medicine*. https://doi.org/10.1056/nejmoa1211851
Guilliams, M., De Kleer, I., Henri, S., Post, S., Vanhoutte, L., De Prijck, S., … Lambrecht, B. N. (2013). Alveolar macrophages develop from fetal monocytes that differentiate into long-lived cells in the first week of life via GM-CSF. *The Journal of Experimental Medicine*. https://doi.org/10.1084/jem.20131199
Haga, S., Akai, K., & Ishii, T. (1989). Demonstration of microglial cells in and around senile (neuritic) plaques in the Alzheimer brain - An immunohistochemical study using a novel

monoclonal antibody. *Acta Neuropathologica*. https://doi.org/10.1007/BF00687883
Hardy, J., & Selkoe, D. J. (2002). The amyloid hypothesis of Alzheimer's disease: Progress and problems on the road to therapeutics. *Science*. https://doi.org/10.1126/science.1072994
Hashimoto, D., Chow, A., Noizat, C., Teo, P., Beasley, M. B., Leboeuf, M., … Merad, M. (2013). Tissue-resident macrophages self-maintain locally throughout adult life with minimal contribution from circulating monocytes. *Immunity*. https://doi.org/10.1016/j.immuni.2013.04.004
Haynes, S. E., Hollopeter, G., Yang, G., Kurpius, D., Dailey, M. E., Gan, W. B., & Julius, D. (2006). The P2Y12 receptor regulates microglial activation by extracellular nucleotides. *Nature Neuroscience*. https://doi.org/10.1038/nn1805
Heneka, M. T., Carson, M. J., Khoury, J. El, Landreth, G. E., Brosseron, F., Feinstein, D. L., … Kummer, M. P. (2015). Neuroinflammation in Alzheimer's disease. *The Lancet Neurology*, *14*(4), 388–405. https://doi.org/10.1016/S1474-4422(15)70016-5
Hoeffel, G, Chen, J., Lavin, Y., Low, D., & Almeida, F. (2015). C-Myb+ erythro-myeloid progenitor-derived fetal monocytes give rise to adult tissue-resident macrophages. *Immunity*. Retrieved from http://www.sciencedirect.com/science/article/pii/S1074761315001259
Hoeffel, Guillaume, Chen, J., Lavin, Y., Low, D., Almeida, F. F., See, P., … Ginhoux, F. (2015). C-Myb + Erythro-Myeloid Progenitor-Derived Fetal Monocytes Give Rise to Adult Tissue-Resident Macrophages. *Immunity*. https://doi.org/10.1016/j.immuni.2015.03.011
Hoeffel, Guillaume, & Ginhoux, F. (2018a). Fetal monocytes and the origins of tissue-resident macrophages. *Cellular Immunology*, *330*(December 2017), 5–15. https://doi.org/10.1016/j.cellimm.2018.01.001
Hoeffel, Guillaume, Wang, Y., Greter, M., See, P., Teo, P., Malleret, B., … Ginhoux, F. (2012). Adult Langerhans cells derive predominantly from embryonic fetal liver monocytes with a minor contribution of yolk sac–derived macrophages. *The Journal of Experimental Medicine*. https://doi.org/10.1084/jem.20120340
Hong, S., Beja-Glasser, V. F., Nfonoyim, B. M., Frouin, A., Li, S., Ramakrishnan, S., … Stevens, B. (2016). Complement and microglia mediate early synapse loss in Alzheimer mouse models. *Science*, *8373*, 1–10. https://doi.org/10.1126/science.aad8373
Hynes, R. O. (1987). Integrins: A family of cell surface receptors. *Cell*. https://doi.org/10.1016/0092-8674(87)90233-9
Hynes, R. O. (2002). Integrins: bidirectional, allosteric signaling machines. *Cell*.
Inlay, M. A., Serwold, T., Mosley, A., Fathman, J. W., Dimov, I. K., Seita, J., & Weissman, I. L. (2014). Identification of multipotent progenitors that emerge prior to hematopoietic stem cells in embryonic development. *Stem Cell Reports*. https://doi.org/10.1016/j.stemcr.2014.02.001
Jakubzick, C., Gautier, E. L., Gibbings, S. L., Sojka, D. K., Schlitzer, A., Johnson, T. E., … Randolph, G. J. (2013). Minimal differentiation of classical monocytes as they survey steady-state tissues and transport antigen to lymph nodes. *Immunity*. https://doi.org/10.1016/j.immuni.2013.08.007
Jay, T. R., Miller, C. M., Cheng, P. J., Graham, L. C., Bemiller, S., Broihier, M. L., … Lamb, B. T. (2015). TREM2 deficiency eliminates TREM2 + inflammatory macrophages and ameliorates pathology in Alzheimer's disease mouse models . *The Journal of Experimental Medicine*. https://doi.org/10.1084/jem.20142322
Joshi, N., Walter, J. M., & Misharin, A. V. (2018). Alveolar Macrophages. *Cellular Immunology*,

330(December 2017), 86–90. https://doi.org/10.1016/j.cellimm.2018.01.005
Jung, B. K., Pyo, K. H., Shin, K. Y., Hwang, Y. S., Lim, H., Lee, S. J., … Shin, E. H. (2012). Toxoplasma gondii infection in the brain inhibits neuronal degeneration and learning and memory impairments in a murine model of alzheimer's disease. *PLoS ONE*. https://doi.org/10.1371/journal.pone.0033312
Jung, S., Aliberti, J., Graemmel, P., Sunshine, M. J., Kreutzberg, G. W., Sher, A., & Littman, D. R. (2002). Analysis of Fractalkine Receptor CX3CR1 Function by Targeted Deletion and Green Fluorescent Protein Reporter Gene Insertion. *Molecular and Cellular Biology*. https://doi.org/10.1128/mcb.20.11.4106-4114.2000
Keren-Shaul, H., Spinrad, A., Weiner, A., Matcovitch-Natan, O., Dvir-Szternfeld, R., Ulland, T. K., … Amit, I. (2017b). A Unique Microglia Type Associated with Restricting Development of Alzheimer's Disease. *Cell*, *169*(7), 1276-1290.e17. https://doi.org/10.1016/j.cell.2017.05.018
Kierdorf, K., Erny, D., Goldmann, T., Sander, V., Schulz, C., Perdiguero, E. G., … Prinz, M. (2013a). Microglia emerge from erythromyeloid precursors via Pu.1- and Irf8-dependent pathways. *Nature Neuroscience*, *16*(3), 273–280. https://doi.org/10.1038/nn.3318
Kim, S. K., Karasov, A., & Boothroyd, J. C. (2007). Bradyzoite-specific surface antigen SRS9 plays a role in maintaining Toxoplasma gondii persistence in the brain and in host control of parasite replication in the intestine. *Infection and Immunity*. https://doi.org/10.1128/IAI.01862-06
Kishimoto, T. K., Larson, R. S., Corbi, A. L., Dustin, M. L., Staunton, D. E., & Springer, T. A. (1989). The Leukocyte Integrins. *Advances in Immunology*. https://doi.org/10.1016/S0065-2776(08)60653-7
Kissa, K., & Herbomel, P. (2010). Blood stem cells emerge from aortic endothelium by a novel type of cell transition. *Nature*. Retrieved from http://www.nature.com/nature/journal/v464/n7285/full/nature08761.html
Klein, I., Cornejo, J. C., Polakos, N. K., John, B., Wuensch, S. A., Topham, D. J., … Crispe, I. N. (2007). Kupffer cell heterogeneity: Functional properties of bone marrow-derived and sessile hepatic macrophages. *Blood*. https://doi.org/10.1182/blood-2007-02-073841
Koh, F. M., Lizama, C. O., Wong, P., Hawkins, J. S., Zovein, A. C., & Ramalho-Santos, M. (2015). Emergence of hematopoietic stem and progenitor cells involves a Chd1-dependent increase in total nascent transcription. *Proceedings of the National Academy of Sciences of the United States of America*, *112*(14), E1734-43. https://doi.org/10.1073/pnas.1424850112
Kolios, G., Valatas, V., & Kouroumalis, E. (2006). Role of Kupffer cells in the pathogenesis of liver disease. *World Journal of Gastroenterology*.
Koning, N., Bö, L., Hoek, R. M., & Huitinga, I. (2007). Downregulation of macrophage inhibitory molecules in multiple sclerosis lesions. *Annals of Neurology*. https://doi.org/10.1002/ana.21220
Konishi, H., Kobayashi, M., Kunisawa, T., Imai, K., Sayo, A., Malissen, B., … Kiyama, H. (2017). Siglec-H is a microglia-specific marker that discriminates microglia from CNS-associated macrophages and CNS-infiltrating monocytes. *GLIA*. https://doi.org/10.1002/glia.23204
Kosik, K. S., Joachim, C. L., & Selkoe, D. J. (1986). Microtubule-associated protein tau (tau) is a major antigenic component of paired helical filaments in Alzheimer disease. *Proceedings of the National Academy of Sciences of the United States of America*.
Kumaravelu, P., Hook, L., Morrison, A. M., Ure, J., Zhao, S., Zuyev, S., … Medvinsky, A.

(2002). Quantitative developmental anatomy of definitive haematopoietic stem cells/long-term repopulating units (HSC/RUs): role of the aorta-gonad-mesonephros (AGM) region and the yolk sac in colonisation of the mouse embryonic liver. *Development (Cambridge, England)*.

Lambert, J. C., Ibrahim-Verbaas, C. A., Harold, D., Naj, A. C., Sims, R., Bellenguez, C., … Seshadri, S. (2013). Meta-analysis of 74,046 individuals identifies 11 new susceptibility loci for Alzheimer's disease. *Nature Genetics*. https://doi.org/10.1038/ng.2802

Lampron, A., Lessard, M., & Rivest, S. (2012). Effects of Myeloablation, Peripheral Chimerism, and Whole-Body Irradiation on the Entry of Bone Marrow-Derived Cells into the Brain. *Cell Transplantation*. https://doi.org/10.3727/096368911X593154

Larson, R. S., & Springer, T. A. (1990). Structure and Function of Leukocyte Integrins. *Immunological Reviews*. https://doi.org/10.1111/j.1600-065X.1990.tb00565.x

Lavin, Y., Mortha, A., Rahman, A., & Merad, M. (2015). Regulation of macrophage development and function in peripheral tissues. *Nature Reviews. Immunology*, *15*(12), 731–744. https://doi.org/10.1038/nri3920

Lavin, Y., Winter, D., Blecher-Gonen, R., David, E., Keren-Shaul, H., Merad, M., … Amit, I. (2014). Tissue-resident macrophage enhancer landscapes are shaped by the local microenvironment. *Cell*. https://doi.org/10.1016/j.cell.2014.11.018

Lee, L. K., Ghorbanian, Y., Wang, W., Wang, Y., Kim, Y. J., Weissman, I. L., … Mikkola, H. K. A. (2016). LYVE1 Marks the Divergence of Yolk Sac Definitive Hemogenic Endothelium from the Primitive Erythroid Lineage. *Cell Reports*. https://doi.org/10.1016/j.celrep.2016.10.080

Lee, L. K., Ueno, M., Van Handel, B., & Mikkola, H. K. A. (2010). Placenta as a newly identified source of hematopoietic stem cells. *Current Opinion in Hematology*. https://doi.org/10.1097/MOH.0b013e328339f295

Lemere, C. A., Spooner, E. T., LaFrancois, J., Malester, B., Mori, C., Leverone, J. F., … Duff, K. E. (2003). Evidence for peripheral clearance of cerebral Aβ protein following chronic, active Aβ immunization in PSAPP mice. *Neurobiology of Disease*. https://doi.org/10.1016/S0969-9961(03)00044-5

López-Rouríguez, C., Nueda, A., Rumo, M., & Corbí, A. L. (1995). Regulation of Expression of the LFA-1 and p150,95 Leukocyte lntegrins: Involvement of the CD11a and CD11c Gene Promoters. *Immunobiology*, *193*(2–4), 315–321. https://doi.org/10.1016/S0171-2985(11)80560-7

Lowe, L. A., Yamada, S., & Kuehn, M. R. (2000). HoxB6-Cre transgenic mice express Cre recombinase in extra-embryonic mesoderm, in lateral plate and limb mesoderm and at the midbrain/hindbrain junction. *Genesis*, *26*(2), 118–120. https://doi.org/10.1002/(SICI)1526-968X(200002)26:2<118::AID-GENE5>3.0.CO;2-S

Lum, A. F. H., Green, C. E., Lee, G. R., Staunton, D. E., & Simon, S. I. (2002). Dynamic regulation of LFA-1 activation and neutrophil arrest on intercellular adhesion molecule 1 (ICAM-1) in shear flow. *Journal of Biological Chemistry*. https://doi.org/10.1074/jbc.M202223200

Luo, B.-H., Carman, C. V., & Springer, T. A. (2007). Structural Basis of Integrin Regulation and Signaling. *Annual Review of Immunology*, *25*(1), 619–647. https://doi.org/10.1146/annurev.immunol.25.022106.141618

Lux, C. T., Yoshimoto, M., McGrath, K., Conway, S. J., Palis, J., & Yoder, M. C. (2008). All primitive and definitive hematopoietic progenitor cells emerging before E10 in the mouse

embryo are products of the yolk sac. *Blood*, *111*(7), 3435–3438. https://doi.org/10.1182/blood-2007-08-107086
Mantovani, A., Biswas, S. K., Galdiero, M. R., Sica, A., & Locati, M. (2013). Macrophage plasticity and polarization in tissue repair and remodelling. *Journal of Pathology*. https://doi.org/10.1002/path.4133
Marsh, S. E., Abud, E. M., Lakatos, A., Karimzadeh, A., Yeung, S. T., Davtyan, H., … Blurton-Jones, M. (2016). The adaptive immune system restrains Alzheimer's disease pathogenesis by modulating microglial function. *Proceedings of the National Academy of Sciences*. https://doi.org/10.1073/pnas.1525466113
Masliah, E., Mallory, M., Alford, M., DeTeresa, R., Hansen, L. A., McKeel, D. W., & Morris, J. C. (2001). Altered expression of synaptic proteins occurs early during progression of Alzheimer's disease. *Neurology*. https://doi.org/10.1212/WNL.56.1.127
McGrath, K. E., Frame, J. M., Fegan, K. H., Bowen, J. R., Conway, S. J., Catherman, S. C., … Palis, J. (2015). Distinct Sources of Hematopoietic Progenitors Emerge before HSCs and Provide Functional Blood Cells in the Mammalian Embryo. *Cell Reports*, *11*(12), 1892–1904. https://doi.org/10.1016/j.celrep.2015.05.036
Medvinsky, A., & Dzierzak, E. (1996). Definitive hematopoiesis is autonomously initiated by the AGM region. *Cell*. https://doi.org/10.1016/S0092-8674(00)80165-8
Menzel, F., Kaiser, N., Haehnel, S., Rapp, F., Patties, I., Schöneberg, N., … Bechmann, I. (2018). Impact of X-irradiation on microglia. *GLIA*. https://doi.org/10.1002/glia.23239
Merad, M., Ginhoux, F., & Collin, M. (2008). Origin, homeostasis and function of Langerhans cells and other langerin-expressing dendritic cells. *Nature Reviews Immunology*. https://doi.org/10.1038/nri2455
Merad, M., Manz, M. G., Karsunky, H., Wagers, A., Peters, W., Charo, I., … Engleman, E. G. (2002). Langerhans cells renew in the skin throughout life under steady-state conditions. *Nature Immunology*. https://doi.org/10.1038/ni852
Mikkola, H. K. A., Gekas, C., Orkin, S. H., & Dieterlen-Lievre, F. (2005). Placenta as a site for hematopoietic stem cell development. *Experimental Hematology*. https://doi.org/10.1016/j.exphem.2005.06.011
Mildner, A., Schmidt, H., Nitsche, M., Merkler, D., Hanisch, U.-K., Mack, M., … Prinz, M. (2007). Microglia in the adult brain arise from Ly-6ChiCCR2+ monocytes only under defined host conditions. *Nature Neuroscience*. https://doi.org/10.1038/nn2015
Mizutani, M., Pino, P. A., Saederup, N., Charo, I. F., Ransohoff, R. M., & Cardona, A. E. (2011). The Fractalkine Receptor but Not CCR2 Is Present on Microglia from Embryonic Development throughout Adulthood. *The Journal of Immunology*. https://doi.org/10.4049/jimmunol.1100421
Monks, C. R. F., Freiberg, B. A., Kupfer, H., Sciaky, N., & Kupfer, A. (1998). Three-dimensional segregation of supramolecular activation clusters in T cells. *Nature*. https://doi.org/10.1038/25764
Moore, M. A. S., & Metcalf, D. (1970). Ontogeny of the Haemopoietic System: Yolk Sac Origin of In Vivo and In Vitro Colony Forming Cells in the Developing Mouse Embryo. *British Journal of Haematology*, *18*(3), 279–296. https://doi.org/10.1111/j.1365-2141.1970.tb01443.x
Moynagh, P. N. (2005). The interleukin-1 signalling pathway in astrocytes: A key contributor to inflammation in the brain. *Journal of Anatomy*. https://doi.org/10.1111/j.1469-7580.2005.00445.x

Mrdjen, D., Pavlovic, A., Hartmann, F. J., Schreiner, B., Utz, S. G., Leung, B. P., … Becher, B. (2018). High-Dimensional Single-Cell Mapping of Central Nervous System Immune Cells Reveals Distinct Myeloid Subsets in Health, Aging, and Disease. *Immunity*. https://doi.org/10.1016/j.immuni.2018.01.011

Müller, A. M., Medvinsky, A., Strouboulis, J., Grosveld, F., & Dzierzakt, E. (1994). Development of hematopoietic stem cell activity in the mouse embryo. *Immunity*, *1*(4), 291–301. https://doi.org/10.1016/1074-7613(94)90081-7

Muzumdar, M. D., Tasic, B., Miyamichi, K., Li, N., & Luo, L. (2007). A global double-fluorescent cre reporter mouse. *Genesis*. https://doi.org/10.1002/dvg.20335

Naik, S. H., Sathe, P., Park, H. Y., Metcalf, D., Proietto, A. I., Dakic, A., … Shortman, K. (2007). Development of plasmacytoid and conventional dendritic cell subtypes from single precursor cells derived in vitro and in vivo. *Nature Immunology*. https://doi.org/10.1038/ni1522

Naito, M., Takahashi, K., & Nishikawa, S. I. (1990). Development, differentiation, and maturation of macrophages in the fetal mouse liver. *Journal of Leukocyte Biology*. https://doi.org/10.1002/jlb.48.1.27

Naito, Makoto, Hasegawa, G., Ebe, Y., & Yamamoto, T. (2004). Differentiation and function of Kupffer cells. *Medical Electron Microscopy*. https://doi.org/10.1007/s00795-003-0228-x

Nayak, D., Zinselmeyer, B. H., Corps, K. N., & McGavern, D. B. (2012). In vivo dynamics of innate immune sentinels in the CNS. *IntraVital*. https://doi.org/10.4161/intv.22823

Nguyen, M. T., Zhu, J., Nakamura, E., Bao, X., & Mackem, S. (2009). Tamoxifen-dependent, inducible Hoxb6CreERT recombinase function in lateral plate and limb mesoderm, CNS isthmic organizer, posterior trunk neural crest, hindgut, and tailbud. *Developmental Dynamics*, *238*(2), 467–474. https://doi.org/10.1002/dvdy.21846

Nguyen, P. D., Hollway, G. E., Sonntag, C., Miles, L. B., Hall, T. E., Berger, S., … Currie, P. D. (2014). Haematopoietic stem cell induction by somite-derived endothelial cells controlled by meox1. *Nature*, *512*(7514), 314–318. https://doi.org/10.1038/nature13678

Nimmerjahn, A., Kirchhoff, F., & Helmchen, F. (2005). Neuroscience: Resting microglial cells are highly dynamic surveillants of brain parenchyma in vivo. *Science*. https://doi.org/10.1126/science.1110647

Nishikawa, S. I., Nishikawa, S., Kawamoto, H., Yoshida, H., Kizumoto, M., Kataoka, H., & Katsura, Y. (1998). In vitro generation of lymphohematopoietic cells from endothelial cells purified from murine embryos. *Immunity*. https://doi.org/10.1016/S1074-7613(00)80581-6

Oakley, H., Cole, S. L., Logan, S., Maus, E., Shao, P., Craft, J., … Vassar, R. (2006). Intraneuronal beta-Amyloid Aggregates, Neurodegeneration, and Neuron Loss in Transgenic Mice with Five Familial Alzheimer's Disease Mutations: Potential Factors in Amyloid Plaque Formation. *Journal of Neuroscience*. https://doi.org/10.1523/JNEUROSCI.1202-06.2006

Onai, N., Obata-Onai, A., Schmid, M. A., Ohteki, T., Jarrossay, D., & Manz, M. G. (2007). Identification of clonogenic common Flt3+M-CSFR+ plasmacytoid and conventional dendritic cell progenitors in mouse bone marrow. *Nature Immunology*. https://doi.org/10.1038/ni1518

Orkin, S. H., & Zon, L. I. (2008). Hematopoiesis: an evolving paradigm for stem cell biology. *Cell*. https://doi.org/10.1016/j.cell.2008.01.025

Ottersbach, K., & Dzierzak, E. (2005). The murine placenta contains hematopoietic stem cells within the vascular labyrinth region. *Developmental Cell*.

https://doi.org/10.1016/j.devcel.2005.02.001
Palis, J. (2001). Yolk-sac hematopoiesis The first blood cells of mouse and man. *Experimental Hematology*, *29*(8), 927–936. https://doi.org/10.1016/S0301-472X(01)00669-5
Palis, J, Robertson, S., Kennedy, M., Wall, C., & Keller, G. (1999). Development of erythroid and myeloid progenitors in the yolk sac and embryo proper of the mouse. *Development (Cambridge, England)*.
Palis, James. (2014). Primitive and definitive erythropoiesis in mammals. *Frontiers in Physiology*. https://doi.org/10.3389/fphys.2014.00003
Palis, James. (2016). Hematopoietic stem cell-independent hematopoiesis: emergence of erythroid, megakaryocyte, and myeloid potential in the mammalian embryo. *FEBS Letters*. https://doi.org/10.1002/1873-3468.12459
Paolicelli, R. C., Bolasco, G., Pagani, F., Maggi, L., Scianni, M., Panzanelli, P., … Gross, C. T. (2011). Synaptic pruning by microglia is necessary for normal brain development. *Science*. https://doi.org/10.1126/science.1202529
Parkhurst, C. N., Yang, G., Ninan, I., Savas, J. N., Yates, J. R., Lafaille, J. J., … Gan, W. B. (2013). Microglia promote learning-dependent synapse formation through brain-derived neurotrophic factor. *Cell*, *155*(7), 1596–1609. https://doi.org/10.1016/j.cell.2013.11.030
Pham, T. H. M., Baluk, P., Xu, Y., Grigorova, I., Bankovich, A. J., Pappu, R., … Cyster, J. G. (2010). Lymphatic endothelial cell sphingosine kinase activity is required for lymphocyte egress and lymphatic patterning. *The Journal of Experimental Medicine*, *207*(1), 17–27. https://doi.org/10.1084/jem.20091619
Ransohoff, R. M., Kivisäkk, P., & Kidd, G. (2003). Three or more routes for leukocyte migration into the central nervous system. *Nature Reviews Immunology*. https://doi.org/10.1038/nri1130
Rhodes, K. E., Gekas, C., Wang, Y., Lux, C. T., Francis, C. S., Chan, D. N., … Mikkola, H. K. A. (2008). The Emergence of Hematopoietic Stem Cells Is Initiated in the Placental Vasculature in the Absence of Circulation. *Cell Stem Cell*. https://doi.org/10.1016/j.stem.2008.01.001
Rodero, M. P., Poupel, L., Loyher, P. L., Hamon, P., Licata, F., Pessel, C., … Boissonnas, A. (2015). Immune surveillance of the lung by migrating tissue monocytes. *ELife*. https://doi.org/10.7554/eLife.07847
Russ, T. C., & Morling, J. R. (2012). Cholinesterase inhibitors for mild cognitive impairment. *Cochrane Database of Systematic Reviews*. https://doi.org/10.1002/14651858.cd009132.pub2
Sadleir, K. R., Eimer, W. A., Cole, S. L., & Vassar, R. (2015). Aβ reduction in BACE1 heterozygous null 5XFAD mice is associated with transgenic APP level. *Molecular Neurodegeneration*. https://doi.org/10.1186/1750-1326-10-1
Saederup, N., Cardona, A. E., Croft, K., Mizutani, M., Cotleur, A. C., Tsou, C. L., … Charo, I. F. (2010). Selective chemokine receptor usage by central nervous system myeloid cells in CCR2-red fluorescent protein knock-in mice. *PLoS ONE*. https://doi.org/10.1371/journal.pone.0013693
Salas, A., Shimaoka, M., Phan, U., Kim, M., & Springer, T. A. (2006). Transition from rolling to firm adhesion can be mimicked by extension of integrin α L β 2 in an intermediate affinity state. *Journal of Biological Chemistry*. https://doi.org/10.1074/jbc.M512472200
Samokhvalov, I. M., Samokhvalova, N. I., & Nishikawa, S. (2007). Cell tracing shows the contribution of the yolk sac to adult haematopoiesis. *Nature*, *446*(7139), 1056–1061.

https://doi.org/10.1038/nature05725
Schafer, D. P., Lehrman, E. K., Kautzman, A. G., Koyama, R., Mardinly, A. R., Yamasaki, R., … Stevens, B. (2012). Microglia sculpt postnatal neural circuits in an activity and complement-dependent manner. *Neuron*. https://doi.org/10.1016/j.neuron.2012.03.026
Schmits, R., Kündig, T. M., Baker, D. M., Shumaker, G., Simard, J. J., Duncan, G., … Hickstein, D. D. (1996). LFA-1-deficient mice show normal CTL responses to virus but fail to reject immunogenic tumor. *The Journal of Experimental Medicine*.
Schneider, L. S. (2012). Pharmacological treatment of alzheimer's disease. In *Alzheimer's Disease: Modernizing Concept, Biological Diagnosis and Therapy*. https://doi.org/10.1159/000335407
Schulz, C., Perdiguero, E. G., Chorro, L., Szabo-Rogers, H., Cagnard, N., Kierdorf, K., … Geissmann, F. (2012). A lineage of myeloid cells independent of myb and hematopoietic stem cells. *Science*. https://doi.org/10.1126/science.1219179
Schwartz, M., & Kipnis, J. (2011). A conceptual revolution in the relationships between the brain and immunity. *Brain, Behavior, and Immunity*. https://doi.org/10.1016/j.bbi.2010.12.015
Sedgwick, J. D., Schwender, S., Imrich, H., Dorries, R., Butcher, G. W., & ter Meulen, V. (2006). Isolation and direct characterization of resident microglial cells from the normal and inflamed central nervous system. *Proceedings of the National Academy of Sciences*. https://doi.org/10.1073/pnas.88.16.7438
Seita, J., Sahoo, D., Rossi, D. J., Bhattacharya, D., Serwold, T., Inlay, M. A., … Weissman, I. L. (2012). Gene expression commons: An open platform for absolute gene expression profiling. *PLoS ONE*. https://doi.org/10.1371/journal.pone.0040321
Selkoe, D. J., & Podlisny, M. B. (2002). Deciphering the genetic basis of Alzheimer's disease. *The Annual Review of Genomics and Human Genetics*. https://doi.org/10.1146/annurev.genom.3.022502.103022
Semmrich, M., Smith, A., Feterowski, C., Beer, S., Engelhardt, B., Busch, D. H., … Holzmann, B. (2005). Importance of integrin LFA-1 deactivation for the generation of immune responses. *The Journal of Experimental Medicine*. https://doi.org/10.1084/jem.20041850
Shaw, S. K., Ma, S., Kim, M. B., Rao, R. M., Hartman, C. U., Froio, R. M., … Luscinskas, F. W. (2004). Coordinated Redistribution of Leukocyte LFA-1 and Endothelial Cell ICAM-1 Accompany Neutrophil Transmigration. *The Journal of Experimental Medicine*. https://doi.org/10.1084/jem.20040965
Shechter, R., Miller, O., Yovel, G., Rosenzweig, N., London, A., Ruckh, J., … Schwartz, M. (2013). Recruitment of Beneficial M2 Macrophages to Injured Spinal Cord Is Orchestrated by Remote Brain Choroid Plexus. *Immunity*. https://doi.org/10.1016/j.immuni.2013.02.012
Sheng, J., Ruedl, C., & Karjalainen, K. (2015). Most Tissue-Resident Macrophages Except Microglia Are Derived from Fetal Hematopoietic Stem Cells. *Immunity*, *43*(2), 382–393. https://doi.org/10.1016/j.immuni.2015.07.016
Shukla, A. K., McIntyre, L. L., Marsh, S. E., Schneider, C. A., Hoover, E. M., Walsh, C. M., … Inlay, M. A. (2018). CD11a expression distinguishes infiltrating myeloid cells from plaque‐associated microglia in Alzheimer's disease. *Glia*, (July), 1–13. https://doi.org/10.1002/glia.23575
Siddiqui, S. S., Springer, S. A., Verhagen, A., Sundaramurthy, V., Alisson-Silva, F., Jiang, W., … Varki, A. (2017). The Alzheimer's Disease–protective CD33 splice variant mediates adaptive loss of function via diversion to an intracellular pool. *Journal of Biological Chemistry*. https://doi.org/10.1074/jbc.M117.799346

Sierra, A., Encinas, J. M., Deudero, J. J. P., Chancey, J. H., Enikolopov, G., Overstreet-Wadiche, L. S., … Maletic-Savatic, M. (2010). Microglia shape adult hippocampal neurogenesis through apoptosis-coupled phagocytosis. *Cell Stem Cell*. https://doi.org/10.1016/j.stem.2010.08.014

Simard, A. R., Soulet, D., Gowing, G., Julien, J. P., & Rivest, S. (2006). Bone marrow-derived microglia play a critical role in restricting senile plaque formation in Alzheimer's disease. *Neuron*, *49*(4), 489–502. https://doi.org/10.1016/j.neuron.2006.01.022

Squarzoni, P., Oller, G., Hoeffel, G., Pont-Lezica, L., Rostaing, P., Low, D., … Garel, S. (2014). Microglia Modulate Wiring of the Embryonic Forebrain. *Cell Reports*. https://doi.org/10.1016/j.celrep.2014.07.042

Stelzmann, R. A., Norman Schnitzlein, H., & Reed Murtagh, F. (1995). An english translation of alzheimer's 1907 paper, "über eine eigenartige erkankung der hirnrinde." *Clinical Anatomy*. https://doi.org/10.1002/ca.980080612

Stephan, A. H., Barres, B. A., & Stevens, B. (2012). The Complement System: An Unexpected Role in Synaptic Pruning During Development and Disease. *Annual Review of Neuroscience*. https://doi.org/10.1146/annurev-neuro-061010-113810

Stevens, B., Allen, N. J., Vazquez, L. E., Howell, G. R., Christopherson, K. S., Nouri, N., … Barres, B. A. (2007). The Classical Complement Cascade Mediates CNS Synapse Elimination. *Cell*. https://doi.org/10.1016/j.cell.2007.10.036

Stremmel, C., Schuchert, R., Wagner, F., Thaler, R., Weinberger, T., Pick, R., … Schulz, C. (2018). Yolk sac macrophage progenitors traffic to the embryo during defined stages of development. *Nature Communications*, *9*(1). https://doi.org/10.1038/s41467-017-02492-2

Swiers, G., de Bruijn, M., & Speck, N. A. (2010). Hematopoietic stem cell emergence in the conceptus and the role of Runx1. *International Journal of Developmental Biology*. https://doi.org/10.1387/ijdb.103106gs

Taoudi, S., Gonneau, C., Moore, K., Sheridan, J. M., Blackburn, C. C., Taylor, E., & Medvinsky, A. (2008). Extensive hematopoietic stem cell generation in the AGM region via maturation of VE-Cadherin+CD45+ pre-definitive HSCs. *Cell Stem Cell*. https://doi.org/10.1016/j.stem.2008.06.004

Thion, M., Squarzoni, P., Coralie-Anne, M., Low, D., Ginhoux, F., Audinat, E., & Garel, S. (2015). Microglia in the early development of inhibitory cortical circuits. *GLIA*. https://doi.org/http://dx.doi.org/10.1002/glia.22870

Tober, J., Koniski, A., McGrath, K. E., Vemishetti, R., Emerson, R., De Mesy-Bentley, K. K. L., … Palis, J. (2007). The megakaryocyte lineage originates from hemangioblast precursors and is an integral component both of primitive and of definitive hematopoiesis. *Blood*. https://doi.org/10.1182/blood-2006-06-031898

Tripathy, D., Thirumangalakudi, L., & Grammas, P. (2007). Expression of macrophage inflammatory protein 1-α is elevated in Alzheimer's vessels and is regulated by oxidative stress. *Journal of Alzheimer's Disease*. https://doi.org/10.3233/JAD-2007-11405

Valladeau, J., Ravel, O., Dezutter-Dambuyant, C., Moore, K., Kleijmeer, M., Liu, Y., … Saeland, S. (2000). Langerin, a novel C-type lectin specific to langerhans cells, is an endocytic receptor that induces the formation of Birbeck granules. *Immunity*. https://doi.org/10.1016/S1074-7613(00)80160-0

van de Laar, L., Saelens, W., De Prijck, S., Martens, L., Scott, C. L., Van Isterdael, G., … Guilliams, M. (2016). Yolk Sac Macrophages, Fetal Liver, and Adult Monocytes Can Colonize an Empty Niche and Develop into Functional Tissue-Resident Macrophages.

Immunity. https://doi.org/10.1016/j.immuni.2016.02.017
van Furth, R., Cohn, Z. A., Hirsch, J. G., Humphrey, J. H., Spector, W. G., & Langevoort, H. L. (1972). The mononuclear phagocyte system: a new classification of macrophages, monocytes, and their precursor cells. *Bulletin of the World Health Organization*.
von Bernhardi, R., Eugenín-von Bernhardi, L., & Eugenín, J. (2015). Microglial cell dysregulation in brain aging and neurodegeneration. *Frontiers in Aging Neuroscience*. https://doi.org/10.3389/fnagi.2015.00124
Wang, Y., Ulland, T. K., Ulrich, J. D., Song, W., Tzaferis, J. A., Hole, J. T., … Colonna, M. (2016). TREM2-mediated early microglial response limits diffusion and toxicity of amyloid plaques. *The Journal of Experimental Medicine*. https://doi.org/10.1084/jem.20151948
Watanabe, T., & Fan, J. (1998). Atherosclerosis and inflammation mononuclear cell recruitment and adhesion molecules with reference to the implication of ICAM- 1/LFA-1 pathway in atherogenesis. In *International Journal of Cardiology*. https://doi.org/10.1016/S0167-5273(98)00147-8
Westphalen, K., Gusarova, G. A., Islam, M. N., Subramanian, M., Cohen, T. S., Prince, A. S., & Bhattacharya, J. (2014). Sessile alveolar macrophages communicate with alveolar epithelium to modulate immunity. *Nature*. https://doi.org/10.1038/nature12902
Winkler #1, E. A., Nishida, Y., Sagare, A. P., Rege, S. V, Bell, R. D., Perlmutter, D., … Author, N. N. (2015). GLUT1 reductions exacerbate Alzheimer's disease vasculoneuronal dysfunction and degeneration HHS Public Access Author manuscript. *Nat Neurosci*. https://doi.org/10.1038/nn.3966
Winkler, E. A., Bell, R. D., & Zlokovic, B. V. (2011). Central nervous system pericytes in health and disease. *Nature Neuroscience*. https://doi.org/10.1038/nn.2946
Wu, X., Briseño, C. G., Durai, V., Albring, J. C., Haldar, M., Bagadia, P., … Murphy, K. M. (2016). Mafb lineage tracing to distinguish macrophages from other immune lineages reveals dual identity of Langerhans cells . *The Journal of Experimental Medicine*. https://doi.org/10.1084/jem.20160600
Yoder, M. C., Hiatt, K., & Mukherjee, P. (2002). In vivo repopulating hematopoietic stem cells are present in the murine yolk sac at day 9.0 postcoitus. *Proceedings of the National Academy of Sciences*. https://doi.org/10.1073/pnas.94.13.6776
Yoder, M., & Hiatt, K. (1997). Engraftment of embryonic hematopoietic cells in conditioned newborn recipients. *Blood*. Retrieved from http://www.bloodjournal.org/content/89/6/2176.short
Yoder, Mervin C, Hiatt, K., Mukherjee, P., & Wells, H. B. (1997). In vivo repopulating hematopoietic stem cells are present in the murine yolk sac at day 9.0 postcoitus (transplantationontogenycell differentiation). *Developmental Biology*.
Yona, S., Kim, K. W., Wolf, Y., Mildner, A., Varol, D., Breker, M., … Jung, S. (2013). Fate Mapping Reveals Origins and Dynamics of Monocytes and Tissue Macrophages under Homeostasis. *Immunity*. https://doi.org/10.1016/j.immuni.2012.12.001
Zenaro, E., Piacentino, G., & Constantin, G. (2017). The blood-brain barrier in Alzheimer's disease. *Neurobiology of Disease*. https://doi.org/10.1016/j.nbd.2016.07.007
Zhao, Z., Nelson, A. R., Betsholtz, C., & Zlokovic, B. V. (2015). Establishment and Dysfunction of the Blood-Brain Barrier. *Cell*. https://doi.org/10.1016/j.cell.2015.10.067
Zhao, Z., Sagare, A. P., Ma, Q., Halliday, M. R., Kong, P., Kisler, K., … Neurosci, N. (2015). Central role for PICALM in amyloid-β blood-brain barrier transcytosis and clearance HHS Public Access Author manuscript. *Nat Neurosci*. https://doi.org/10.1038/nn.4025

Zhou, F., Li, X., Wang, W., Zhu, P., Zhou, J., He, W., … Liu, B. (2016). Tracing haematopoietic stem cell formation at single-cell resolution. *Nature*, *advance on*. https://doi.org/10.1038/nature17997

Zhou, X., Xie, Q., Xi, G., Keep, R. F., & Hua, Y. (2014). Brain CD47 expression in a swine model of intracerebral hemorrhage. *Brain Research*. https://doi.org/10.1016/j.brainres.2014.06.003

Zlokovic, B. V. (2013). Cerebrovascular effects of apolipoprotein E: Implications for Alzheimer disease. *JAMA Neurology*. https://doi.org/10.1001/jamaneurol.2013.2152

Zovein, A. C., Turlo, K. A., Ponec, R. M., Lynch, M. R., Chen, K. C., Hofmann, J. J., … Iruela-Arispe, M. L. (2010). Vascular remodeling of the vitelline artery initiates extravascular emergence of hematopoietic clusters. *Blood*, *116*(18), 3435–3444. https://doi.org/10.1182/blood-2010-04-279497